TURBINE TRIP EVENT ANALYSIS IN A BOILING WATER REACTOR USING RELAP5/MOD3.4

TURBINE TRIP EVENT ANALYSIS IN A BOILING WATER REACTOR USING RELAP5/MOD3.4

By RAMAZAN BAYRAM ÇAKIR,

A Thesis Submitted to the School of Graduate Studies in Partial Fulfillment of the Requirements for the Degree Master of Applied Science

August 2023

McMaster University

MASTER OF APPLIED SCIENCE (2023)

Hamilton, Ontario, CANADA (Department of Engineering Physics)

TITLE:	Turbine Trip Event Analysis in a Boiling Water Reactor Using RELAP5/MOD3.4
AUTHOR:	Ramazan Bayram ÇAKIR Mechanical Engineering (BS), Kırıkkale University, Kırıkkale/TÜRKİYE
SUPERVISOR:	Dr. David NOVOG
NUMBER OF PAGES:	xx, 141

Lay Abstract

This research investigates the response of the Laguna Verde Boiling Water Reactor to a turbine trip event using the RELAP5/Mod3.4 themal-hydraulic analysis code. From reactor safety perspective a best-estimate case is evaluated, as well as three additional hypothetical scenarios. Findings are compared with the Boiling Water Reactor Turbine Trip II Benchmark results. Additionally, sensitivity analyses focusing on plant parameters such as shutdown rod behavior, gamma heating coefficient, turbine stop valve, and steam bypass valve characteristics conducted to determine their impact on the results. Insights from these analyses aim to enhance safety protocols and refine best practices in boiling water reactor management.

Abstract

This study explores the behavior of a Boiling Water Reactor (BWR) during a turbine trip scenario initiated by the abrupt closure of the turbine stop valve. The RELAP5/Mod3.4 code is employed to make calculations using the Laguna Verde Nuclear Power Plant input model provided by Innovative Software Systems Company. The event sequences and initial boundary conditions are sourced from the Boiling Water Reactor Turbine Trip 2 Benchmark created by NEA. Results are subsequently compared against the benchmark values.

In order to gauge the risk of a turbine trip event leading to elevated power, which could in turn cause Critical Heat Flux (CHF)-related issues in cladding temperature, a best-estimate case is developed. Our findings indicate that the closure of the turbine stop valve (TSV) resulted in a collapse of the void fraction within the reactor core. Although the core power doubled the initial level, the negative feedback mechanism effectively suppressed the power pulse. Throughout the transient phase, the maximum cladding temperature stayed below the CHF threshold, a fact attributable to the fuel's conductivity and the rapid progression of the transient.

We further analyzed three hypothetical scenarios to test the computational boundaries of the plant model. The third scenario, which combines conditions from the first two, produced elevated outcomes (6500MW core power, 598K cladding temperature,

and 7900kPa dome pressure) as expected. Notably, while the CHF limit remained unbreached in this scenario, literature reviews suggest potential core meltdown risks in subsequent stages of this calculation.

Our sensitivity analyses determined that variations in the gamma heating coefficient or the maximum time step of the calculations have little to no impact on core power or peak cladding temperature. Conversely, we noted a significant reduction, approximately 35%, in the power peak, underscoring the high sensitivity of the parameters to the initial triggering of the SCRAM mechanism. Our results also recommend rapid and early actuation of the BPV as a measure to dampen the pressure wave, consequently decreasing both the power peak and peak cladding temperatures.

Dedication

I dedicate this work to my mother, and members of my family, who have always stood by my side with encouragement and unwavering belief in my future.

I also would like to thank my friends Muse and Nurten for their friendship and endless support.

Finally, a heartful of thank goes to the love of my life, my fiancee Ayşenur ŞEREF. Her love, patience, and never-ending support have been my stronghold. She have filled my life with meaning and made this journey all the more special.

Acknowledgements

I would like to extend my sincerest gratitude to my supervisor, Dr. NOVOG. His guidance, encouragement, and invaluable insights enlightened my path. His unwavering support and mentorship have been instrumental in shaping my academic journey.

On behalf of Dr. NOVOG I also thank to the distinguished professors and helpful members of McMaster University.

I genuinely thankful for Dr. Chris Allison and his team in Innovative Software Systems for their support.

I also thank Dr. Anuj Trivedi for helping me during the learning phase of my studies.

I am grateful to the Ministry of National Education of the Republic of Türkiye for their financial support. This generous assistance made my pursuit of higher education possible.

A special acknowledgment is extended to my mentor, Mr. Ali ÖZKARA, in the Nuclear Regulatory Authority in Türkiye for his guidance.

Contents

List of Figures

List of Tables

Nomenclature

$\dot{Q}$	Heat transfer rate
k	Thermal conductivity
h	Convection coefficient, specific enthalpy
v	Kinematic viscosity
f	Friction loss coefficient
Re	Reynolds number
Nu	Nusselt number
Pr	Prandtl number
T	Temperature
t	Time
σ	Stefan-Boltzman coefficient
ϵ	Surface roughness
Γ	Volumetric mass exchange rate

α	Void fraction
ρ	Density, reactivity in reactor kinetics
FIF,FIG	Interphase drag coefficient [liquid,vapor]
FWF,FWG	Wall drag coefficients [liquid,vapor]
$DISS$	Energy dissipation function
C	Virtual mass coefficient
χ	Lockhart-Martinelli function
B	Body force
A	Cross-sectional area, coefficient in pressure and velocity equations
G	Mass flux
Φ	Lockhart-Martinelli two-phase parameter
Ψ	Fission rate
Σ_f	Fission cross-section
Λ	Prompt neutron generation time
λ	Friction factor, interface velocity parameter, decay constant
β	Effective delayed neutron fraction in reactor kinetics

List of Abbreviations

AEC	Atomic Energy Commission
AGR	Advanced Gas-Cooled Reactor
ANL	Argonne National Laboratory
BEMUSE	Best Estimate Methods, Uncertainty and Sensitivity Evaluation
BORAX	Boiling Water Reactor Experiment
BPV	Steam Bypass Valve
BWR	Boiling Water Reactors
CANDU	Canadian Deuterium Uranium Reactor
CNSNS	National Commission of Nuclear Safety and Safeguards
CRD	Control Rod Drive System
EBWR	Experimental Boiling Water Reactor
ECCS	Emergency Core Cooling
GCR	Gas-Cooled Reactors

HPCS	High-Pressure Core Spray System
HTR	High-Temperature Reactors
IAEA	International Atomic Energy Agency
IEA	International Energy Agency
INEL	Idaho National Engineering Laboratory
ISS	Innovative Systems Software
LBLOCA	Large Break Loss of Coolant Accident
LGR	Liquid Graphite Reactors
LMFBR	Liquid Metal Fast Breeder Reactor
LOFT	Loss of Fluid Test Circuit
LPCI	Low-Pressure Injection System
LPCS	Low-Pressure Core Spray System
LVNPP	Laguna Verde Nuclear Power Plant
OECD	Organisation for Economic Co-operation and Development
PBTT	Peach Bottom Turbine Trip Test
PHWR	Pressurized Heavy Water Reactors
PWR	Pressurized Water Reactors
RBMK	Reactor Bolshoy Moshchnosti Kanalniy

RCIC	Reactor Core Isolation Cooling
RELAP	Reactor Excursion and Leak Analysis Program
RETRAN	Reactor Transient Analysis
RPV	Reactor Pressure Vessel
RWCU	Reactor Water Cleanup System
SLC	Standby Liquid Control System
SNAP	Symbolic Nuclear Analysis Package
TDJ	Time-Dependent Junction
TDV	Time-Dependent Volume
TRAC	Transient Reactor Analysis Code
TRACE	TRAC/RELAP Advanced Computational Engine
TSV	Turbine Stop Valve
UO2	Uranium Dioxide
USNRC	United States Nuclear Regulatory Commission
VVER	Voda Vodyanoi Energetichesky Reactor

Declaration of Academic Achievement

Declaration of Academic Achievement go here.

1

Introduction

Almost every day new gadgets and devices are introduced into day-to-day life thanks to the advancements in the various fields of science and technology. It is well-known that rapidly developing technologies and increasing population also increase energy demand. According to the United Nations (UN), the global population is expected to increase by almost 2 billion by 2050 [23]. The parties who signed the Paris Agreement in 2015 promised to meet this increasing demand using clean and sustainable sources in conjunction with the Net Zero Emission commitment [2].

The efforts to improve and popularize alternative energy production methods show the high potential of these sources. However, the dependence on fossil fuels in power and electricity production is still considered strong. Findings revealed that in 19 years following the year 2000, the global energy-related carbon dioxide emission rose to 33.3 Gt. The pandemic in 2020 brought a drop by 4%, however; the fast recovery of the sectors after the pandemic has jumped the emission rates by 5% in 2021 [27].

Constant emission of smoke and greenhouse gasses into the atmosphere has a toll on the world's natural balance. Among all known effects, climate change stands out as

the most widely accepted example of many other threats. Due to the changing precipitation cycles and climate conditions, even the most reliable food, water, and energy sources are not as dependable as they were in the past. Therefore, decarbonization of electricity, heat, and power production has crucial importance in globally achieving the net zero emission goal by 2050. According to a report by the International Energy Agency (IEA), this goal can not be achieved without benefiting from the capacity of nuclear energy [27].

Moreover, geopolitics already revealed its potential to create a widespread food and energy crisis even in the most secure and wealthy territories such as those experienced during the war in Ukraine that began in 2022. Governments who can secure clean and reliable food, water, and energy sources also can secure the interest and well-being of their nation and citizens. Therefore, Zohuri draws attention to the capacity of nuclear power production facilities substituting approximately 50,000 barrels of oil being consumed per day in the production of electricity [50]. For widespread electrification of transportation, industry, and agriculture it is very apparent that growth in nuclear baseload generation, in addition to intermittent renewables, will be required.

To address the increasing energy demand nuclear power generation technologies have been constantly improving instruments. Many countries such as the USA, Canada, Russia, and Japan played a pioneering role in the development of nuclear systems. However, the discovery of new horizons in the nuclear field also brought along new risks and challenges. The unforeseen threats resulted in unprecedented accidents such as the ones that happened in Three Mile Island, Chernobyl, and last

but not least Fukushima [22]. These and many other accidents highlighted the importance of nuclear reactor safety and led to the development of safety principles. The application of the safety analysis methods becomes a crucial part of both the plant design and operation for providing safer yet more efficient solutions to remain competent in the market and comply with regulatory rules.

Many safety analyses showed that transient events and accidents actually can happen more frequently than they were expected. One of the most significant examples of this occurred in the Salem II reactor in 1991. In the accident, the uncontrolled turbine overspeed transient caused an internal missile accident. This accident caused a 6 months of outage which is a significant loss in a reactor's operating life. Investigations showed that the particular accident occurred in a shorter frequency than the frequency specified by the designer.

For this very reason, we decided to conduct a safety analysis investigating the effects of the Turbine Trip Event on a Boiling Water Reactor since it is one of the most established and used reactor designs. During the course of this study, we benefited from the safety analysis tools, the results of publicly available studies, and the Boiling Water Reactor Turbine Trip II Benchmark created by the Nuclear Energy Agency (NEA). Within the scope of this thesis, we also conducted a series of transient cases in addition to the steady-state calculation. Findings from our work are also compared against publicly available data and the benchmark results. Additionally, to identify the influence of the plant parameters on the transient simulations, various sensitivity analyses have been conducted.

In Chapter 2, we discuss the evolution and development of nuclear studies, as well as the fundamentals of fission reactions. Building on this foundation, we introduce

methods of nuclear power generation, various designs of nuclear power reactors, and the safety aspects of their operation.

In Chapter 3, we present our findings from the literature survey on turbine trip analysis for boiling water reactors. We introduce the Boiling Water Reactor Turbine Trip Benchmark and provide an in-depth review of related works in the literature. Later in this chapter, we cover the principles and methods related to the uncertainty and sensitivity assessment in nuclear reactor analysis.

In Chapter 4, we discuss the methods and tools employed during our research. The theory section outlines the computational framework. Later in this chapter, we provide design specifications of the reference power plant and a description of the plant computer model.

In Chapter 5, we share the problem description and analysis results from the steady-state run, code testing routine, reference case calculation, and hypothetical scenarios. Comparisons are made with relevant literature and the benchmark.

In Chapter 6, we present our findings from analyzing selected sensitive cases, including maximum time steps for calculation, gamma heating coefficients, different valve operation characteristics, and the effect of control rod movement.

In Chapter 7, we summarize the work undertaken in this thesis and offer an overall conclusion based on the results presented. We also provide comments on potential future work in this field.

2

Background

2.1 History of the Nuclear Studies

Nuclear reactors are systems designed to benefit from the energy released due to electromagnetic interactions at the sub-atomic level. They are an excellent base-load electricity generation option and have very low carbon emissions per MWh of energy produced. Hence a combination of large reactors and Small Modular Reactors may help meet the challenges for low-carbon energy in the future. Therefore a brief explanation of the sub-atomic structure and behavior of the radioactive material would be helpful for better representation of the nuclear energy production systems.

In history, the radioactivity phenomenon has been a subject of scientific study for over a century. In 1896, Henri Becquerel discovered the radioactivity (emission of beta radiation and alpha particles) from an ore (pitchblende) containing radium and uranium. Villard later found a third type of radiation (gamma rays which are similar to X-rays) from the same substance. In 1902 Ernest Rutherford proved the potential of creating different elements via radioactivity. Nine years later, Frederick Soddy discovered that naturally radioactive elements had several different isotopes

(radionuclides) with the same chemistry. Almost two decades later (in 1932) James Chadwick announced the discovery of the neutron. This was a breakthrough in the history of nuclear studies, because, in the following year, Enrico Fermi proved that it is possible to create a much greater variety of artificial radionuclides with the help of neutrons.

By the end of 1938, Otto Hahn and Fritz Strassmann showed that the atomic fission reaction had occurred in uranium, as they discovered that the new lighter elements created were about half the mass of the fissioned uranium. Lise Meitner and Otto Frisch explained this discovery by suggesting that some neutron was captured by the nucleus, causing severe vibration leading to the nucleus splitting into two unequal parts. They calculated the energy release from this fission as almost 200 million electron volts. This figure was also confirmed experimentally by Frisch in January 1939.

A significant part of these historical achievements have been accomplished under the shadow of the First and Second World Wars. The tense climate of WW II also brought the need for superior firepower. The race to develop the first atomic bomb had pushed the nations to control the fission reactions to derive a detrimental force out of that. Ultimately, the efforts to harness this energy had started giving yields in both military and peaceful areas. In December 1942 the first controlled fission chain reaction was achieved by Enrico Fermi and his colleagues with an experimental facility built beneath the football field of the University of Chicago [50]. This accomplishment is considered a pioneer in nuclear studies.

Almost a decade later, construction of the first nuclear power reactor was completed under the directory of Walter Zinn in Idaho. The project was successful enough

to produce electricity (about 45 kW) sufficient for the operation of the facility itself [10] [40].

2.2 Fundamentals of Fission Reactions

It is a fact that all matter is comprised of atoms, which are made up of nuclei containing protons and neutrons in the core, and electrons orbiting on various energy levels around the nuclei. The combination of neutrons and protons in the nucleus of each atom gives rise to different isotopes observed in nature and laboratories. Some of these isotopes are stable over very long periods of time, while others are unstable and transform into more stable nuclei via emitting radiation.

Free neutrons can also cause the transformation of an isotope to another isotope and change the target nuclei's properties and their stability. The neutron-nucleus collision can occur in three possible scenarios: Elastic Scattering, Inelastic Scattering, and Capture. Should a fissile heavy nucleus such as Uranium-235 or Plutonium-239 capture a neutron, in certain situations the total energy imparted to the nucleus can cause fission and the release of some of the nuclear binding energy in the nucleus. Figure 2.1 is a schematic representation of a core splitting as a result of neutron capture by the Uranium-235 nucleus. The possibility of causing the target nucleus to become unstable and split (fission) into two smaller (lighter) nuclei strongly depends on the state of the target nuclei, energy of the incident neutron, and dynamics of the collision [33]. For other elements like U-238, fission does not readily take place unless the neutron has a very high incident velocity, and absorption reactions tend to produce heavier isotopes (e.g., Pu-239).

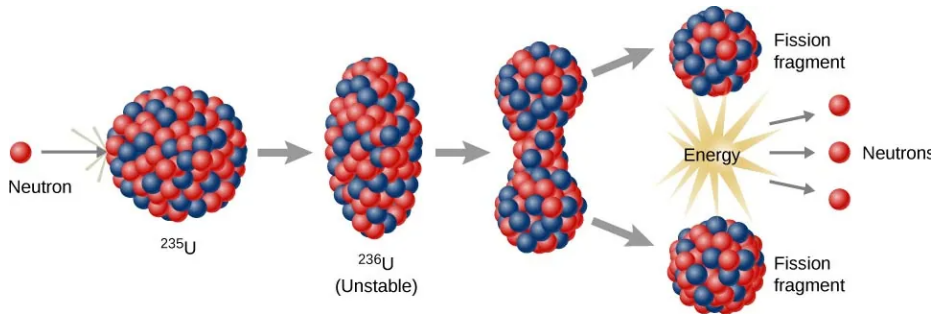

Figure 2.1: Diagram of a fission reaction following a neutron strike

Resulting lighter elements are often named as fission fragments (or products). An average of two to three excess neutrons are emitted from the fission reaction. The additional neutrons play an important role in the continuation of the series of fission reactions. The reason is that these extra neutrons can trigger the excitement of other heavy nuclei in the vicinity, thus could lead to a self-sustaining chain reaction.

As a byproduct of the fission reaction, a substantial amount of energy is also released in the form of kinetic energy and electromagnetic radiation. Although the actual amount of the total energy release can vary depending on how the nucleus is broken up this value is calculated by Frisch as approximately 200 MeV. This energy is deposited mostly in the fragments and results in increased temperature/energy locally. Nuclear reactor coolant systems absorb this energy and transport it to steam production facilities that ultimately drive a turbine system.

Since, fission reactions occur very fast, controlling these reactions is crucial to achieving a meaningful and convertible energy from these interactions. Therefore many decades were needed from the discovery of the fundamentals of the sub-atomic behavior to the development of nuclear energy production methods.

2.3 Nuclear Power Generation

Nuclear fission is a process of transforming high-energy atoms into lower-energy atoms. The driving force behind this transition is to achieve a more stable energy level. This mechanism may work spontaneously without external excitement/design. Even though this is a very low probability event, the first natural self-sustained nuclear reactor was discovered in Gabon in 1972 by French physicist Francis Perrin [32]. However, the geological conditions for a self-sustaining natural reaction are quite rare. Therefore, nuclear reactors are designed to facilitate and control the fission process, thereby utilizing the heat to produce electricity. This process bears a resemblance to power plants that are fueled by fossil fuels [10].

Since the first appearance of nuclear reactors, many reactors have been designed both for peaceful and military purposes. Besides electric power production purposes, nuclear reactors have been employed for the propulsion of vessels, rockets, and satellites, for medical use and research [10]. During the WWII era, nuclear projects were conducted under top-secret conditions which created different designs in different nations. In the following years, this difference in disciplines was combined with the differences in economy and safety culture. These all together led to the emergence of diverse designs of nuclear rectors among leading nuclear powers in the world. Some of the examples are American Pressurized Water Reactors (PWRs) and Boiling Water Reactors (BWRs), Canadian Deuterium Uranium (CANDUs), Soviet Reactor Bolshoy Moshchnosti Kanalniy (RBMKs), and Voda Vodyanoi Energetichesky Reactor (VVERs) [10].

2.4 Nuclear Power Reactor Designs

In the literature, there are several ways to categorize nuclear power plants. Some may consider the fuel type, reactor generation, moderator material, coolant, or reactor scale, etc. Since there is no strict method for classification, the method observed by researchers can vary based on the purpose of the work.

According to Dr. Rubin from McMaster University, reactors can be investigated under five groups: Pressurized Water Reactors (PWRs), Boiling Water Reactors (BWRs), Pressurized Heavy Water Reactors (PHWRs), Gas-Cooled Reactors (GCRs), Liquid-Cooled Graphite Reactors (LGRs), and Liquid Metal Fast Breeder Reactor (LMFBRs) [47].

2.4.1 Gas-Cooled Reactors

The Gas Cooled Reactors are types of nuclear reactors using gas as a coolant in a separate circuit from the primary circuit. The use of gas coolant allows for reaching higher coolant temperatures and hence achieving a high-efficiency steam cycle. Due to the high temperatures graphite is a more suitable moderator than water. Graphite blocks with channels are used to house the fuel elements and direct the flow of the gas coolant. Early gas-cooled reactors were called Magnox, while later ones were called advanced gas-cooled reactors (AGRs) and used a different type of fuel that allowed for higher operating temperatures. By changing the coolant from carbon dioxide to helium, even higher temperatures could be achieved, resulting in the designation of high-temperature reactors (HTRs). These reactors have the advantage of high cycle

efficiency, comparable to fossil fuel-fired power plants. Recent developments in gas-cooled reactors, such as the pebble bed modular reactor (PBMR), use a direct cycle with helium as the coolant passing directly to a helium turbine.

2.4.2 Liquid-Cooled Graphite Reactor

The Liquid Cooled Graphite Reactor is a type of nuclear reactor that uses a graphite block core for moderation. Fuel elements are positioned inside pressure tubes similar to those of the pressurized heavy water reactor, which passes through vertical holes in the graphite core. The use of graphite as a moderator allows for high efficiency and a compact design. Light water coolant flows upwards over the fuel and within the tubes. Boiling occurs around the fuel, producing steam that is separated from the water in an external drum. The water is then recirculated, and the saturated steam is sent to the turbine for electricity generation.

2.4.3 Liquid Metal Fast Breeder Reactor

The Liquid Metal Fast Breeder Reactor (LMFBR) is a unique type of reactor that employs a liquid metal, usually sodium, as the primary coolant. In this design, the heat generated in the fuel is carried away by the primary coolant and then transferred to a secondary sodium circuit in a heat exchanger. The secondary circuit, in turn, transfers the heat to the steam circuit in a steam generator. Using sodium as the coolant eliminates the need for thick-pressure vessels because sodium remains in a liquid state at high temperatures without being pressurized. Ultimately this improves the cycle efficiency. Unlike the other reactor types, the LMFBR does not require a moderator to reduce the energy of the neutrons, which is why it is referred to as

a "fast" reactor. The surplus neutrons produced by the fission process are utilized to convert fertile material into fissile fuel, earning it the designation of a "breeder" reactor. The use of fast-spectrum neutrons can provide many benefits such as a reduction in the production of long-lived actinide waste.

2.4.4 Pressurized Heavy Water Reactors

Pressurized Heavy-Water Reactors (PHWRs) are the third most common type of nuclear reactors in the World [7]. PHWRs are commonly used in Canada, where they are known as CANDU reactors, and they are also used in other countries such as India, Argentina, Romania, Pakistan, and China. The unique design of PHWRs allows online refueling, which allows for more flexible and efficient operation. In this design, the heavy water (D2O) acts both as a coolant and a moderator. The use of heavy water allows natural uranium to be used as fuel. This makes PHWRs a cost-effective option for countries with access to natural uranium reserves.

2.4.5 Pressurized Water Reactors

The Pressurized-Water Reactor (PWR) was initially developed as a nuclear propulsion system for US submarines due to its ability to provide high power and long range while requiring infrequent refueling [11]. The reactor designs for the PWR program were developed by the Argonne National Laboratory, while Westinghouse Electric Corporation was building the land-based prototypes. By August 1950, significant progress had been made on the Mark I land-based PWR prototype at the Bettis laboratory of Westinghouse.

While the Atomic Energy Commission (AEC) primarily supported the Navy's nuclear propulsion program through the Argonne Laboratory, they were also strongly advocating the development of nuclear power as a heat source for central electric generating stations [22]. The first commercial PWR nuclear power project in Shippingport Pennsylvania was built by Westinghouse in December 1957. In the following years, Russia developed the water-cooled, water-moderated power reactor (VVER), a similar design to PWR.

In a PWR design, the pressure vessel is a fundamental component of a nuclear power plant that performs several critical functions. It is a robust, thick-walled pressure chamber that encloses the fuel bundles and reactivity control equipment while also serving as a passive barrier, preventing the release of radioactive materials into the atmosphere in case of a leakage.

PWRs typically consist of two to four separate major coolant loops, with the primary loop circulating water inside the reactor core to remove heat generated by the nuclear material. The water in the PWR is maintained at high pressure, around 15 MPa, and exits the vessel at a temperature of about 325°C. Since the water in the PWR is maintained at high pressure, it does not boil during normal operation, requiring external steam generators to activate the turbines that generate electricity. This steam generator or heat exchanger acts as a bridge between the superheated, high-pressure water in the primary loop and the working fluid in the secondary loop. The fluid in the secondary circuit is turned into dry steam to drive the turbine blades, activating the generator attached to the turbine shaft.

PWR reactors use slightly enriched uranium dioxide (UO2) as fuel in the form of a black ceramic material with a high melting point of approximately 2,800°C [11].

UO2 is shaped into small cylindrical pellets, roughly 1 cm in diameter and 2 cm long, and loaded into sealed stainless steel or Zircaloy3 tubes (cladding) around 4 m long. The Zircaloy tubes provide support for the fuel pellets and prevent the fission products-especially fission product gases- released in the pellets from escaping. The fuel assemblies are arranged in a tightly packed lattice configuration, with either a square or triangular pitch, depending on the reactor type. Assemblies are individually handled and relocated in the core. Efficient manipulation and proper sequencing of the fuel assemblies from various burnup levels ensure that the reactor operates efficiently, and reactor generates power safely and reliably.

2.4.6 Boiling Water Reactors

The bulk of this thesis looks at examining the behavior and sensitivity of Boiling Water Reactors to Turbine Trip events. One of the motivations of this study is that Ontario is considering the construction of up to 4 BWRs at its Darlington site. Hence more detail on the design is provided in the following section. The technology behind the Boiling Water Reactors (BWR) and Pressurized Water Reactors (PWR) nuclear plants, initially emerged from the U.S. Navy's nuclear submarine program during the 1950s [31].

Before the development of the BWR technology, many believed that allowing water to boil in a reactor would cause hazardous instability due to uneven formation and movement of steam bubbles. However, Samuel Untermyer, a scientist at Argonne National Laboratory (ANL), proposed a different perspective. He postulated that if water bubbled or steamed in an overheating reactor core, the chain reaction, as opposed to the common belief, would actually slow down. Today, this concept is

known as the negative void reactivity feedback.

In 1953, Walter Zinn, the director of the Argonne Laboratory, decided to investigate the potential use of boiling water in reactor cores as a control mechanism for power production. This research resulted in the creation of the Boiling Water Reactor Experiment (BORAX) BORAX-I reactor, which proved the effectiveness of using steam formation as a self-limiting control mechanism during power surges [31].

During the course of experiments, ANL made several modifications to the BORAX reactor design in order to gain a comprehensive understanding of the parameters required for the safe operation of a BWR. The ultimate objective was to develop a reactor suitable for electrical generation. The initial BORAX experiments provided evidence of the inherent safety and stability of the BWR [22].

In a significant milestone, the BORAX-III reactor supplied nuclear power to the town of Arco, Idaho for the first time ever achieved a historic feat on July 17, 1955. Following these successful experiments, ANL constructed the Experimental BWR (EBWR), which became the first operational BWR power plant. Initially designed to generate 20 MWe, the EBWR functioned from 1956 to 1967. Over time, the power level and reliability of the plant were gradually increased, eventually enabling it to provide electricity to the entire ANL facility. Construction of the first commercial BWR is the Vallecitos plant with a 5 MWe capacity located near San Jose, California (1957). Vallecitos nuclear plant marked a significant milestone by producing electricity for a grid successfully and safely. Following the Vallecitos, the first large-scale BWR reactor Dresden 1 was constructed in 1960 [22].

The key feature of BWR is the occurrence of bulk boiling within the reactor core. In a BWR flow to the pressure vessel is provided by the main feedwater pumps

which take low-pressure water from the condenser and raise its pressure to the vessel pressure. The reactor vessel houses the reactor core, acts as a boundary for the reactor coolant, supports and aligns the fuel and control rods, facilitates the circulation of coolant around the fuel, removes moisture from the steam as it leaves the reactor vessel, restricts the downward motion of control rods in the event of a control rod drive housing failure, and provides an internal volume that can be reflooded [31]. The flow of coolant within the core is pressurized by pumps located either outside or inside the reactor vessel (depending on the vintage of the design, with the newest designs relying on natural convection of core circulation). These pumps actively drive the flow of coolant through the fuel. In contrast, a natural circulation design relies on the density difference between the single-phase fluid present in the downcomer region and the two-phase mixture (liquid and vapor) found in the core to drive flow through the fuel. This density difference is the driving force of the circulation of coolant within the reactor core, eliminating the need for internal/external core circulation pumps.

In the mid-1960s, the first large direct cycle BWRs (Oyster Creek and Nine Mile Point Unit 1) emerged. These were distinguished by two notable features: the elimination of steam generators and the utilization of five external recirculation loops to facilitate forced circulation flow through the reactor core. Further simplifications in reactor systems were achieved through the introduction of internal jet pumps to drive core flow. This development led to a reduction in the number of external recirculation loops required. This also avoided the risk of a LOCA in a recirculation line which was generally located below the top-of-active fuel (thus could result in core uncovery events). Consequently, this reduction in the number of loops resulted in a decrease in associated piping, valves, pumps, and large vessel nozzles. The control of reactivity

in BWRs is achieved through a combination of control rods and variations in coolant recirculation flow within the core. Jet pumps are utilized to adjust the ratio of liquid to steam and alter the fraction of steam and liquid water surrounding the fuel elements, thereby reducing the reliance on control rods.

Another significant milestone was the introduction of two technical innovations: the internal steam separator and the steam dryer. The internal steam separator effectively separates the steam from the boiling water within the reactor core. Additionally, the steam dryer plays a crucial role in ensuring that the steam leaving the reactor core is adequately dried prior to entering the turbine generator set. This eliminates excess moisture and enhances the overall efficiency of the BWR system [21].

Since the first example of the BWR reactors, there has been a constant effort to improve the technology. Since the 1960s, eight successive generations of the BWRs developed and went online (namely BWR I, BWR II, BWR III, BWR IV, BWR V, BWR VI, ABWR, and ESBWR).In Figure 2.2 major milestones in the history of the BWR technology development have been highlighted. Throughout these advancements, experts have tried to achieve a simpler, safer, and more efficient reactor design. Currently, there are investments to build new reactors and develop more financially economical designs such as BWRX. Even though it is technically a small modular reactor, its design principles are significantly related to the BWR design.

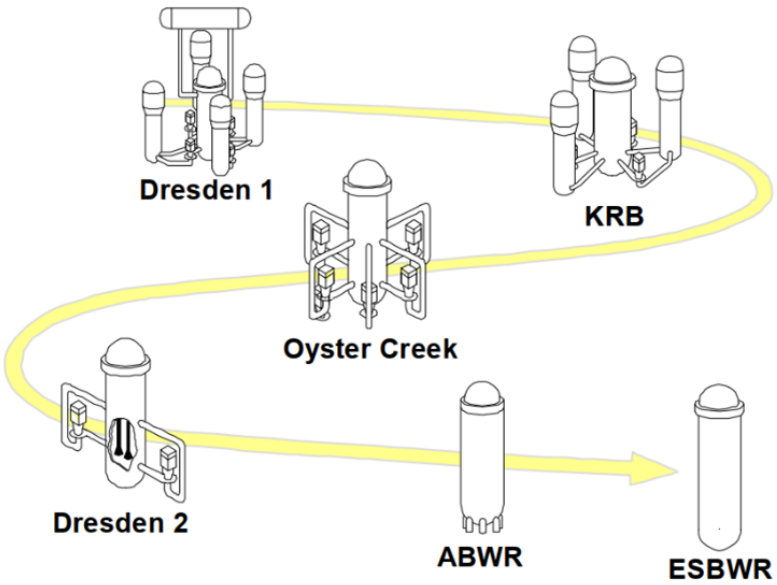

Figure 2.2: Evolution of Boiling Water Reactor technology adopted from [42]

The containment structure is a cylindrical prestressed concrete barrier with an embedded steel liner. It encloses the reactor, reactor coolant pressure, and important ancillary systems. Throughout the development of boiling water reactors (BWRs), three major containment designs were implemented: Mark I, Mark II, and Mark III. These containment designs all rely on the principle of pressure suppression to manage the loss of coolant accidents effectively. The primary function of the containment is to condense steam and confine fission products released during a loss of coolant accident. By doing so, these designs prevent exceeding the predefined radiation dose limits. Additionally, the containment serves as a heat sink and water source for specific safety-related equipment. While the Mark I and Mark II designs consist of a drywell and a wetwell (suppression pool) the Mark III consists of a primary containment and a drywell [21].

The radiation shielding requirements for the energy conversion side of a BWR

plant are still subject to controversy in the scientific community [42] [10]. This is because, in PWR systems, steam is generated in separate steam generators attached to the reactor pressure vessel (RPV). This system is known as the "Indirect Cycle". On the contrary, the steam is directly produced inside the RPV, which is then sent to a steam-driven turbine in the BWRs. Since the same fluid travels along the core, steam lines, and turbines, this process is called "Direct Cycle" [16]. Some experts contend that it is necessary to provide shielding for all components of the steam utilization system, including turbines, condensers, reheaters, pumps, and piping, to mitigate the risks of radiation exposure. However, others argue that the majority of radioactive materials in the BWR coolant remain in the liquid water and do not carry over into the steam, thereby reducing the need for extensive shielding measures.

The main characteristics of a BWRs can be summarized as:

- The typical operating temperature is around 290 - 320°C.
- The normal operating conditions result in two phases the core: a subcooled liquid phase; and a saturated steam-water mixture.
- The BWR core consists of several fuel assemblies enclosed in a casing called a fuel channel. Fuel rods (slightly enriched Uranium fuel 2% to 5% U-235 by weight) in assembly arranged in a N $\times$ N square lattice.
- The reactor power control consists of control rods and recirculation flow control. A power change rate of 2% full power per sec using control rods. A power change rate of 30% full power per minute using recirculation pumps.
- The turbine inlet valves, and turbine bypass valves control the steam dome pressure.

- Dry steam is generated within steam separators and dryers.
- A separate steam bypass line is dedicated to discarding the steam flow directly to the condenser.

Advantages of the BWR compared to the PWR are:

- Substantially lower operating pressure in the reactor vessel (about 7 MPa) compared to a PWR (about 15 MPa).
- The fuel operates at a lower temperature.
- Steam generators and pressurizers are eliminated.
- The risk of embrittlement is reduced, and the operational lifespan of the pressure vessel is prolonged due to the less irradiation exposure resulting from the greater distance between the core and the vessel walls.

Disadvantages of a BWR are:

- Two-phase flow conditions in the boiling region of the core require more complex thermal-hydraulic calculations.
- BWR system needs a larger reactor pressure vessel.
- Radiation exposure risk in the vicinity of the main steam line and turbines might require shielding.

2.4.7 Nuclear Power Plants Around the World

Currently, several countries are installing or planning to install nuclear power plants. According to a report published by the International Atomic Energy Agency (IAEA)

as of December 2021, there are 56 ongoing reactor projects in different phases of construction and installation. The report also states that there are 437 active nuclear reactors across the globe having a total rated capacity of 389,5 GW(e). With the commissioning of 6 new reactors, the total capacity is increased by approximately 5200 MW(e) in the year 2021. By the end of these projects, it is predicted that the total rated nuclear energy production capacity all around the world would be 444,7 GW(e) an increase of almost 14.91%. There are also 70 reactors in the planning or approval phase as well as 56 under construction [7]. Popularity differences among various designs of power plants will be clearer when these figures are analyzed more deeply. The majority of the current reactors are Generation II models which began operation in the late 1960s. The report also shows that the Pressurized Water Reactors (PWR) comprise the largest group of 303 reactors with a total rated capacity of 299,2GW(e) while the second most preferred design Boiling Water Reactors (BWR) consists of 61 reactors with 61849 MW(e) capacity [7].

2.5 Nuclear Reactor Safety

Nuclear power plants benefit from the energy arising from the fission reaction of radioactive elements. Due to their fragile nature and potential risks, nuclear-related processes and materials should be handled, monitored, and controlled responsibly. Thus, nuclear reactors require reliable materials and technological instruments for safe and sustainable operation. However, combining various mechanical, electrical, thermal, hydraulic, and optic components creates highly sophisticated and delicate systems. Regardless of how robust and reliable these systems are, various irregularities in the rector's behavior may arise in expected and unexpected circumstances. The

goal of Safety Analysis is to demonstrate using computational methods that the design meets all safety requirements for a wide range of postulated failures or events.

At a nuclear power plant, events can be identified and classified into categories primarily based on the frequency of the occurrence [3].

- Normal Operation
- Anticipated Operational Occurrences
- Design Basis Accidents
- Beyond Design Basis Accidents

According to IAEA "the protection of employees, the public, and the environment from the harmful radiological effects that the nuclear facilities can cause could be ensured by establishing the highest safety standards." [5].
Measures to achieve the highest standards of safety are summarized as:

- To restrict the radiation exposure of workers and the public and the dispersion of radioactive material to the environment.
- To reduce the possibility of events that could cause a loss of control over a nuclear reactor core, fission chain reaction, radioactive material, depleted radioactive fuel, or nuclear waste.
- To minimize the impacts of such events in case they were to happen. The fundamental safety objective is the backbone of the safety requirements, and it applies to all phases of design, construction, commissioning, licensing, operation, decommissioning, and nuclear waste management.

2.5.1 Defence in Depth Concept

Nuclear power plants must be equipped with adequate safety systems and procedures to ensure their safe operation. One of the most significant concepts in plant safety is the Defence-in-Depth Method. This concept's application extends to all safety-related activities. It encompasses organizational, behavioral, and design aspects across various operational states. This comprehensive approach ensures that all safety-related activities have multiple independent layers of provisions. If a failure occurs at one level of protection or barrier, subsequent levels or barriers are in place to provide continued safety assurance [25].

There are five levels of defense:

- First Level: to avert any deviations from standard operation and to prevent malfunctions of safety-critical components.
- Second Level: to detect and control deviations from standard operational conditions before they escalate to accident conditions.
- Third Level: To equip the plant with inherent and/or engineered safety features that are capable of preventing damage and returning the plant to a safe state.
- Fourth Level: To prevent accident progression.
- Fifth Level: To reduce the potential radiologic impact of radioactive discharges.

2.5.2 Safety Assessment Methods

Adequacy of the safety barriers to minimize the amount of radioactive material released while maintaining their integrity is demonstrated by the means of a range of

varied quantitative studies for assessing and addressing potential safety risks using both deterministic and probabilistic methodologies [4].

The safety analysis is required to ensure that the defense-in-depth approach has been integrated into the plant's design. It must demonstrate that the nuclear power plant can comply with acceptable limits on radioactive releases and adhere to the dose limits across all operational states, as well as maintain acceptable limits during accident scenarios.

Providing satisfactory answers and supporting materials for this fundamental safety discipline may require calculations, measurements, and simulations which are demanding in terms of time, funding, and manpower. Computer technologies play a crucial role in conducting detailed calculations and simulations. Computer codes are valuable pieces of nuclear analysts' tool sets for the assessment of various operating and accident conditions. The results obtained from these studies help scientists and operators to predict the system behavior under real and anticipated reactor conditions [50].

According to the IAEA [6], the nuclear analysis codes can be categorized according to discipline as:

- Fuel Behavior Codes
- Reactor Kinetic Codes
- Thermal-Hydraulics Codes
- Containment Analysis Codes
- Atmospheric Dispersion and Dosimetry Codes
- Structural Analysis Codes

2.5.3 Thermal Hydraulics Analysis Codes

Nuclear power plants are rather complex and heterogeneous systems. Therefore, understanding of their operation and potential accidents requires sophisticated physical and mathematical models. The heat and fluid transfer processes within the reactor core are particularly intricate, necessitating computer codes that can accurately simulate both local and system-wide behavior under normal, transient, and accident conditions. The complexity of these systems underscores the importance of rigorous modeling and testing to ensure safe and reliable operation. To ensure that these codes are functioning correctly, they are regularly assessed using experimental data in a process known as code validation. The validation of these codes for complex reactor designs and for such a wide range of potential transients makes the validation costly, with a strict level of Quality Assurance applied at each stage of the process.

While many codes were originally designed with one-dimensional models of the reactor vessel and piping, two and three-dimensional representations of the vessel and coolant system structures are now also commonly utilized. Thermal-hydraulic codes are usually not tailored to specific designs and can be utilized across a range of conditions. Several of the thermal-hydraulic codes for systems have been expanded by incorporating severe accident models, which enables them to handle diverse accident scenarios, ranging from transients and design basis accidents to beyond design basis and severe accident transients.

Some of the most developed and widely accepted code examples are TRAC (Transient Reactor Analysis Code), TRACE (TRAC/RELAP Advanced Computational Engine), RETRAN (Reactor Transient Analysis), SNAP (Symbolic Nuclear Analysis Package), and RELAP (Reactor Excursion and Leak Analysis Program) [6].

2.5.4 Reactor Excursion and Leak Analysis Program

Within the context of this work, we will be employing the RELAP5 code to investigate the steady state and transient conditions in a BWR reactor. RELAP5/Mod3.4 is a thermal-hydraulics analysis code used for simulating the response of a thermal-hydraulic system of a nuclear power plant under steady and transient operating conditions. The code is designed to predict system behavior by analyzing two-phase flow conditions based on six phasic equations: two mass conservation equations, two momentum conservation equations, and two energy conservation equations [24].

The code was originally developed by the United States Nuclear Regulatory Commission (NRC) at the Idaho National Engineering Laboratory (INEL) in 1979 [6]. It serves various purposes, including rulemaking, licensing audits, assessing operator guidelines, and forming the foundation for a nuclear plant analyzer. RELAP5 is a versatile and generic program capable of not only calculating the behavior of a reactor coolant system during transients but also simulating a wide range of hydraulic and thermal events in both nuclear and non-nuclear systems. This includes scenarios involving mixtures of steam, water, noncondensable gases, and solute substances.

Because of its extensive modeling capabilities, it is employed in a broad range of PWR, BWR, and PHWR analyses. Some of the application areas are operational transients, loss of coolant, loss of feedwater, station blackout, turbine trip, etc. Due to the extensive open literature related to the code and applications, code has a wide basis of users ranging from world-class thermal-hydraulics experts to novice users with limited experience in the field of thermal-hydraulic phenomena.

3

Literature Review

In this section, we present analysis methods and results from some of the most significant research conducted to identify the reactor behavior during turbine trip transient. While the turbine trip transients encompass a broad area of interest, our primary focus encompasses the thermal-hydraulic perspective. It is important to note that other turbine trip analyses utilizing different thermal-hydraulic analysis software packages are also investigated, but they are not presented in this section.

3.1 Peach Bottom Turbine Trip Benchmark

Advancements in hardware and software technologies provided both academia and industry with strong computation tools. Especially the thermal-hydraulics analysis codes have been improved significantly since the earliest examples. However, improvements in this field brought the need for verification and validation of the codes for their intended applications. There have been considerable efforts to establish benchmark projects for examining the capabilities of coupled codes. The Peach Bottom Turbine Trip Test (PBTT2) Benchmark by NEA is a significant example of many other benchmarking projects. The importance of this benchmark for this thesis is

that it constitutes outlines of the analyses conducted. Especially during the formulation of the best estimate case the event sequences and boundary conditions provided in the benchmark have been adopted accordingly for this thesis.

Turbine trip transient is selected purposefully for the benchmark since it is a dynamically complex event with rapidly changing reactor operating variables. Experts decided that such a scenario would comprise a good challenge for coupled codes on both neutronic/thermal-hydraulic coupling and core/plant system coupling. BWR turbine trips typically involve a surge of cold water into the core thereby elevating reactivity via moderator feedback and void collapse phenomena. The increase in reactivity/power leads to changes in fuel temperature as well as many other thermal-hydraulic parameters.

Peach Bottom Atomic Power Station Unit 2 utilizes General Electric BWR/4 design reactors. It has a rated thermal power output of 3,293 MW, a rated core flow of 12915 kg/s, a rated steam flow of 1685 kg/s, and a turbine inlet pressure of 6.65 MPa [8]. In April 1977 three tests were conducted in Unit 2 at the End of Cycle 2 at different reactor power levels. The results from the second test were selected to establish the benchmark since it has the highest quality measured dataset [28].

Three main exercises are suggested in the benchmark for a complete and accurate representation of the real plant conditions in the digital domain. The objective of the first exercise is to assess the response of the thermal-hydraulic system and initialize the participants' system models for the second and third exercises involving coupled 3-D kinetics/system thermal-hydraulics simulations. The second exercise involves conducting coupled-core boundary conditions calculations to test and initiate

the participants' core models, using the provided core inlet pressure, core exit pressure, core inlet temperature, and core inlet flow as thermal-hydraulic core boundary conditions. Exercise three, involves the best estimate of coupled 3D core/thermal-hydraulic system modeling, combining elements of the first two exercises to analyze the transient in its entirety [41].

3.2 Related Work

In 2002 Salah and D'Auria from the University of Pisa conducted a series of studies to evaluate the capabilities of RELAP5/Mod3.2 [12]. In this work, the first exercise in the PBTT2 Benchmark is conducted. This way the thermal-hydraulic coolant system response is tested by fixing the time-dependent reactor power input data. In the structure of the model, the core region is modeled as two separate regions, namely the active zone (representing the fuel assembly region) and the non-active zone (representing the core bypass line). The core fuel rods are lumped into one homogenized component which is axially divided into 26 meshes. While the first and last meshes are dedicated to the non-active zone, the remaining 24 meshes comprise the active core height. Meanwhile, only one steam line and 2 jet pumps are modeled. Apart from these, researchers adjusted some singular pressure coefficient losses to match the inlet core coolant flow rate in the report. The steady-state initialization of the model took 200 seconds. During this period most of the thermal-hydraulic parameters achieved stable trends. Comparison between experimental data and results showed good agreement. The transient was rapid (5 seconds) in comparison to steady state calculation. Overall, results achieved very similar trends with experimental data. Some of the key parameters highlighted in the report are predicted well. However,

the pressure response in the vessel to the valve closure is calculated to be occurring 0.1 second later than the actual measured pressure response of the plant. According to the authors, the reason for this delay is the accuracy of the plant dimensions. A series of sensitivity analyses are conducted to identify the influence of the key transient parameters on the test conditions. Uncertainties regarding the vessel steam dome volume and the steam bypass valve flow area are particularly investigated. Tuning these parameters 120 to 80% of their reference value revealed that the transient behaviour is particularly sensitive to these assumptions. [12].

In 2004 researchers from the University of Pisa and the Pennsylvania State University tested RELAP5/Mod3.3/PARCS/2.3 coupled code against the PBTT2 Benchmark [14]. The use of a coupling mechanism allowed the team to use data from both codes simultaneously. The generated data from each code supported the calculation procedure of the other code. PARCS/2.3 used the values from the thermal-hydraulic system as input to predict the time-dependent core power distribution. Similarly, RELAP5/Mod3.3 takes this power profile into account to simulate the thermal-hydraulic behavior of the system. This coordination between codes is established through a parallel virtual machine (PVM) method.

The numerical simulation of the experiment is performed systematically in three steps:

- Running RELAP5 in stand-alone mode to reach a steady state.
- Running coupled codes for steady-state calculation
- Running coupled codes for transient calculation

Since the steady state calculation was performed in the previous study [12], the

group proceeded with the remaining steps. The coupled steady state calculation shows that the axial void profile, an axial profile of fuel temperature, and an average axial power profile follow the same trend as the experimental data. It is noted that the axial distribution of calculated power is underestimated the peak power point. The transient calculations reasonably predicted the amplitude of the pressure wave and the trend of the increase in pressure in response to the water hammer effect caused by sudden TSV closure. However, the time response is calculated with a 0.1 second error. The reason for this mismatch is attributed to the dimensions of the coolant flow path model. Also, the rate of increase of the power response at the beginning of the excursion phase was found to be faster than the calculated value. Due to the lack of measured data on void and fuel temperature, only two possible causes for this discrepancy are mentioned:

- Underestimated prompt positive feedback effects during the excursion phase.
- Underestimated prompt negative feedback effects.

Three major issues that could cause the shift from the experimental results are;

- Insufficient code capability
- Inaccuracy of cross-section table
- Lack of prompt feedback mechanisms in coupled codes.

The team conducted a series of sensitivity analyses to qualify the disparity related to feedback modeling. The turbine trip without scram is selected as a base case since the prediction of self-limiting power behavior is the primary concern. Three cases were evaluated along with the base case. Results show that self-limiting power behavior

is simply because of the delayed feedback mechanisms. On the other hand, prompt feedback effects are responsible for the experimental power quenching [14].

Based on the model built in this study Bousbia-Salah and D'Auria conducted another extensive sensitivity analysis covering 10 sensitive cases including the base case [13]. By the means of sensitive cases, the positive and negative prompt and delayed feedback responses are evaluated. Findings from this study support the arguments generated in previous work. In terms of suggestions for achieving better results, the team encourages the use of finer cross-section tables, better representation of prompt void feedback, and the impact of the valve action/timing on local parameters.

In 2005 a research team from the University of Pisa published an article about RELAP5/Mod3.3/PARCS/2.4 coupled code assessment against the PBTT2 benchmark [15]. Special attention was paid to the nodalization of the steam line considering the importance of the pressure wave propagation on the kinetic and thermal-hydraulic feedback mechanisms. The travel of the shock wave along the steam dome and core area was compared against the experimental data. The pressure response of the system was found to be in good agreement with measured values. However, the code predicted the power response earlier and higher in comparison to the benchmark. The decreasing period of the exponentially rising power shows possible uncertainties in kinetics feedback or thermal-hydraulic parameters which affect the void calculations. Sensitivity analyses are divided into two groups. The first group focuses on the code capability of predicting pressure wave dynamics. The second group considers the effect of the cross-section data on feedback mechanisms. In sensitivity analyses, the team investigated how the different opening and closure times of the TSV and BPV influence the pressure response of the system. This is found to be especially

important since there is an information gap in terms of valve characteristics. The closure time of TSV is adjusted by plus and minus 20%. The resultant power peak and amplitude of the pressure wave variation remained within the acceptable limit (2%). Likewise, node sizes smaller than 2.0 meters were found not to be affecting the pressure wave amplitude significantly. On the other hand, during the excursion phase, the power response does not match the experimental results. This is mainly linked to inadequate cross-section and void fraction modeling. It is stated that disparity occurs due to the non-linear dependence of the cross-section modeling concerning moderator density. Additionally, the void correlation of the RELAP5 is compared against Bestion's (1990) and Koncar-Mavko's (2003) equations. Findings suggest that better void correlations can help to improve the prediction of the power response [15].

Although in the above works, we mainly focused on the application of RELAP5 on the Peach Bottom Turbine Trip 2 Benchmark, several other participants made contributions to the benchmarking activities. Findings from each work were compared on code-to-data and code-to-code basis. Results were summarized and published following Exercise 1, Exercise 2, and Exercise 3 respectively.

The PBTT2 Benchmark Exercise 1 is aimed at evaluating thermal-hydraulic system models. In total 14 organizations from multiple countries using different codes contributed. The participants analyzed the thermal-hydraulic parameters during the steady-state and turbine trip transient, finding the results largely consistent with reference solutions, despite model complexities. The exercise also provided an opportunity for sensitivity studies on various modeling issues, helping participants to understand the effects of different thermal-hydraulic models and identify critical parameters for accurate turbine trip modeling. In conclusion, Exercise 1 successfully

helped participants initialize and test, the thermal-hydraulic system models, serving as a valuable platform for improving reactor simulations [8].

The second exercise centered on coupled-core boundary condition calculations, with the aim of testing and initiating participants' core models. The benchmark team provided a cross-section library to participant organizations, removing uncertainties arising from various cross-section generation and modeling processes. Key thermal-hydraulic boundary conditions were also provided by the benchmark team. With 18 organizations from 9 countries participating, the results were used for code-to-code comparisons and further statistical analysis. This analysis revealed several sources of modeling uncertainties, including factors like core pressure drop, void feedback model, time step size, and fuel heat transfer parameters among others [29].

The third exercise aimed at building and verifying the thermal-hydraulic system model, the coupled core model, and the integrated core/system model, involving a 3D kinetics/thermal-hydraulics analysis for the reactor core and a 1D evaluation for the rest of the plant components. Five scenarios were simulated to evaluate the coupling and feedback modeling. Results from fourteen participants from eight countries were used for code-to-data and code-to-code comparisons. Despite some limitations and uncertainties, the findings indicated good agreement in integral parameters, core-averaged axial distributions, and time histories. Accurate prediction of radial power distribution, however, hinged heavily on the number of thermal-hydraulic channels and the mapping scheme, with the void fraction modeling also posing challenges. The study concluded that further research is needed for precise predictions of void fraction by core thermal-hydraulics models [30].

3.3 Uncertainty and Sensitivity Analysis

Some thermal-hydraulic codes incorporate physical models that have been intentionally biased in a pessimistic direction to provide "conservative" safety predictions. In cases where best estimate codes are used for licensing analysis, a pessimistic bias may be introduced by utilizing conservative input data, particularly for parameters that significantly impact the results [26]. During the review of licensing analysis, regulators often seek to determine the degree of a margin between the presented results of accident analysis and any significant changes that might occur in those results if conditions were to vary suddenly (known as the 'cliff edge' effect). To measure these margins, the uncertainty analysis is employed. Overly conservative approaches may occasionally hide safety concerns by ignoring significant physical phenomena (i.e., transients become non-physical and hence cannot be judged against actual plant responses). However, uncertainty analysis can help gauge the level of uncertainty in safety margins and provide assurance about their adequacy. This can help regulatory decision-making, particularly for low-probability events within the scope of the design basis.

There are three major sources of uncertainty in accident analysis: Code or Model Uncertainty, Representation or Simulation Uncertainty, and Plant Uncertainty [26].

Model Uncertainty: The uncertainty involved in modeling and correlations, the solution methodology, model choices, unmodeled processes, data libraries, and inadequacies of the computer software are some of the factors that contribute to uncertainty.

Simulation Uncertainty: The inability to model complex geometries with accuracy, as well as three-dimensional effects, scaling, control, and system simplifications, can introduce uncertainty into the representation or idealization of the actual plant.
Plant Uncertainty: Measuring or monitoring a real plant can introduce uncertainty due to factors such as reference plant parameters, measuring instrument error, instrument response time, and reference data set points.

- Identification and ranking
- Determining the span of the uncertainty
- Sensitivity analysis
- Calculating the combined uncertainty

The various individual uncertainty components must be identified and combined to determine an overall uncertainty in each parameter, then compared with an acceptance criterion. However, because of the complexity of the system analysis codes and the large number of individual uncertainties involved, this can quickly become unmanageable without simplifying assumptions. As a result, many approaches rely on expert judgment to reduce the computational burden and save time.

Computer codes are employed for demonstration of the behavior of nuclear power plants under hypothetical scenarios. Essentially, the codes are mathematical algorithms representing the dynamics of the real physical world and substances. Despite the advancements in science and computer technology, many physical phenomena are yet to be completely discovered. Besides, during the process of creating computer codes and plant models, some of the data might be uncertain. Altogether these

uncertainties constitute of a certain inaccuracy for the computer code and system model. From a safety point of view dependency of the results to these inadequacies must be considered during the evaluation and decision-making process. Sensitivity analysis is a method for describing the level of dependency of any output value on uncertain input parameters. Sensitivity analysis is valuable for decision-making because it provides insights into the robustness and reliability of models and identifies critical factors affecting the results.

Before starting the sensitivity analyses, we investigated the methods applied for the BEMUSE (Best Estimate Methods, Uncertainty, and Sensitivity Evaluation) program [35], [36]. BEMUSE program is a benchmarking project aiming to create a database for the uncertainty aspect of the best estimate analysis of the large break loss of coolant accident (LBLOCA) of the pressurized water reactors. While the accident and reactor design is different than that studied in this thesis, it is a good example of an investigation of code uncertainty and sensitivity.

The program has been conducted in two sections each consisting of three phases. While for the first section, participants evaluated the large break loss of fluid test (LOFT) circuit, in the second section ZION PWR has been analyzed. Some of the sensitivity analysis parameters that were specified in the publications for Phase 2 and Phase 4 were adopted for this thesis. Although the program was conducted mainly for PWR reactors, publications are rather helpful in developing an understanding and methodology towards sensitivity assessment discipline.

4

Methodology

4.1 Theory

The urge to control the ambient conditions has its roots in the genes of species. Throughout history, mankind fed this urge with discoveries. Starting from ancient times improvements in critical and analytical thinking paved the way to a better understanding of heat transfer and fluid mechanics. Studies revealed that the ancient Egyptians developed significant skills and expertise in the use of thermodynamic principles well beyond keeping themselves warm and cooking food. According to a study, Egyptian masters created air-conditioned temples and palaces [43].

In the early days of modern technology, thermodynamics gained more importance as a field of study involving the dynamics of heat transfer and fluid mechanics. Today, thermodynamics continues to be an essential part of new applications and technologies from nano-technology resistors to large-scale nuclear power plants. Engineers and scientists are pushing the boundaries of the possibility of achieving higher performance and efficiency.

Safety is also another major consideration for nuclear power plants. Constant

cooling of the hot fuel in the core has the utmost importance for the integrity of the system. At high temperature and pressure conditions disturbances or failures in the components may result in a lack of cooling and even radiological release. For a better representation of the boiling water reactor systems and the transients acting on them, the introduction of the fundamental thermal-hydraulic analysis methods might be beneficial.

4.1.1 Fundamentals of Thermal-Hydraulic Analysis

Starting from the 18th century the scientific ground of heat transfer began emerging. Until it was proven to be wrong by Benjamin Thompson (1753-1814) the "caloric" theory of Antoine Lavoisier (1743-1794) was a highly common perception about heat transfer. Thompson challenged the validity of Lavoisier's theory explaining how heat could be generated through work[18]. In the same years, Joseph Fourier (1768-1830) established the principles of continuum mechanics in his article about the conduction of heat in solids (Fourier's Law). Another crucial contribution was made by James Clerk Maxwell (1831-1879) by declaring the heat as a mode of motion. In his study, Maxwell explained how energy is transferred between touching gas molecules. Following the discipline established by the pioneers, numerous scientists such as Bragg, Nusselt, Reynolds, and Prandtl created works representing the milestones of heat transfer studies.

In his ground-breaking work "The Analytical Theory of Heat" Fourier explained the principles of heat conduction, which states that the rate of heat transfer through a material is proportional to the negative gradient of the temperature and thermal conductivity of the material. He mathematically expressed this approach in the following

formula:

$$\dot{Q}_{\text{cond}} = -kA\frac{dT}{dx} \tag{4.1.1}$$

In this formula, dT/dx is the temperature gradient representing the slope of the temperature curve. Therefore, this gradient declares that heat conduction in a certain direction is directly linked to the temperature gradient in the same direction. While A is the area perpendicular to the direction of conduction, a negative sign ensures that the conduction has a positive value in a positive direction. Constant k is a material property describing the ability to conduct heat.

Convection is the transmission of energy between a solid boundary and nearby mobile fluid (gas or liquid) particles. Sir Isaac Newton is credited with the Law of Cooling, which determines the rate at which heat is transferred from a hot surface to a cooler surrounding fluid.

$$\dot{Q}_{\text{conv}} = hA_s\left(T_s - T_\infty\right) \tag{4.1.2}$$

According to Newton's Law of Cooling, the rate of heat transfer through convection is proportional to the difference between surface temperature and fluid temperature. Unlike the conduction coefficient k, the convection coefficient is not a property of the material, instead, it is an experimentally determined value. Should the movement of the fluid over a surface be induced externally by a fan, pump, or wind, convection is referred to as "Forced Convection". The increased number of fluid particles touching the surface also increases the heat transfer rate. In the case of fluid motion driven

by buoyancy forces that arise from variations in fluid density resulting from temperature differences within the fluid the mode of convection is referred as to "Natural Convection". This type of heat transfer is deliberately employed as a passive safety system in certain types of reactors as a backup plan in case of loss of pumping force.

Thermal radiation is a unique mode of heat transfer occurring through electromagnetic waves emitted by bodies due to their temperature. This sets it apart from other forms of electromagnetic radiation types, such as X-rays, gamma-rays, microwaves, and radio waves because these are not associated with the body's temperature. All objects release and absorb thermal radiation based on factors like surface properties, body temperature, and the surrounding environment. However, the Stefan-Boltzman Law constrains the maximum rate at which a surface can emit radiation.

$$\dot{Q}_{\text{emit, max}} = \sigma A_s T_s^4 \tag{4.1.3}$$

In this equation, T_s determines the surface temperature while A_s represents the surface area. Another major element of this formula is the Stefan-Boltzman coefficient:

$$\sigma = 5.670 \times 10^{-8}\ \text{W/m}^2 \cdot \text{K}^4 \tag{4.1.4}$$

Internal forced convection is one of the most employed heat removal solutions in engineering systems. It refers to the process of transferring heat from or to a fluid flowing through a confined space, like a pipe or duct. The driving force behind the flow is created by mechanical accelerators like pumps or fans. The movement of the particles has an increasing effect on the heat transfer rate from the surface. The absence of a free surface on the fluid is the distinguishing feature of internal flow from

the free stream. This feature is important when explaining boundary layer theory.

Similar to the flow velocity, there are several other important factors governing the convection in forced flow conditions, including fluid properties, flow regime, geometry and surface characteristics, and temperature differences. Despite the fact that many subjects in the fluid flow area are well explained, for most of the cases the empirical relations and experimental data plays important role in the solution process. In these solution methods, dimensionless numbers such as Nusselt number, Reynolds number, and Prandtl number are significantly important.

Fluids with lower flow velocity or higher viscosity often move in a regular and stable manner. Fluid particles slide on top of each other in parallel layers. This smooth, regular, and orderly movement of fluid particles with minimal mixing between the layers is called laminar flow.

$$\mathrm{Re} = \frac{V_{\mathrm{avg}} D}{v} \tag{4.1.5}$$

Osborne Reynolds proposed a dimensionless number (Re) (ratio of inertial forces to viscous forces) which can be used to determine the flow regime. In the formula above the v represents the kinematic viscosity of the fluid, V_{avg} is the average velocity of the fluid in the pipe, and D is the diameter of the pipe. For the Re values lower than 2300 flow regime is considered to be laminar.

In the thermal-hydraulic system determination of the pressure drop and heat transfer rate along the piping system is vitally important for performance and safety. Julieus Weisbach developed a relation based on the Bernoulli principle to determine

the pressure drop as a function of the pipe diameter, material type, and fluid velocity.

$$\Delta P_L = f\frac{L}{D}\frac{\rho V_{\text{avg}}^2}{2} \tag{4.1.6}$$

Accurate description of pressure loss and heat transfer rate strongly related to the determination of frictional losses f. In fully developed laminar flow, the friction factor is solely dependent on the Re number.

$$f = \frac{64}{Re} \tag{4.1.7}$$

For convection rate analysis on fully developed laminar flow in circular tubes Nusselt number (Nu) related to the temperature profile should be evaluated. This is done by investigating the energy balance of a differential volume in the system. Under a load of constant surface heat flux conditions, the Nu number regarding the fully developed laminar flow in a circular pipe is constant and independent of Re and Pr.

$$Nu_D \equiv \frac{hD}{k} = 4.36 \tag{4.1.8}$$

Similarly, the Nu number for a fully developed laminar flow in a circular pipe subjected to a constant surface temperature is constant.

$$Nu_D = 3.66 \tag{4.1.9}$$

Cengel suggests the use of constant heat flux over constant surface temperature conditions. The fact that the Nu number for the latter is 16% lower shows laminar flow is more sensitive to the constant heat addition through the pipe walls. On the

other hand, the fully developed turbulent flow shows no significant change with the varying surface thermal boundary conditions.

Unlike the laminar flow, the turbulent flow is known for its chaotic and irregular nature. Due to the higher heat transfer coefficients comes along with the mixing action inside the flow. In literature turbulent flow its seen that turbulent flow occurs when Re is greater than 4000. However, to reach a fully turbulent flow regime Re number must extend beyond 10,000 [17].

Panton [38] draws the outline of the characteristics of turbulent flow as: turbulent flows have irregular fluctuations of velocity in all three dimensions, and a gradient in the mean velocity must exist for turbulence to be self-sustaining. The irregularities in velocity in turbulent flows have spatial structures called eddies, which exist at many scales. Eddies transport momentum, heat, and mass from low to high velocity, temperature, and concentration. The energy can be transferred from large to small eddies and ultimately dissipated by viscosity.

In the beginning of the 20th century, a group of scholars made an effort to use Prandtl's boundary layer theory to analytically predict the friction factor. Colebrook and White (1939) proposed an equation that can predict the friction factor for the Re values within the transition region. This equation was combining the formulas developed by Prandtl and Nikuradse [49].

$$\frac{1}{\sqrt{f}} = -2\log_{10}\left[\frac{\varepsilon/D}{3.70} + \frac{2.51}{\mathrm{Re}\sqrt{f}}\right] \tag{4.1.10}$$

In 1944 Lewis Ferry Moody plotted a diagram today known as Moody's diagram to be used in combination with the Colebrook and White equation to determine the friction factor.

Turbulence is often responsible for increased drag and enhanced heat transfer rate over or inside solid surfaces. Hence, this type of flow regime is often employed in various engineering applications. For the turbulent flow conditions, the Nu number does not react to the changes in the thermal conditions on the surface of the pipe. Therefore, the determined Nu number can be used interchangeably between constant heat flux and temperature loads.

For fully developed turbulent flow in a smooth pipe, the Dittus–Boelter equation may be employed to obtain the Nu number.

$$\mathrm{Nu} = 0.023\,\mathrm{Re}^{0.8}\,\mathrm{Pr}^{n} \qquad \begin{pmatrix} 0.7 \leq \mathrm{Pr} \leq 160 \\ \mathrm{Re} > 10,000 \end{pmatrix} \tag{4.1.11}$$

When dealing with flow cases characterized by large variations in fluid properties Sieder and Tate equation can be employed within the application range.

$$Nu_D = 0.027\,\mathrm{Re}_D^{\frac{4}{5}}\,\mathrm{Pr}^{\frac{1}{3}}\left(\frac{\mu_b}{\mu_s}\right)^{0.14} \qquad \begin{bmatrix} 0.7 \leq \mathrm{Pr} \leq 16,700 \\ \mathrm{Re}_D \geq 10,000 \end{bmatrix} \tag{4.1.12}$$

Preceding equations are widely accepted for educational and professional purposes due to their simplicity and wide range of applications. However, for upper-level applications, the accuracy provided by the above formulas may show deviations around 25%. When higher accuracy equations were needed, several more accurate (error reduced to around 10%) but also complex equations were developed by different contributors. The Second Petukhov equation (also known as the Petukhov-Popov equation) is a significant example of improved correlations. It is an extension of Gnielinski's equation and includes a correction factor to account for the effect of the pipe length

for thermally developing flow.

$$\mathrm{Nu} = \frac{(f/8)\,\mathrm{Re}\,\mathrm{Pr}}{1.07 + 12.7(f/8)^{0.5}\left(\mathrm{Pr}^{2/3} - 1\right)} \quad \left[\begin{array}{l} 0.5 \leq \mathrm{Pr} \leq 2000 \\ 10^4 < \mathrm{Re} < 5 \times 10^6 \end{array}\right] \tag{4.1.13}$$

For the applications with fluids at relatively lower Re number Piotr Gnielinski's empirical equation may be a better option. This equation is particularly applied to the heat exchanger and cooling systems.

$$\mathrm{Nu} = \frac{(f/8)(\mathrm{Re} - 1000)\,\mathrm{Pr}}{1 + 12.7(f/8)^{0.5}\left(\mathrm{Pr}^{2/3} - 1\right)} \quad \left[\begin{array}{l} 0.5 \leq \mathrm{Pr} \leq 2000 \\ 3 \times 10^3 < \mathrm{Re} < 5 \times 10^6 \end{array}\right] \tag{4.1.14}$$

4.1.2 Boundary Layer Theory

Investigation of the flow behavior and heat transfer on a smaller scale is an important subject. Because the heat convection dynamics and fluid velocity profile may differ downstream due to the changes in the properties of fluid and surface in both the radial and axial direction. For analysis of the flow, a no-slip condition is assumed for the sake of simplicity. According to this approach, the fluid particles adjacent to the wall are considered to be stationary. Fluid molecules that come to a complete stop on the surface slow the adjacent fluid particles as well. This interaction occurs because the viscous forces are dominant in the zone near the wall. These relatively slow particles constitute the boundary layer. The development boundary layer in a pipe is graphically represented in Figure 4.1.

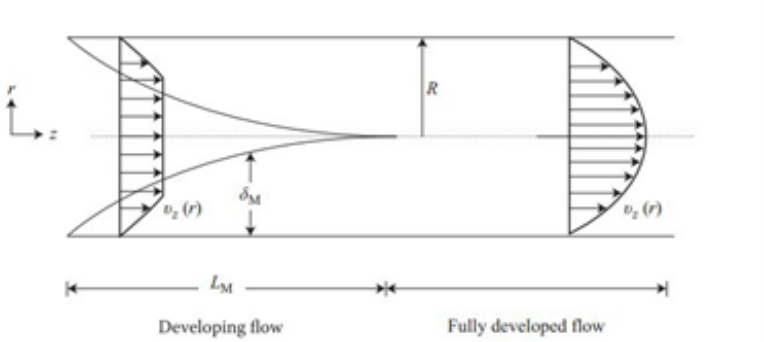

Figure 4.1: Development of the liquid boundary layer adopted from [10]

This approach suggested by Prandtl in 1904 allows the fluid flow separation in two regions as boundary layer and irrotational flow region. He also developed a dimensionless number for determining the relative thickness of the thermal or velocity boundary layer.

$$\mathrm{Pr} = \frac{\text{momentum diffusivity}}{\text{thermal diffusivity}} = \frac{\nu}{\alpha} = \frac{C_p \mu}{k} \tag{4.1.15}$$

In external flow the boundary layer can infinitely grow downstream; however, in internal flow conditions, growing boundary layers from adjacent walls ultimately meet in the middle and cover the entire flow area. After this point the flow is said to be fully developed and the velocity profile does not change in the flow direction.

Similar to the boundary layer in fluid mechanics, another notion is also needed for the analysis of the forced convection with a thermal consideration. Thermal boundary layer theory explains how the temperature difference between the fluid and pipe surface creates a temperature gradient and hence a convection path inside the pipe. Figure 4.2 provides a graphical demonstration of this behavior.

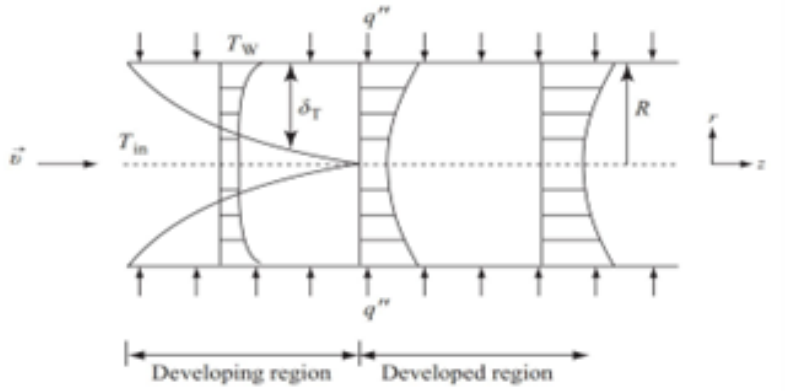

Figure 4.2: Development of the thermal boundary layer adopted from [10]

The thickness of the thermal boundary layer gradually increases downstream until it occupies the whole flow area. This state is considered to be a thermally steady state. Starting from this point the flow is considered to be thermally fully developed. In fully developed flow analysis dimensionless numbers such as Re, Pr, and Nu play an important role.

4.1.3 Fundamentals of Boiling

Boiling and condensation are essential in heat transfer in different engineering applications. A comprehensive understanding of these processes and categorizing them according to temperature conditions and fluid motion enables engineers to enhance thermal performance. Within the context of this text, we will pay special attention to boiling.

Boiling is a convection process that transfers heat from or to a solid surface. Boiling is known for corresponding high heat transfer coefficients due to latent heat and buoyancy-driven flow mechanisms. An essential part and physical sign of the boiling process is bubble nucleation and growth.

Bubbles act as energy carriers, transferring heat from the hot surface to the liquid body as they absorb heat from the surface and release it into the liquid. The temperature difference between the vapor inside a bubble and the surrounding liquid is what drives the heat transfer between the two phases. The growth and behavior of vapor bubbles have a strong impact on liquid motion near the surface, and thus strongly influence the heat transfer coefficient. Therefore, for the thermal-hydraulic system optimization, analysis of the dynamics of bubbles and their effect on heat transfer coefficients is a requirement.

Boiling is classified into two types -pool boiling and flow boiling- based on the presence of bulk fluid motion. Based on the bulk liquid temperature, pool, and flow boiling are further classified as subcooled boiling or saturated boiling.

During the pool boiling the fluid body is in a stationary position and there it is not forced to by the means of external devices. This type of boiling is known for the natural movement of liquid and vapor bubbles under buoyancy forces. Since bubbles (vapor bubbles) are essential features of boiling, their dynamics of should be investigated comprehensively.

Boiling can occur through homogeneous or heterogeneous nucleation. For homogeneous nucleation, a group of liquid molecules with sufficiently high energy come together to create a vapor nucleus. Naturally occurring embryo vapor bubbles are mostly in molecular size, so the difference between the liquid temperature and the saturation temperature must be very high for homogeneous nucleation to occur. Thus, it only takes place in the event of rapid depressurization or when the liquid temperature is significantly above the saturation temperature.

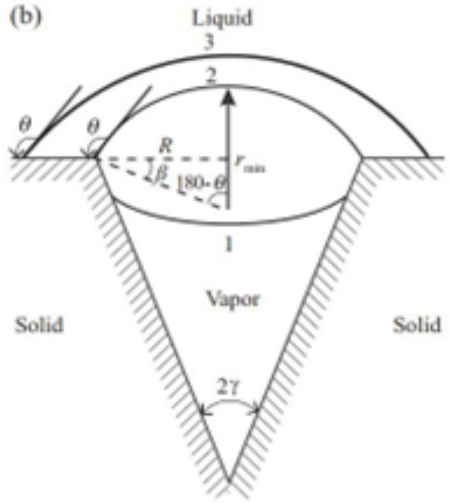

Figure 4.3: Schematic representation of bubble nucleation site adopted from [10]

As shown in Figure 4.3 the surface pits, cavities, and irregularities can provide locations for inhomogeneous nucleation of bubbles. The microcavities that can serve as nucleation sites must be able to trap and retain vapor when the surface is flooded. Whether a cavity fills with liquid depends on factors such as the contact angle, geometry, and relative temperatures of the liquid interface and cavity surface.

The boiling process at the surface can commence if the coolant temperature near the surface is high enough for the pre-existing vapor at the cavity site to attain sufficient pressure to initiate the growth of a vapor bubble at that location. Upon the completion of the nucleation phase, the bubble tends to rise and join the fluid. This process is controlled by the combination of the inertia of the surrounding liquid and the diffusion rate of heat into the vapor bubble.

When a liquid comes into contact with a surface that is kept at a temperature higher than the liquid's saturation temperature, boiling starts at the imperfections on the solid surface in contact with the liquid. In the event of boiling, vapor bubbles

form quickly at the solid-liquid interface. Once they reach a certain size, they detach from the surface and try to rise to the liquid's free surface.

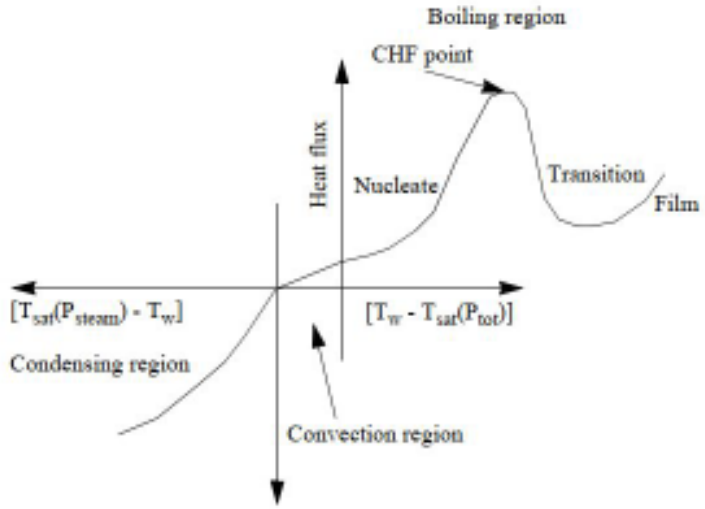

Figure 4.4: Representation of boiling and condensation chart in RELAP5 adopted from [48]

Figure 4.4 represents the boiling curve used in RELAP5 to govern the selection of the wall heat transfer correlations when the wall surface temperature is above the saturation temperature (superheated relative to the saturation temperature based on total pressure).

4.1.4 Boiling Transition and Thermal Limits

Boiling is the dominant heat transfer mechanism in BWR systems. Bubbles forming under the thermal and hydrodynamic effects act as carriers of heat from the heated surface to the liquid body. As shown in Figure 4.4 the heat flux experiences a substantial increase following the onset of the nucleate boiling.

However, due to the localized flooding condition beyond a certain superheating level, the maximum achievable heat flux value is physically limited. Beyond this point, the heat transfer coefficient experiences a significant reduction due to the vapor film preventing the liquid from contacting the heated surface. Therefore, the maximum achievable heat flux without establishing a vapor blanket is known as the Critical Heat Flux (CHF). Terminologically this condition is separated into two mechanisms, Departure from Nucleate Boiling (DNB) observed at low-quality conditions and Dry-out observed at high-quality conditions. The term Dryout is mostly used to describe the critical flow conditions in BWR systems.

The most widely used measure of the thermal margin is the Critical Power Ratio (CPR). It is defined as the ratio of critical channel power to the operating channel power. The CPR as a thermal margin is a practically useful approach since it is easy to interpret in terms of power rather than heat flux. For instance, when CPR=1.20 in a system where other parameters are held constant if power is increased by 20% boiling transition could be expected. In [31] the factors increasing the critical power performance are stated as the mass flux and inlet subcooling.

4.1.5 Field Equations

The RELAP5 hydrodynamic model is a one-dimensional model for the flow of a two-phase steam-water mixture that can contain soluble components in the steam phase and/or in the water phase. The two-fluid equations of motion that are used as the basis for the RELAP5 hydrodynamic model are formulated in terms of volume and time-averaged parameters of the flow. The system model is solved numerically using a semi-implicit finite-difference technique. Phenomena such as friction and

heat transfer, are formulated using empirical transfer coefficients in terms of the bulk properties.

A total of eight field equations for eight variable types are solved in the thermal-hydraulic model numerical scheme. The basic field equations for the two-fluid nonequilibrium model consist of two phasic continuity equations, two phasic momentum equations, and two phasic energy equations [48].

Mass continuity equations come from the one-dimensional phasic mass equations. Generally, the flow does not include mass sources or sinks other than the transfers between each phase through boiling, evaporation, or condensation. The continuity rule requires that the liquid generation term be the negative of the vapor generation.

$$\Gamma_{\mathrm{f}} = -\Gamma_{\mathrm{g}} \tag{4.1.16}$$

For the vapor phase;

$$\Gamma_g = \frac{\partial}{\partial t}\left(\alpha_g \rho_g\right) + \frac{1}{A}\frac{\partial}{\partial x}\left(\alpha_g \rho_g v_g A\right) \tag{4.1.17}$$

For the liquid phase;

$$\Gamma_f = \frac{\partial}{\partial t}\left(\alpha_f \rho_f\right) + \frac{1}{A}\frac{\partial}{\partial x}\left(\alpha_f \rho_f v_f A\right) \tag{4.1.18}$$

The phasic momentum conservation equations are synthesized from one-dimensional phasic momentum equations. For simplicity, certain assumptions have been made such as no Reynolds stress, equal phasic and interfacial pressures within a node, adequately modeled normal wall forces, and the unity of the covariance terms. Also,

some properties have been neglected such as interfacial momentum storage and phasic viscous stresses. Since the development of the numerical scheme is convenient (can be reduced to Bernoulli's equation for frictionless steady incompressible flow) the expanded forms of the equations are used.

For the vapor phase:

$$\alpha_g\rho_g A\frac{\partial v_g}{\partial t}+\frac{1}{2}\alpha_g\rho_g A\frac{\partial v_g^2}{\partial x}=-\alpha_g A\frac{\partial P}{\partial x}+\alpha_g\rho_g B_x A-\left(\alpha_g\rho_g A\right)FWG\left(v_g\right)+\Gamma_g A\left(v_{gI}-v_g\right)$$
$$-\left(\alpha_g\rho_g A\right)FIG\left(v_g-v_f\right)-C\alpha_g\alpha_f\rho_m A\left[\frac{\partial\left(v_g-v_f\right)}{\partial t}+v_f\frac{\partial v_g}{\partial x}-v_g\frac{\partial v_f}{\partial x}\right] \tag{4.1.19}$$

For the liquid phase:

$$\alpha_f\rho_f A\frac{\partial v_f}{\partial t}+\frac{1}{2}\alpha_f\rho_f A\frac{\partial v_f^2}{\partial x}=-\alpha_f A\frac{\partial P}{\partial x}+\alpha_f\rho_f B_x A-\left(\alpha_f\rho_f A\right)FWF\left(v_f\right)-\Gamma_{\mathrm{g}}\mathrm{A}\left(\mathrm{v_{fI}}-\mathrm{v_f}\right)$$
$$-\left(\alpha_{\mathrm{f}}\rho_{\mathrm{f}}\mathrm{A}\right)\mathrm{FIF}\left(\mathrm{v_f}-\mathrm{v_g}\right)-C\alpha_f\alpha_g\rho_m A\left[\frac{\partial\left(v_f-v_g\right)}{\partial t}+v_g\frac{\partial v_f}{\partial x}-v_f\frac{\partial v_g}{\partial x}\right] \tag{4.1.20}$$

The force terms on the right-hand side of the momentum equations for liquid and vapor phases include the pressure gradient, body force, wall friction, interface mass transfer related momentum transfer, interfacial friction drag, and virtual mass-related force. While FWG and FWF are part of the wall frictional drag, the FIG and FIF are part of the interfacial friction drag.

The value of the virtual mass coefficient (C) is determined based on the flow regime. For bubbly or dispersed flow patterns C>1/2 is acceptable, and presently this value is used for all flow regimes.

The phasic energy conservation equations come from the one-dimensional phasic thermal energy equations. For simplicity, certain assumptions have been made such as no Reynolds heat flux, unified covariance multipliers, no interfacial energy storage,

and no internal phasic heat transfer.

For the vapor phase:

$$\frac{\partial}{\partial t}\left(\alpha_g \rho_g U_g\right)+\frac{1}{A}\frac{\partial}{\partial x}\left(\alpha_g \rho_g U_g v_g A\right) = -P\frac{\partial \alpha_g}{\partial t}-\frac{P}{A}\frac{\partial}{\partial x}\left(\alpha_g v_g A\right)+Q_{wg}+Q_{ig}+\Gamma_{ig}h_g^*+\Gamma_w h_g'+DISS_{\mathrm{g}} \tag{4.1.21}$$

For the liquid phase:

$$\frac{\partial}{\partial \mathrm{t}}\left(\alpha_{\mathrm{f}} \rho_{\mathrm{f}} \mathrm{U_f}\right)+\frac{1}{\mathrm{A}}\frac{\partial}{\partial \mathrm{x}}\left(\alpha_{\mathrm{f}} \rho_{\mathrm{f}} \mathrm{U_f v_f A}\right) = -\mathrm{P}\frac{\partial \alpha_{\mathrm{f}}}{\partial \mathrm{t}}-\frac{\mathrm{P}}{\mathrm{A}}\frac{\partial}{\partial \mathrm{x}}\left(\alpha_{\mathrm{f}} \mathrm{v_f A}\right) \&+\mathrm{Q_{wf}}+\mathrm{Q_{if}}-\Gamma_{\mathrm{ig}}\mathrm{h_f^*}-\Gamma_{\mathrm{w}}\mathrm{h_f'}+\mathrm{DISS_f} \tag{4.1.22}$$

The final expression for the total interface mass transfer:

$$\Gamma_{\mathrm{g}} = \Gamma_{\mathrm{w}} - \frac{\mathrm{H_{ig}}\left(\mathrm{T^s}-\mathrm{T_g}\right)+\mathrm{H_{if}}\left(\mathrm{T^s}-\mathrm{T_f}\right)}{\mathrm{h_g^*}-\mathrm{h_f^*}} \tag{4.1.23}$$

DISS_g and DISS_f are the phasic energy dissipation terms. They represent the sums of wall friction and pump effects. The wall friction dissipations are defined as:

$$\begin{aligned} \mathrm{DISS} &= \mathrm{DISS_g}+\mathrm{DISS_f} \\ \mathrm{DISS_g} &= \alpha_{\mathrm{g}}\rho_{\mathrm{g}}\mathrm{FWG}\,\mathrm{v_g^2} \\ \mathrm{DISS_f} &= \alpha_{\mathrm{f}}\rho_{\mathrm{f}}\mathrm{FWF}\,\mathrm{v_f^2} \end{aligned} \tag{4.1.24}$$

4.1.6 Constitutive Models

The constitutive relations are developed for defining flow regimes and related models for interphase drag and shear, the coefficient of virtual mass, wall friction, wall heat transfer, interphase heat and mass transfer, and direct (sensible) heat transfer. The

constitutive relations include flow regime effects for which simplified mapping techniques have been developed to control the use of constitutive relation correlations. Four flow regime maps are used: a horizontal map for flow in pipes; a vertical map for flow in pipes, annuli, and bundles; a high mixing map for flow in pumps; and an ECC mixer map for flow in the horizontal pipe near the ECC injection port.

Vertical Volume Flow Regime Map

In RELAP5 nine regimes -four for pre-CHF heat transfer, four for post-CHF heat transfer, and one for vertical stratification- are modeled for the vertical flow.

The flow regime maps are based on the work of Taitel and Dukler. The post-critical heat flux (post-CHF) regimes are adopted from the work of Ishii. For the transition between the flow regimes the semi-empirical Taitel and Dukler relations are simplified for better application in the code.

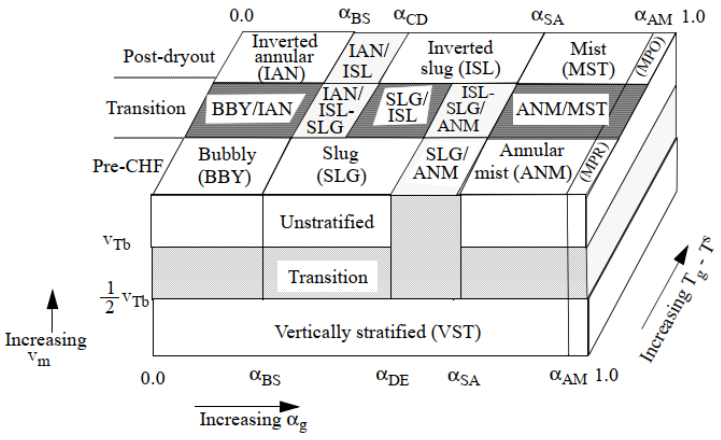

Figure 4.5: Flow regime map used in RELAP5 adopted from [48]

The pre-CHF heat transfer regimes are the bubbly, slug, annular-mist, and mist-pre-CHF regimes while the post-CHF heat transfer regimes (inverted annular, inverted slug, and mist regimes) are suggested by suggested by Ishii.

Figure 4.5 represents the pre-CHF, post-CHF, and transition regimes of the vertical flow as functions of the boiling regime, void fraction (α_g), and average mixture velocity (v_m). Several criteria are used to decide the state of the flow regime in transition zones.

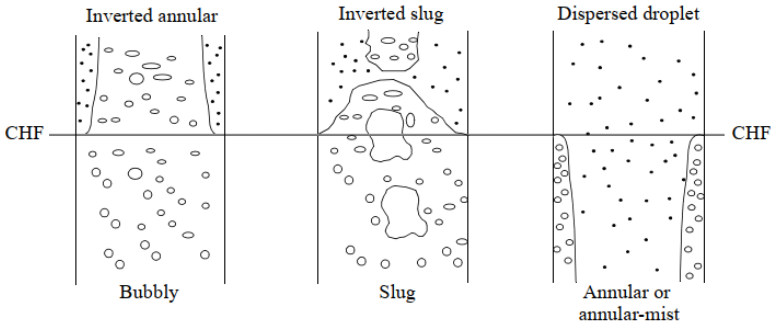

Figure 4.6: Schematic representation of vertical flow regimes in RELAP5 adopted from [48]

Figure 4.6 provides an illustration of the flow patterns used in RELAP5. For a smooth transition between the flow regimes, certain rules have been developed. In Table 4.1 these transition regions and transition rules are introduced for both pre-CHF and post-CHF flow conditions.

BUBBLY / INVERTED BUBBLY
$\mathrm{G_m} \leq 2000\ \mathrm{kg/m^2 \cdot s}$ $\alpha_{BS} = 0.25 \min\left[1.0, \left(\frac{\mathrm{D^*}}{22.22}\right)^8\right]$ $2000 < \mathrm{G_m} < 3000\ \mathrm{kg/m^2 \cdot s}$ (4.1.25) $\alpha_{BS} = \alpha_L + 0.001\,(0.5 - \alpha_L)\,(G_m - 2000)$ $G_m \geq 3000\ \mathrm{kg/m^2\ s}$ $\alpha_{BS} = 0.5$
SLUG / INVERTED SLUG
$\alpha_{\mathrm{SA}} = \min\left(\alpha^{\mathrm{f}}_{\mathrm{crit}}, \alpha^{\mathrm{e}}_{\mathrm{crit}}\right)$ (4.1.26) $\alpha_{DE} = \max\left(\alpha_{BS}, \alpha_{SA} - 0.05\right)$
ANNULAR MIST / INVERTED ANNULAR MIST
$\alpha_{\mathrm{AM}} = 0.9999$ (4.1.27)
MIST PRE-CHF / MIST POST-CHF

Table 4.1: Transition rules between flow regimes

Coefficient of Virtual Mass

The junction flow regime map is used to determine the coefficient of virtual mass in RELAP5. Based on an objective and symmetric formulation of the relative acceleration the dynamic drag is calculated. In the phasic momentum equation, the inertial drag force per unit volume is written as;

$$FA_{gf} = -C\alpha_g\,(1 - \alpha_g)\,\rho\left[\frac{\partial}{\partial t}\,(v_g - v_f)\right] \tag{4.1.28}$$

where the virtual mass coefficient is given as

$$C = \frac{1}{2}\frac{(1+2\alpha_g)}{(1-\alpha_g)} \text{ for } 0 \leq \alpha_g \leq \frac{1}{2} \tag{4.1.29}$$

$$C = \frac{1}{2}\frac{(3-2\alpha_g)}{\alpha_g} \text{ for } 1/2 \leq \alpha_g \leq 1 \tag{4.1.30}$$

Wall Friction

The flow regime map is used to determine the wall friction. The wall friction model is based on a two-phase multiplier approach in which the two-phase multiplier is calculated from the Heat Transfer and Fluid Flow Service (HTFS)-modified Baroczy correlation.

The Lockhart-Martinelli model computes the overall friction pressure drop in terms of the liquid-alone wall friction pressure drop

$$\left(\frac{d\mathrm{P}}{d\mathrm{x}}\right)_{2\phi} = \phi_{\mathrm{f}}^2 \left(\frac{d\mathrm{P}}{d\mathrm{x}}\right)_{\mathrm{f}} \tag{4.1.31}$$

Throughout the current literature, the overall two-phase friction pressure gradient is calculated using two-phase friction multiplier correlations. The multipliers may be interrelated using the Lockhart-Martinelli ratio defined as

$$\chi^2 = \frac{\left(\frac{\mathrm{dP}}{\mathrm{dx}}\right)_{\mathrm{f}}}{\left(\frac{\mathrm{dP}}{\mathrm{dx}}\right)_{\mathrm{g}}} = \frac{\phi_{\mathrm{g}}^2}{\phi_{\mathrm{f}}^2} \tag{4.1.32}$$

The HTFS correlation for the two-phase friction multiplier is expressed as

$$\phi_{\mathrm{f}}^2 = 1 + \frac{\mathrm{C}}{\chi} + \frac{1}{\chi^2} \tag{4.1.33}$$

$$\phi_{\mathrm{g}}^2 = \chi^2 + \mathrm{C}\chi + 1 \tag{4.1.34}$$

The RELAP5 phasic momentum equations can be written in a quasistatic form except that the wall friction terms are in terms of the RELAP5 wall friction coefficients instead of phasic wall shear stresses.

The overall quasi-static, two-phase wall friction pressure gradient as

$$\left(\frac{dP}{dx}\right)\Big|_{2\phi} A = \mathrm{FWF}\left(\alpha_g \rho_f v_f\right) A + FWG\left(\alpha_g \rho_g v_g\right) A \tag{4.1.35}$$

In RELAP5 the Darcy-Weisbach friction factor is computed from correlations for laminar and turbulent flows with interpolation in the transition regime.

The laminar friction factor is calculated as

$$\lambda_{\mathrm{L}} = \frac{64}{\mathrm{Re}\,\Phi_{\mathrm{S}}} \tag{4.1.36}$$

The turbulent friction factor is given by the Zigrang-Sylvester approximation to the Colebrook-White correlation as,

$$\frac{1}{\sqrt{\lambda_{\mathrm{T}}}} = -2\log_{10}\left\{\frac{\varepsilon}{3.7\mathrm{D}} + \frac{2.51}{\mathrm{Re}}\left[1.14 - 2\log_{10}\left(\frac{\varepsilon}{\mathrm{D}} - \frac{21.25}{\mathrm{Re}^{0.9}}\right)\right]\right\} \tag{4.1.37}$$

The friction factor in the transition region between laminar and turbulent flows

is computed by reciprocal interpolation as

$$\lambda_{\mathrm{L,T}} = \left(3.75 - \frac{8250}{\mathrm{Re}}\right)\left(\lambda_{\mathrm{T},3000} - \lambda_{\mathrm{L},2200}\right) + \lambda_{\mathrm{L},2200} \tag{4.1.38}$$

Wall to Fluid Heat Transfer

The energy transfer between the heat structure wall and hydrodynamic volumes is calculated using the wall-to-fluid heat transfer model. The heat transfer correlations in RELAP5 consider fully developed flow since in real nuclear power plants the entrance effect is very small. In RELAP5, different user-defined geometries in the input deck representing the heat structures such as pipes, vertical or horizontal bundles, and parallel plates correspond to different heat transfer correlations. The heat transfer coefficient is determined by the maximum value among laminar flow, forced convection flow, and natural convection flow. Changes in heat transfer regime from single-phase, subcooled boiling, fully developed two-phase, and film boiling are also considered.

The general expression for the total wall heat flux considers heat transfer between wall and liquid in two different phases.

$$\begin{aligned} \mathrm{q}''_{\mathrm{total}} &= hg_g\left(T_w - T_g\right) + hg_{spt}\left(T_w - T_{spt}\right) + hg_{spp}\left(T_w - T_{spp}\right) \\ &\quad + hf_f\left(T_w - T_f\right) + hf_{spt}\left(T_w - T_{spt}\right) \end{aligned} \tag{4.1.39}$$

For easier explanation, the heat transfer modes are represented by numbers. For each of the 12 mode numbers, the convective correlations are employed. Mode numbers indicate the heat transfer regime between heat structure surfaces and the circulating fluid.

The suitable correlation set for a specific surface relies on the hydraulic geometry

of the neighboring fluid, with the flow field near the wall influencing the velocity profile and turbulence. Various geometric configurations of flow paths are contemplated and assigned numbers, but only a selection of these numbers has been addressed in the coding. Pipes, being versatile flow mediums, can be molded to various shapes, but in RELAP5, the correlations are restricted to modeling only circular pipes.

CONDEN	Computes the coefficients by considering the wall temperature when it falls below the saturation temperature.
DITTUS	Use for single-phase liquid or vapor conditions.
PREDNB	Encompasses the correlations for nucleate boiling on all surfaces, except for the horizontal bundles.
PREBUN	Used for the outer face of horizontal bundled tubes.
PSTDNB	Contains transition and film boiling correlations.
CHFKUT	Computes the CHF at horizontal bundles.
CHFCAL	Determines the CHF for the surfaces using a lookup table.
SUBOIL	Calculates the vapor generation rate near the wall when the bulk liquid is subcooled.

Table 4.2: List of logic map subroutines used in RELAP5

In RELAP5 a logic map is used to determine the heat transfer regime and corresponding heat transfer coefficient. Eight subroutines DITTUS, PREDNB, PREBUN, PSTDNB, CONDEN, CHFKUT, CHFCAL, and SUBOIL play important roles in the logic map. The functions and roles of each subroutine are described in Table 4.2.

4.1.7 Point Reactor Kinetics Calculations

The computation of power from reactivity inputs in RELAP uses the space-independent or point kinetics approximation, which presumes that power can be divided into spatial and temporal functions. Utilizing this method, the point reactor kinetics model assesses both the immediate fission power, including the kinetic energy from fission products and neutron moderation, and the power resulting from fission product decay.

The kinetics model executes an integration of ordinary differential equations via a tailored Runge-Kutta technique, using core-average fluid conditions, feedback coefficients, and weighting factors to identify the overall reactivity. This total reactivity guides the kinetics calculation for the complete core power, subsequently apportioned among the fuel heat structures consistently. The generation of decay power comes as the fission products experience radioactive decay, with the selected model for this process being the American National Standard for Decay Heat Power in Light Water Reactors (e.g.ANSI/ANS-5.1-1979).

The point kinetics equations are presented as;

$$\psi(t) = \Sigma_f \varphi(t) \tag{4.1.40}$$

$$P_f(t) = Q_f \psi(t) \tag{4.1.41}$$

$$\frac{d}{dt}\varphi(t) = \frac{[\rho(t) - \beta]\varphi(t)}{\Lambda} + \sum_{i=1}^{N_d} \lambda_i C_i(t) + S \tag{4.1.42}$$

$$\frac{d}{dt}\mathrm{C_i(t)} = \frac{\beta \mathrm{f_i}}{\Lambda}\varphi(\mathrm{t}) - \lambda_\mathrm{i}\mathrm{C_i(t)i} = 1, 2, \ldots, \mathrm{N_d} \tag{4.1.43}$$

The power Psα(t), as defined by the 1979 standard, is expressed in MeV/s and represents a function of time t, originating from a single fission of isotope α when t=0.

$$P_{s\alpha}(t) = \sum_{j=1}^{N_\alpha} \mathrm{a}_{\alpha j} \exp\left(-\lambda_{\alpha j}\mathrm{t}\right) \tag{4.1.44}$$

Following the necessary simplifications and substitutions, the decay power equation is derived for one group corresponding to a single isotope. The interpretation of this equation is twofold: the first term on the right side illustrates the creation of the isotope during the fission process, while the last term signifies the depletion of the isotope as a result of decay.

$$\frac{d}{dt}\gamma(\mathrm{t}) = \frac{\mathrm{a}}{\lambda}\psi(\mathrm{t}) - \lambda\gamma(\mathrm{t}) \tag{4.1.45}$$

The ANS standard employs a correction factor for the energy stemming from fission product decay, and this factor serves to accommodate the impacts of neutron absorption.

$$\mathrm{G(t)} = 1.0 + \left(3.24 \cdot 10^{-6} + 5.23 \cdot 10^{-10}\mathrm{t}\right) \mathrm{T}^{0.4}\psi_\mathrm{g} \tag{4.1.46}$$

The corrected version of the decay power equation is given as

$$\mathrm{P}_\gamma = \mathrm{G(t)P}'_\gamma \tag{4.1.47}$$

The actinide model illustrates the creation of U-239, Np-239, and Pu-239 through

the capture of neutrons by U-238.

$$P_\alpha(t) = \eta_U \lambda_U \gamma_U(t) + \eta_N \lambda_N \gamma_N(t) \tag{4.1.48}$$

$$\frac{d}{dt}\gamma_{\mathrm{U}}(\mathrm{t}) = \mathrm{F_U}\psi(\mathrm{t}) - \lambda_{\mathrm{U}}\gamma_{\mathrm{U}}(\mathrm{t}) \tag{4.1.49}$$

The rate of change in the number of U-239 atoms is calculated by deducting the number of depleted U-239 atoms from the created amount.

$$\frac{d}{dt}\gamma_{\mathrm{N}}(\mathrm{t}) = \lambda_{\mathrm{U}}\gamma_{\mathrm{U}}(\mathrm{t}) - \lambda_{\mathrm{N}}\gamma_{\mathrm{N}}(\mathrm{t}) \tag{4.1.50}$$

The generation of Np-239 occurs as a result of the beta decay of U-239, while the formation of Pu-239 comes from the decay of Np-239.

The total power P_T in units of watts is described as the total of immediate fission power, corrected fission product decay, and actinide decay.

$$P_T(t) = Q_f X \psi(t) + G(t) \sum_{\alpha=1}^{3} \sum_{j=1}^{N_\alpha} \lambda_\alpha X \gamma_{\alpha j}(t) + \eta_U \lambda_U X \gamma_U(t) + \eta_N \lambda_N X \gamma_N(t) \tag{4.1.51}$$

Reactivity Feedback Mechanism

The evaluation of reactivity feedback effects, such as fuel temperature, moderator temperature, moderator density, and boron concentration within the moderator, is conducted by using averages across the hydrodynamic control volumes and corresponding heat structures representing the core.

There are five available feedback options: SEPARABL, TABLE3, TABLE3A, TABLE4, and TABLE4A. Among these, the SEPARABL option is the most straightforward and commonly utilized. It's referred to as the separable option due to the underlying assumption that each feedback mechanism operates independently, with the total reactivity being a cumulative sum of the individual effects. The separable option employs two tables, with one outlining reactivity in relation to volume density and the other in connection to volumetric average fuel temperatures. Under this option, a variation in any one of the three parameters doesn't influence the others. The tables facilitate nonlinear feedback resulting from alterations in moderator density and fuel temperature. A consistent temperature coefficient provides for linear feedback concerning moderator temperature, and supplementary linear feedback related to fuel temperature is also included. Data for the separable option can be sourced from either reactor operating data, reactor physics computations, or a blend of both. The necessary moderator temperature coefficient differs from the quantity that is typically cited.

The reactivity value in the separable model is specified as

$$\begin{aligned} r(t) =& r_o - r_B + \sum_{i=1}^{n_s} r_{si}(t) + \sum_{i=1}^{n_c} V_{ci} + \sum_{i=1}^{n_\rho} \left[W_{\rho i} \cdot R_\rho \left(\rho_i(t) \right) + a_{Wi} \cdot T_{Wi}(t) \right] \\ &+ \sum_{i=1}^{n_F} \left[W_{Fi} \cdot R_F \left(T_{Fi}(t) \right) + a_{Fi} \cdot T_{Fi}(t) \right] + \sum_{i=1} W_{\rho i} \cdot C_b \cdot 10^6 \cdot B_W \end{aligned} \tag{4.1.52}$$

The option utilizing three- and four-dimensional table lookup and interpolation relies on either three or four quantities as the independent variables. Within this framework, two sub-options provide the flexibility to select the independent variables. One option defines the reactivity as a function of moderator density, weighted moderator

temperature, volumetric average fuel temperature, and boron density. This option employs the same variables as the separable choice but adds the effects of boron if a total of four variables are utilized. The second option employs void fraction, liquid moderator temperature, volume-averaged fuel temperature, and boron concentration as the independent variables. This multidimensional interpolation enables the handling of nonlinearities and interaction between feedback effects, but it places a greater demand on the user to acquire an extensive amount of reactivity data. The necessary information can be gathered from either plant data or reactor physics computations. In the tabular reactivity feedback model, the reactivity value is defined with standard independent variables as:

$$r(t) = r_o - r_B + \sum_{i=1}^{n_c} r_{si} + \sum_{i=1}^{n_c} V_{ci} + R\left(\bar{\alpha}_g(t), \bar{T}_f(t), \bar{T}_F(t), \bar{C}_b(t)\right) \tag{4.1.53}$$

4.2 Reference Plant Specifications

The Laguna Verde Nuclear Power Plant (LVNPP) is situated in Veracruz State of Mexico. The plant incorporates two units, each equipped with a fifth-generation boiling water reactor (BWR5) designed by the General Electric Company.

The Unit 1 started operation in 1990 and the Unit 2 in 1995 with rated power levels of 1931 MWt each. A thermal power uprate project was implemented to amplify the energy output. Consequently, the net capacity of each reactor was increased to roughly 2317 MWt, thereby elevating the plant's total capacity to approximately 4634 MWt [34] [19].

The following Figure 4.7 provides a detailed view of the inner components of a

BWR5 reactor vessel. In this chart, many components are named and highlighted. Although all of the systems are important for plant operation and safety some of the most important ones are namely, fuel assemblies, feedwater systems, control rods, jet pump assemblies, in-core monitoring systems, steam separators, and steam dryer assembly. It is noteworthy that while the bottom portion of the vessel is named as lower plenum and is mostly occupied by liquid water, the upper portion mostly contains the dry steam and it is called the vessel head.

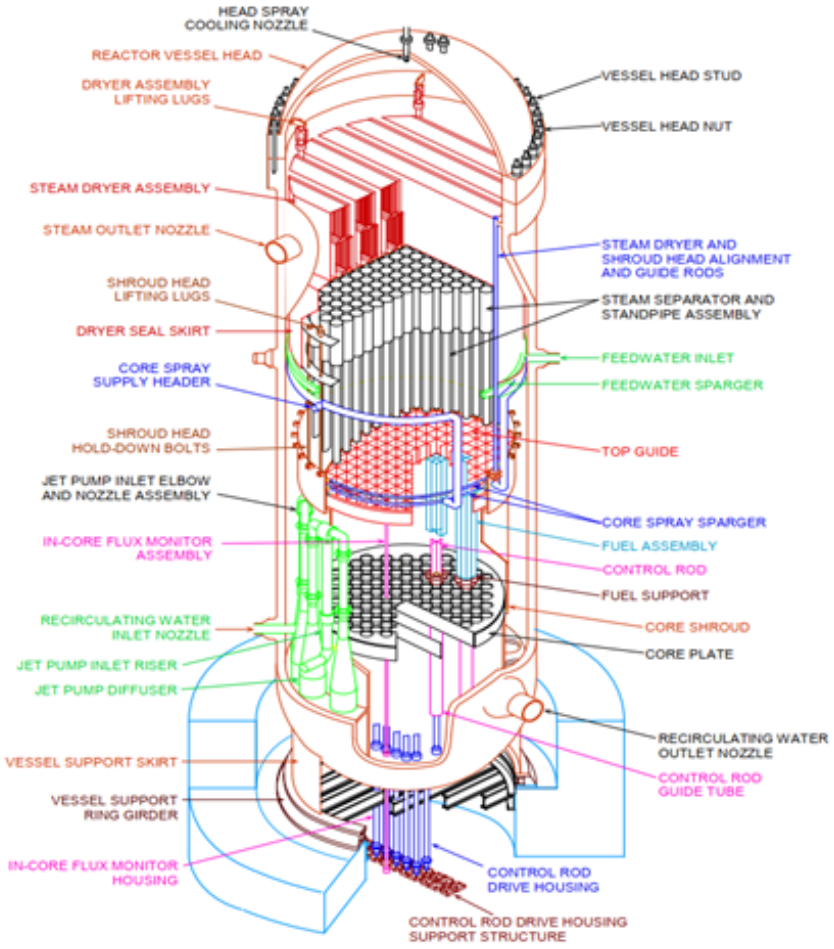

Figure 4.7: Boiling water reactor vessel layout adopted from [1]

Fuel rods in the reactor core consist of slightly enriched uranium dioxide fuel pellets encapsulated in Zircalloy-2 sheaths. Fuel assemblies are composed of 62 fuel rods and 2 water rods positioned in an 8x8 square array. The Figure 4.8 represents a GE-14 fuel assembly. A total of 444 fuel assemblies reside in the reactor core to obtain the desired energy level. A hydraulic control system manipulates the bottom-entry control rods to achieve gross control of the core power. Control rods are cruciform-shaped and dispersed along the lattice of the fuel bundles. However, the cruciform-shaped control rod component is not shown in the fuel assembly.

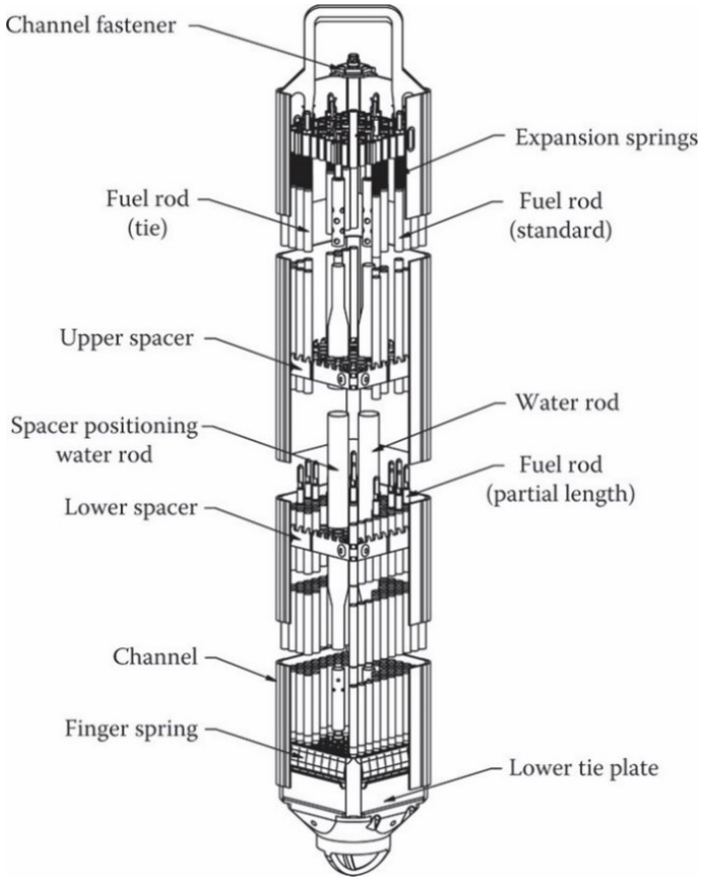

Figure 4.8: BWR fuel assembly diagram adopted from [1]

Twenty internal jet pumps and two recirculation pumps provide a 9600 tonnes/hr

flow rate in the reactor vessel. The system was designed to provide a steam flow rate of 3759 Kton/hr for a gross capacity of 803 MWe. Produced dry steam is used to drive the power conversion system. The power conversion system consists of tandem compound 1800rpm capacity turbines (two low-pressure and one high-pressure turbine) with reheating equipment. An electro-hydraulic control system regulates the turbine for normal operation. The turbine generator is rated at approximately 674,480 kW. The generator is a direct-driven three-phase 60Hz, 22000 volts, 1800rpm hydrogen inner-cooled synchronous machine rated at 750000 kVa with a 0.9 power factor and a short circuit ratio of 0.58 to the design capacity [19].

For operational and safety purposes several other subsystems such as the reactor recirculation system, residual heat removal system, reactor water cleanup system, control rod drive system, and emergency core cooling systems are also employed [1]. Although all the components and systems have significant roles in plant operation and safety, we will be mostly focusing on the reactor core and fuel assembly, emergency cooling systems, and auxiliary units such as turbines and condensers. Following through description of the real system, the sections of the computer model created using RELAP5 thermal-hydraulics code will be explained.

4.3 Plant Input Model Description

In this section design specifications of Laguna Verde Nuclear Reactor RELAP5 code input model are introduced. The SCDAPSIM/RELAP5 input model of the LVNPP is developed by the Mexican National Commission on Nuclear Safety and Safeguards (CNSNS) and is provided by Innovative Systems Software (ISS) to support this research thesis.

Figure 4.9 represents the nodalization layout of the LVNPP systems and components modeled using RELAP5. In this diagram, various components such as pipes, valves, fuel channels, turbines, and volumes are shown, and the connections between the figures represent the flow path. RELAP allows users to define different components using the same tools by applying proper configurations and input specifications. Therefore, even if the two shapes look identical in the nodalization diagram each one can correspond to an entirely different plant component.

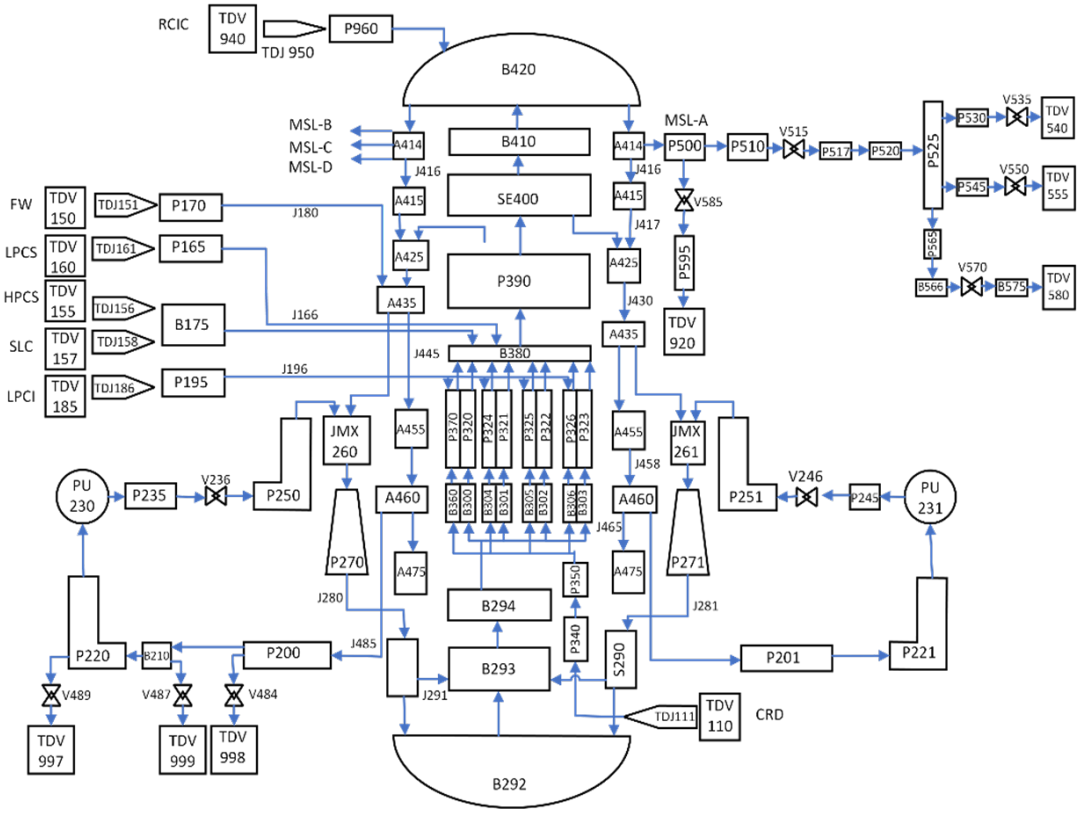

Figure 4.9: Laguna Verde NPP RELAP5 input model nodalisation diagram

The plant model is developed to reflect the real plant specifications as detailed as possible. The model represents numerous features of the main steam lines, emergency core cooling systems, reactor pressure vessels, containment structures, fuel assemblies,

blade boxes, and many other important components. The computer model is designed to be able to calculate a wide range of plant conditions starting from a steady state to an accident scenario resulting in the melting of the reactor core.

The following main elements are modeled in LVNPP input code 1) reactor vessel and internals, 2) reactor core, 3) lower plenum, 4) broken and intact recirculation loops, 5) main steam lines, 6) feed-water system, and 7) engineered safety systems such as Emergency Core Cooling (ECCS) and Reactor Core Isolation Cooling (RCIC).

The thermal-hydraulic nodalisation diagram shown in Figure 4.9 is manually regenerated using the diagrams in the open literature and the actual input model. Detailed information on the CNSNS-developed nodalization and input model is available in the open literature. The validity of this model has been proven to be adequate in several studies [9], [20], [37], [39], [44], [45], [46]. One of the most significant example was conducted following the accident at Fukushima Daiichi to support emergency response activities and further investigate the possibility of such accidents in western nuclear power plant designs. Experts from ISS and other SCDAP Development and Training Program members investigated the possible consequences of a station blackout scenario. This study provided valuable insights into the progression of the accident (fuel melting, hydrogen production, containment failure, etc.). Under the lights of the findings, the team makes suggestions regarding accident management and emergency procedures [9]. This study paved the way for several other studies investigating the various stages and scenarios of station blackout events and severe accident simulations in LVNPP using RELAP5/SCDAPSIM code

4.3.1 Core Components

The reactor core is divided into 8 vertical channels representing flow paths along the core. While four of the channels represent fuel channels, the other four channels are reserved for core bypass flow and core monitoring instrumentation cooling (one and three paths respectively). Fuel assemblies of the reactor model are represented by standard pipe elements (P320, P321, P322, and P323). Each flow channel is modeled as a pipe divided into 14 nodes. The time-dependent volume components (TDV 998 and TDV 999) are employed to represent the boundary condition as a MARK-II environment at constant pressure.

Although not used in this thesis, the code provides the capability to analyze the beyond-design-basis accident cases. In the event of a core meltdown, forecasting the behavior of the molten material on the vessel's bottom is of vital importance. To facilitate this, a two-dimensional, finite element, steady-state, and transient heat conduction computer code, COUPLE, is employed to simulate the increase in heat in the lower head due to the slump of the molten material. The B-292 volume of the BWR model is linked with the COUPLE code to evaluate the transfer of heat and mass from the vessel. In addition, a time-dependent volume known as TDV-750 is used to mimic the heat transfer from the vessel's lower head to the dry well. The computer code accounts for the decay heat and initial internal energy of the slumped debris.

4.3.2 Fuel Rods

Simulation of the energy source in the core is completed by using specialized fuel elements under the core components instead of generic heat elements in RELAP5. The total number of fuel rods in the real reactor core is 27528. Fuel rods and fuel pellets in all groups have been defined with uniform physical properties. Table 4.3 defines the number of fuel rods and the total number of fuel pellets in each group. Each fuel group has a different enrichment level and energy contribution from each group is defined by a multiplier. To specify the in-core age of each fuel group a certain burnup level is also defined.

A total of four fuel channels modeled as representative of fuel assemblies have been divided into four representative groups based on power and fuel enrichment level. The position of the fuel rods in the core is defined by hydrodynamic volumes surrounding the rods.

Group	Enrichment%	Rods	Pellets	Multiplier	Burnup (MWseg/kg)
1	1.76	112	6944	0.313835	433641.6
2	1.76 to 2.19	112	6944	0.307024	433468.8
3	2.19	108	6696	0.248864	374112.0
4	0.711	108	6944	0.130277	188438.4

Table 4.3: Table of fuel rod properties

For thermal analysis of the fuel rods, there are 13 axial nodes and 4 radial nodes assigned on each heat structure. Radial and axial temperature profiles around the fuel rods are defined using these nodes. Also, the share of each assembly in the production of the total power is given in power multiplier value. Along with the fuel

rods, the blade box corresponding to each fuel assembly is also modeled using the core component. To describe the blade boxes the physical properties, oxidation levels, initial temperatures, and volume connections are specified in the model.

4.3.3 Heat Structures

In the RELAP5 the heat transfer mechanisms are represented by generic heat structure elements. Heat structures provide the code with a domain to handle the complex thermal interactions between a solid material and a working fluid. Structures such as vessel walls, steam separators, steam dryers, fuel rod support pieces, pipes, and other necessary reactor internals could be modeled using heat structures. Thermal characteristics of the components are defined by the material properties. Using heat structures specific types of materials, and associated properties such as density, conductivity, and heat capacity can be modeled. These properties play significant roles in determining how heat is transferred and stored within the material. A "left" and a "right" side are designated for each heat structure. These sides can be connected to a hydrodynamic volume to facilitate heat exchange to the surrounding fluid. The code can account for various modes of heat transfer, including conduction, convection, and radiation. In Table, 4.4 components are defined by component name and component number. The number of axial heat structures is defined as well as the number of radial mesh points and assigned material type.

Number	Component Name	Axial Heat Structures	Mesh Points and Material Type
270	Jet Pump 1	3	2(SS304)
271	Jet Pump2	3	2(SS304)
340	Control Rod Drive Housing	1	1(SS) and 2(SS304)
350	Control Rod Guide Tubes	4	2(SS304)
292	Lower Vessel Wall	1	1(SS304) and 3(C-Steel)
294	Core Plate Stiffeners	1	2(SS304)
294	Core Plate	4	2(SS304)
435	Downcomer Vessel Wall	10	1(SS304) and 3(C-Steel)
435	Stand Pipes	2	2(SS304)
450	Middle Core Shroud	17	2(SS304)
475	Lower Core Shroud	2	2(SS304)
293	Shroud Skirt	1	2(SS304)
300	Nose Pieces	1	2(SS304)
301	Nose Pieces	1	2(SS304)
302	Nose Pieces	1	2(SS304)
303	Nose Pieces	1	2(SS304)
410	Dryer Plates	1	1(SS304) and 3(C-Steel)
420	Upper Vessel Wall	1	2(SS304)

Table 4.4: List of heat structures and materials in RELAP5 model of LVNPP

4.3.4 Recirculation Loops

In BWR design the fluid properties and void fraction have a significant importance in reactivity level, and hence power. By adjusting the fluid flow rate through the core void fraction level and hence the reactivity feedback relation is regularly controlled. To accomplish this, BWR5/6 reactors are equipped with two physically and thermodynamically identical recirculation loops. These are modeled using generic RELAP tools such as time-dependent volumes, pumps, pipes, valves, branches, and jet pumps.

Two identical recirculation pumps (P230 and P231) have been modeled for both recirculation loops (with the ability to simulate a break in one of the loops). For defining the properties of pumps single-phase homologous data and two-phase multiplier and difference curves are introduced. Each pump is capable of providing a 27800 gpm flow rate with a 778.14 ft head. To account for 20 internal jet pumps in the reactor vessel two jet pump is modeled in recirculation cycles.

The model is designed to allow users to conduct LB-LOCA analysis using this input model. The guillotine break condition on the piping is applied using motor valves(V483 and V484) that could open instantly located on either side of the broken lines. This method of valve application is particularly important to consider the fluid flowing out from either side of the broken pipe.

4.3.5 Steam Separator and Main Steam Line

In BWR reactors dominant heat transfer method is saturated boiling. In this mode of heat transfer, the generation of steam is observed in every part of the fluid in the core. However, the top portion of the reactor core has a significant role in the

operation of the reactor because this is where the production and accumulation of the dry steam takes place. For BWR reactors obtaining steam with high purity is crucially important for the integrity of the turbine generators. Should a substantial amount of droplets arrive at the turbine, higher-density liquid particles could lead to turbine failure. To prevent this, LVNPP is equipped with a two-stage moisture separator and dryer (SE400 and B410). Water droplets in the steam-water mixture are extracted and passed to the downcomer (A415) to be mixed with recirculation flow and enter back to the core.

Dry steam collected in the steam dome is distributed to the four main steam lines (MSLA, MSLB, MSLC, MSLD). Several valves (SRV, MSIV, and BPV) are located over the length of the steam line leading to the power conversion system. These valves regulate the steam flow to the turbines. In case of an emergency, steam could be partially or fully discarded to the containment volume (TDV920) or condenser (TDV580 or corresponding volume in other main steam lines). Two identical turbines (TDV540 and TDV555) are located at the end of the main steam lines. Instead of specialized turbine components in RELAP5 generic time-dependent volumes are preferred to represent the turbine volume. Prior to the turbines servo valves (V535 and V550 respectively) are located to regulate the steam flow into turbines and hence the turbine speed.

4.3.6 Other Related Systems

The constant supply of fresh water into the core is managed by the feedwater system. In the model, the TDV 150 represents the water supply volume. The flow rate from the supply is controlled with the help of TDJ 151. Water from this source is introduced

into the core through A435 to represent the core annulus in real plants. Following the annulus, water is divided into two branches first leading to the jet mixer (JMX261) and jet pump (P271), and second joining the recirculation loops. The Reactor Water Cleanup System (RWCU) serves to maintain reactor water purity. It extracts water from the recirculation system and then filters and demineralizes it. The RWCU is modeled as a time-dependent volume (TDV997) and a valve (V489) attaching to the recirculation unit. Some of the engineered safety systems are also separately modeled: Low-Pressure Core Spray System (LPCS), Low-Pressure Injection System (LPCI), High-Pressure Core Spray System (HPCS), Reactor Core Isolation Cooling (RCIC), Standby Liquid Control System (SLC) and Control Rod Drive System [1].

The Reactor Core Isolation Cooling (RCIC) system sprays water into the reactor vessel to cool the core when the normal coolant supply is cut off. The system includes a pump attached to a steam-powered turbine and necessary piping. The motive power for the coolant injection comes from the mini-turbine which draws steam from the main steam lines. The pump draws water from storage tanks or the suppression pool, and channels it to the reactor. In the computer model, a time-dependent volume (TDV940) represents the suppression pool. For the sake of simplicity, the flow rate is governed by a time-dependent junction (TDJ950) instead of a pump itself. Under normal operating conditions, this system doesn't supply any flow to the vessel. However, if a low water level is detected in the reactor vessel, an initiation signal triggers the pumps. This is facilitated through a time-dependent junction control with a trip mechanism. Flow is accessible only when the trip mechanism is disengaged, and is non-existent otherwise. The standby liquid control (SLC) system manually stops the reactor chain reaction by injecting neutron-absorbing boron, independently of control

rods. In the computer model, this system only consists of a time-dependent volume (TDV157) and a time-dependent junction (TDJ158) to control the flow. The Control Rod Drive (CRD) system, modeled through time-dependent volume (TDV110) and time-dependent junction (TDJ11), ensures a constant flow into the core during accidents, effectively slowing the progression of core damage. The high-pressure coolant injection (HPCI) system is a standalone emergency mechanism that provides make-up water to cool the reactor vessel during minor to moderate coolant losses. It operates at various pressures, independent of auxiliary AC power, air systems, or external cooling water systems. In the computer model, this system is simplified to include only a time-dependent volume (TDV155) and a time-dependent junction (TDJ156) to manage the flow.

The low-pressure emergency core cooling systems consist of the Low-Pressure Core Spray System (LPCS)and the Low-Pressure Injection System (LPCI)mode of the residual heat removal system, both independent. Low-Pressure Core Spray System (LPCS) pumps water from the suppression pool into the reactor vessel and cools the core by spraying water on fuel assemblies. In the computer simulation, this system is represented simply by a time-dependent volume (TDV160) and a time-dependent junction (TDJ1161) that controls the flow. The LPCI mode of the residual heat removal system provides makeup water for core cooling during coolant loss accidents. During LPCI operation, pumps draw water from the suppression pool and discharge it into the reactor vessel. In the computational model, this system is reduced to just a time-dependent volume (TDV185) and a time-dependent junction (TDJ186) for controlling the flow.

4.3.7 Trip Inputs and Control Variables

In RELAP5, the trip system is typically designed to model various features of a thermal-hydraulic network that are set to automatically respond when certain conditions are met. These conditions, or "trip inputs," are defined as part of the input data for the RELAP5 simulation. Detailed explanations regarding how the trip inputs are built and organized are available in guidebooks and input manual [48]. Trips serve as binary logical operators in RELAP, capable of holding either a true or false status at any given moment. The value of a trip statement is that it enables this binary data to be wholly integrated into a computational process.

A trip statement can utilize any computed parameter like temperature, pressure, or flow rate, and conduct a comparison to determine if the current state is true or false. On the flip side, a trip's status can trigger a specific response within the problem at hand, such as initiating the opening of a valve when the trip becomes true. In other words, trip capability has two dimensions: (a) discerning when a trip event has transpired, and (b) deciding the subsequent course of action upon the occurrence of a trip. While each trip statement represents an individual logical statement, the capacity for trip statements to reference other trip statements enables the formation of complex logical statements.

RELAP5 makes use of two fundamental categories of trips, namely variable trips and logical trips. A variable trip is utilized to compare a computed parameter with another one, or with a constant, to establish a true or false status. Comparison of the inputs is conducted using one of the following relationships: equal (EQ), not equal (NE), greater than or equal (GE), greater than (GT), less than or equal (LE), or less than (LT).

RELAP5 logical trips are used to relate the status of two variable trips (also logical trips and even the logical trip itself) using standard logical operators. These logical operators are AND, OR (inclusive), and XOR (exclusive).

In the logical trip inputs a positive trip number means the original trip value; a negative number means the complement value. Complement means reversing the true and false values; that is, the complement of true is false.

Control variables possess the capability to handle both algebraic and ordinary differential equations, making them ideal for simulating the control logic of hydrodynamic systems and other similar phenomena. They have versatile applications beyond simulating control system logic. They can be employed to establish relationships between different types of calculated data and perform mathematical and logical operations. When used in conjunction with trip inputs, control variables allow the user to collect and process system data as well as make changes in system parameters triggering specific actions within a model.

To do these complex tasks RELAP5 offers several different operators. By utilizing suitable combinations of control variables, it becomes possible to execute a wide range of algebraic, logical, and functional actions within the model. Furthermore, uncalculated variables that are typically disregarded can be recorded for later use. In this section, to provide a clearer representation of the LVNPP model, we highlight some of the user-defined trip inputs and control mechanisms.

Recirculation Loop Break Trips: The pipe break in the recirculation cycle is modeled by attaching motor valves (V484 and V487) on either side of the broken pipe. Valves trip mechanisms are set to open the valves at the desired time and angle to simulate the loss of coolant accident scenario.

Water Level Trips: With the help of control variables water levels are sensed from various parts of the reactor core such as the downcomer, lower plenum, and fuel channels. Based on the liquid and steam ratio in the sensed water level 5 collapsed water level trip setpoints (4 low water level and 1 high water level signal) are assigned to be used as input for other trips or control variables.

Core Flow Control Mechanism: In the control system definition the Total Core Flow is initially defined as 7748.87 gpm. This number is then calculated as the "sum" of the flows supplied by jet pumps (P270 and P271) into the core. This calculated value is recorded as cntrlvar116. Similarly, the Total Fuel Channel Flow is initially defined as 6973.98 gpm. The sum of the mass flows through nose pieces (B300, B301, B302, and B303) is recorded as cntrlvar117. Following the same steps using values from B304, B305, B306, and B360 gives the Bypass Flow as cntrlvar119. Using the values of cntrlvar117 and cntrlvar119 the Total Core Inlet Flow is computed and saved as cntrlvar020. This number is then used to measure the core flow rate using other control variables.

4.3.8 Initial Boundary Conditions

In this section, we introduce the initial boundary conditions of the major components and systems in the LVNPP computer model.

As we stated in the earlier sections a point reactor kinetics model is employed for computation of neutronics behavior in the model. The core is designed to generate 2317 MW total power at steady state. For the reactivity feedback system, the separable option is employed to individually handle the feedback effects from fuel temperature, moderator temperature, and moderator density. To achieve the desired

power production in the core a total of 27528 fuel rods are divided into 4 different enrichment levels as shown in Table 4.3. While initial temperatures range between 1164 and 2351 K defined for the center of the fuel pins, initial temperatures of the fuel claddings lie between 559 and 573 K.

The user-defined initial pressure values in the reactor vessel change by location in the core. The initial pressure in the lower plenum region is defined as about 7185 kPa while in the vessel dome, it is 7000 kPa.

The coolant in the reactor is driven by two recirculation pumps and two jet pumps. Each recirculation pump is designed to rotate at 17035 rpm to provide 28700 gpm mass flow rate. Altogether the core is supplied with a total core flow rate of 7748.87 gpm while a significant portion (6973.98 gpm) is delivered to the fuel channel.

In order to initiate the transient, the turbine stop valve on the main steam line is assumed to be linearly switching from 100% open position to 0% open position within 50 milliseconds. Similarly, the bypass valve is designed to follow a linear progression, starting from complete closure at 0.3 seconds and reaching fully open within 0.9 seconds.

In case of a shutdown, the reactor control rods can provide a total of -37.2 dollars in reactivity to the core when fully inserted. The control rod insertion speed and corresponding reactivity worth are given in Table 4.5.

Time After Signal (s)	Reactivity Worth ($)
0.0	0.0
0.5	0.0
1.0	-0.5
1.3	-0.6
1.4	-0.8
1.5	-1.0
1.6	-1.2
1.7	-1.5
1.8	-1.7
1.9	-1.8
2.0	-2.0
2.1	-2.5
2.2	-2.9
2.3	-3.1
2.4	-3.8
2.5	-4.2
2.6	-5.0
2.7	-6.0
2.8	-7.5
2.9	-8.8
3.0	-10.5
3.1	-13.0
3.2	-16.0
3.3	-20.0
3.4	-27.0
3.5	-32.5
3.6	-35.5
3.8	-37.2
3.9	-37.2
4.0	-37.2

Table 4.5: Control Rod Insertion Rate vs. Time

5

Reference Turbine Trip Analysis Results

In this section, we present results from the thermal-hydraulic analysis of the Laguna Verde Nuclear Power Plant (LVNPP) model using the RELAP5-Mod3.4 computer code. The research encompasses a range of tests and analyses to understand plant behavior during a transient event. The comprehensive understanding of plant behavior under steady state and transient scenarios not only provides a solid foundation for future investigations involving advanced transient analyses, safety evaluations, and design optimizations but also contributes significantly to the broader scientific understanding of nuclear power plant thermal-hydraulics.

The purpose of the steady-state test is to verify the code's capability to accurately represent the thermal-hydraulic behavior of the LVNPP under normal operating conditions. Key parameters, core power, including reactor vessel dome pressure, coolant temperature, core mass flow rate, core void fraction level, and core collapsed liquid level, were compared against the results from the open literature and plant data where possible.

In the transient analyses, we conducted a series of computer tests on a nuclear power plant model to evaluate its performance under various scenarios. Our objective

was to evaluate whether the transient behavior poses any safety risk regarding the thermal limits. Comparisons with findings in the open literature were made to assess the reliability of the results. Given BWR behavior is new to the Canadian landscape, these simulations provide a valuable starting point for the development of new models and methods for BWRS in Canada. The results show that the simulation models and inputs provide the correct qualitative behavior.

Sensitivity analyses were carried out to assess the impact of selected parameters on the thermal-hydraulic performance of the plant.

5.1 Steady State Results

The steady-state simulations of the LVNPP were performed to establish the accuracy and reliability of the computer code and reactor model in capturing key thermal and hydraulic parameters under normal operating conditions and to assess the appropriateness of the boundary conditions. These results were compared to plant data available in open literature.

The power source in the LVNPP RELAP model has been developed using 4 fuel structures which constitute fuel components for the point reactor kinetics module. The power generated by the core is the product of both prompt and decay neutrons. Therefore, the total power term is used to cover energies supplied from both sources. The plant nominal power is set to generate 2317 MW total power at steady state which is the upper allowed operational power limit [34].

The steady-state simulation allows for all the thermal-hydraulic parameters (i.e., fuel temperatures, moderator temperatures, and water levels) and their associated reactivity feedbacks to reach equilibrium (i.e., zero total reactivity), thus the stable

and self-consistent solution of the thermal-hydraulics and physics parameters, for the steady-state. In this section, we present Figure 5.1 showing the total power behavior during startup and steady-state run while Figure 5.2 shows the dome pressure response and Figure 5.3 the maximum core surface temperature.

The steady-state calculation has been conducted for the thermal-hydraulic parameters to reach their stable trend. Additional simulations of 300s showed no significant deviations from the steady-state calculation results.

As shown in Figure 5.1, the code successfully achieves a steady power level of 2317 MW by the end of the calculation time. The oscillations following the initiation of the calculation may result in the termination of the calculation unless a suitable maximum time step value is defined (i.e. the maximum time step must be below some threshold to limit power oscillations).

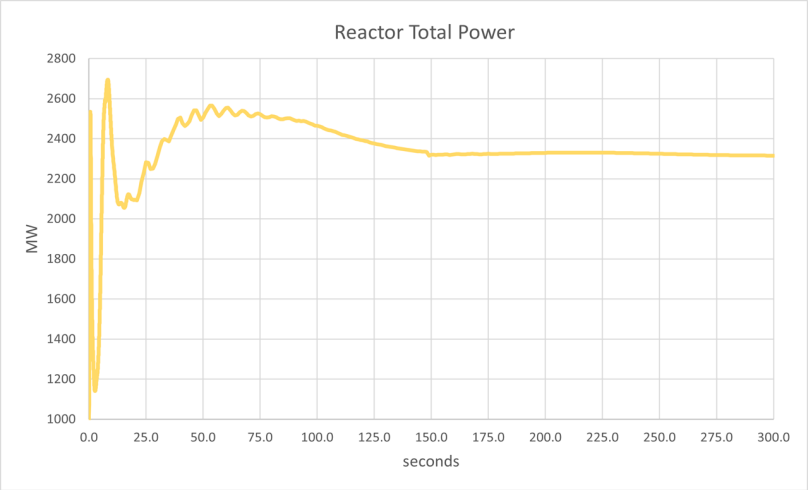

Figure 5.1: Total power production at steady state

The reactor vessel dome pressure, a vital parameter for assessing the plant's stability and safety, was analyzed. Figure 5.2 demonstrates that the calculated pressure level for the reactor vessel dome successfully maintained a stable level during the

calculation period. The steady-state value of the dome pressure is demonstrated in excellent agreement with the design value (7050 kPa) [19] and data in literature [45].

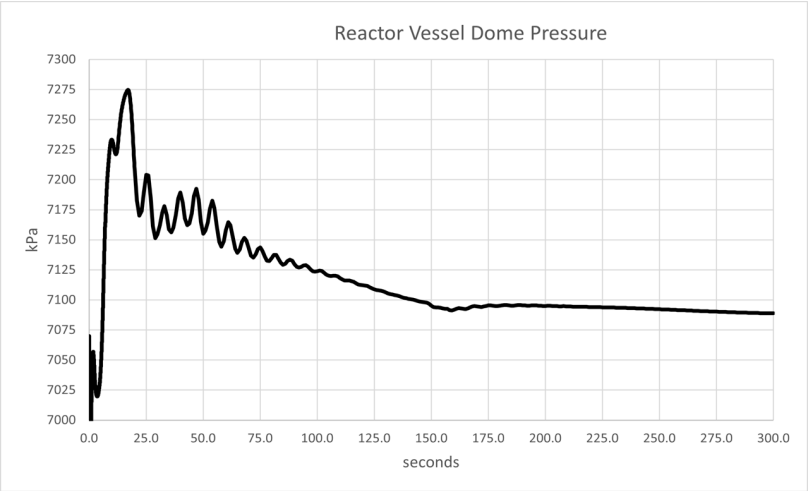

Figure 5.2: Vessel dome pressure level at steady state

The accurate prediction of cladding temperature is crucial for ensuring the optimal thermal performance and safety of the nuclear power plant. Therefore thermal resilience of the fuel sheath is an important acceptance criterion. In a previous study [45] Trivedi investigates the effects of a possible blackout scenario in LVNPP. His computed maximum core surface temperature at steady state before transient calculations is found to be around 600K. As shown in Figure 5.3 our model can reproduce a cladding temperature of roughly 590K at the steady-state. The strong relation between the results validates the capability of the code and reactor model to capture the complex heat transfer phenomena occurring within the reactor core.

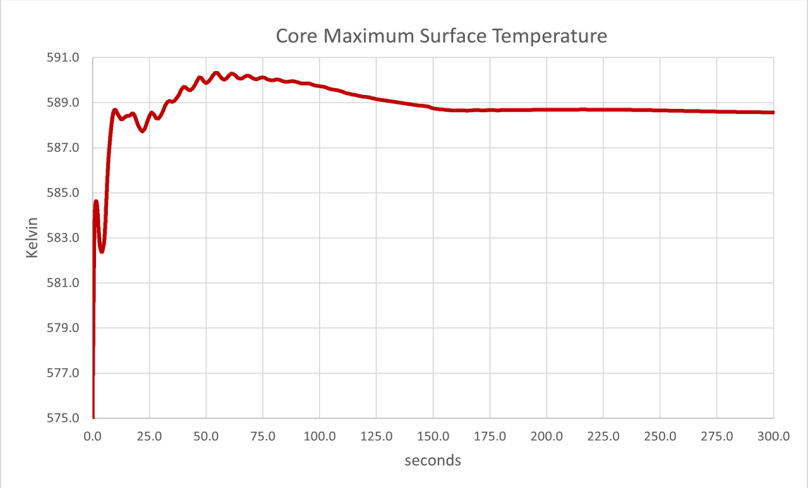

Figure 5.3: Maximum fuel cladding temperature at steady state

The collapsed liquid level signifies the height of the liquid coolant around the fuel bundles. It is an important parameter for effective cooling and for the prediction of void-reactivity effects. In post-accident modeling conditions, the liquid level ensures the fuel remains covered at all times. For example, the initial void (core level) plays an important role in TT events since the amount of void available to collapse at the steady state influences the power pulse magnitude and speed. The plotted data for the collapsed liquid level in the LVNPP model demonstrated a good agreement with the steady-state values presented in the literature [45]. This agreement indicates the capability of the code and reactor model to accurately predict the void fraction level in the core.

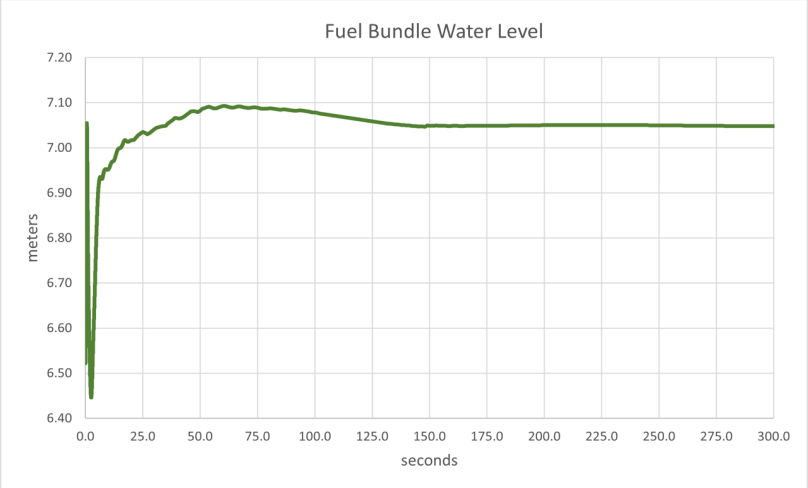

Figure 5.4: Hot channel water level at steady state

The successful validation of the code and reactor model through the steady state analyses provides a solid foundation for further analyses, including power transient and turbine trip transient simulations. These subsequent analyses will investigate the plant's response to dynamic events and transient conditions, providing valuable insights for safety evaluations, operational decision-making, and design optimizations.

5.2 Code Testing Routine

As a part of the code testing routine, a power pulse test was conducted on the LVNPP input model to evaluate its response under various power transients. The test included a power drop, where the plant's power level decreased from a steady-state value of 100% full power (2317MW) to 2000MW. Figure 5.5 shows the total power during the ramp while Figure 5.6 shows the dome pressure and Figure 5.7 the sheath temperature.

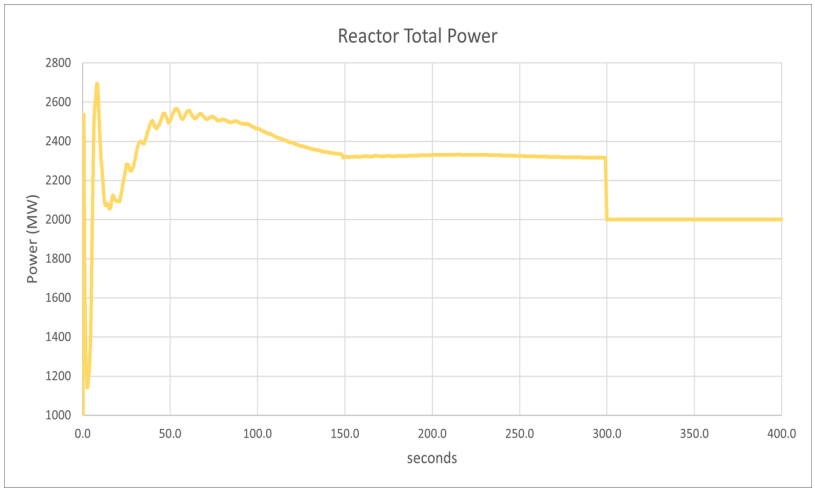

Figure 5.5: Reactor total power response following a negative power pulse

The effect of a negative power pulse at 300 sec is clearly visible in the power history in Figure 5.5. The system experiences a 14% drop in core power level. One thing to note at this point, usually a change in power level brings about an oscillation in the outputs. However, for this particular example, the conditions of the feedback mechanism do not allow oscillatory behavior. Instead, the generated response resembles a step function since the pulse is introduced as a step change.

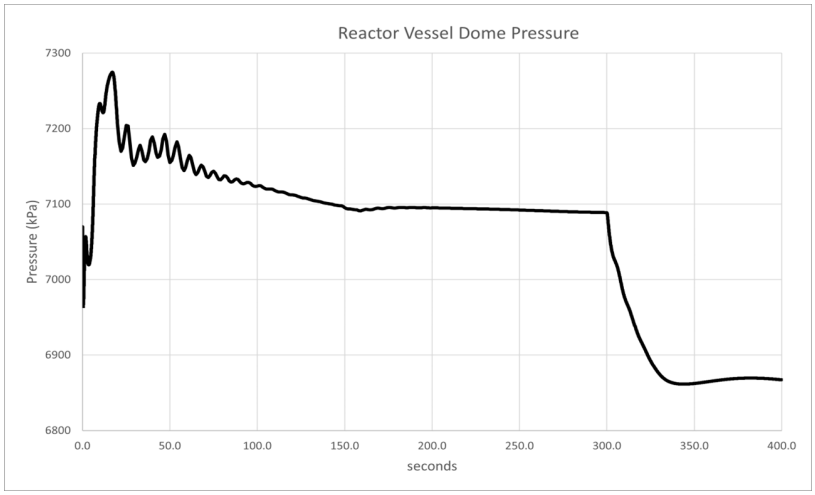

Figure 5.6: Dome pressure evaluation following a negative power pulse

The vessel dome pressure response in Figure 5.6 experiences a slightly more natural behavior than the power behavior. While the pressure level is at a balance of around 7100 kPa before the power drop test, it dropped by roughly 250 kPa as a result of the change in the power level. It means that a 14% change in the power level caused an almost 3.5% change in the dome pressure level. However, despite the step change in the power level, the dome pressure showed a more natural course.

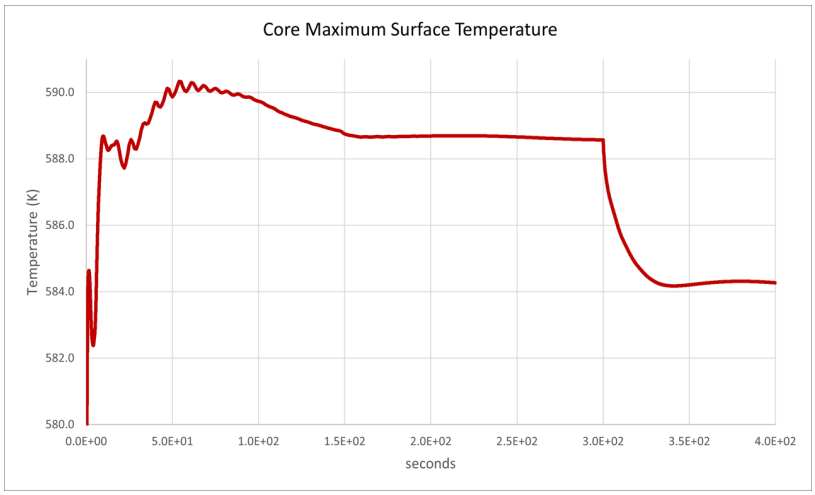

Figure 5.7: Maximum cladding temperature behavior following negative power pulse

In response to the 14% change in the power level, the maximum core surface temperature shows a slight change from the steady-state level. The cladding temperature under 2000 MW core power is calculated to be around 584K.

Overall, the plant model demonstrated stable behavior and successfully maintained the new plant parameters till the end of the simulations. These results provide compelling evidence that the model can reliably and predictably handle perturbations in reactor power levels. Such findings instill confidence in the plant's operational stability and underscore its capability to adapt to power fluctuations effectively.

5.3 Reference Turbine Trip Case Results

In a BWR the reactor vessel is directly linked to the turbine, meaning that the heat energy from steam produced in the reactor core is transformed into mechanical energy in the turbines to generate electricity. However, this cooperative mechanism could be disrupted by a turbine trip incident, which can cause either an influx of cold liquid or a surge in vessel pressure depending on system availability. Hence an increase in reactor power. The increase in power can pose a risk to the cladding temperature through the occurrence of CHF on the sheath.

Within the scope of this thesis, a best-estimate case is formulated to offer a thorough evaluation of the turbine trip event. This section introduces Figure 5.11a showing the dome pressure response, Figure 5.8 shows the change in the void fraction, Figure 5.10a represents the total power behavior during transient, Figure 5.9a shows the variation of the reactivity level, Figure 5.12a the maximum core surface temperature, and Figure 5.13 comparing the reactivity level against the change in the void fraction. To evaluate the accuracy, the results have been compared against the relevant benchmark results. Where the calculated values are compared against the benchmark, the trends corresponding to the study by UPISA (University of Pisa) are considered.

Before conducting the transient calculation, the code have been run for 300 seconds to reach steady state values. Upon successfully achieving the steady state, another restart problem was run using the data from steady-state calculations. The transient is induced with the sudden closure of the turbine stop valve (TSV) at t = 301.0 seconds within 50 milliseconds. The reactor system is equipped with a steam bypass

valve (BPV) to discard the excess amount of steam through a condenser. This is important to prevent further increase in vessel pressurization, and protection of the steam turbines as well. Bypass valve operation is set to be linear from a fully closed position at 0.3 seconds to a fully opened position at 1.2 seconds.

Sudden closure of the turbine stop valve generates pressure waves downstream the main steam line. The pressure waves travel along the pipe at the speed of sound and ultimately reach the reactor core through different channels. Once the pressure waves enter the core, the balance between pressure and temperature is disturbed [15]. As it is shown in Figure 5.8 this disturbance in the core balance parameters results in the core void collapse by almost 4%.

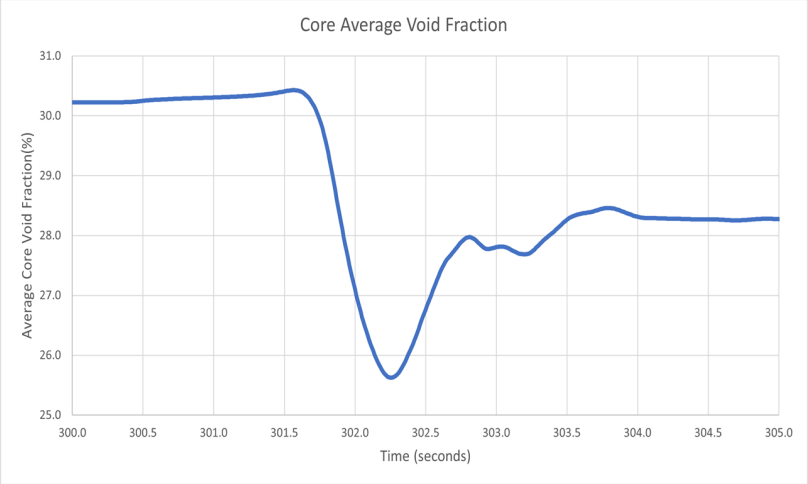

Figure 5.8: Void fraction collapse during turbine trip transient

The total reactivity behavior before the scram is dominated by the void reactivity feedback mechanism. The reactivity excursion due to the change in the void fraction is shown in Figure 5.9a. From the figure, it is clear that roughly a 4% decrease in the void fraction caused a prompt insertion of almost 0.45 dollars reactivity. However, in the benchmark, the maximum marginal reactivity insertion rate is predicted to be

around 0.8 dollars in Figure 5.9b.

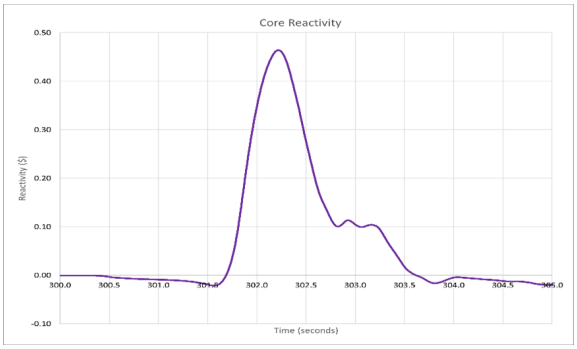

(a) Core reactivity level during turbine trip transient

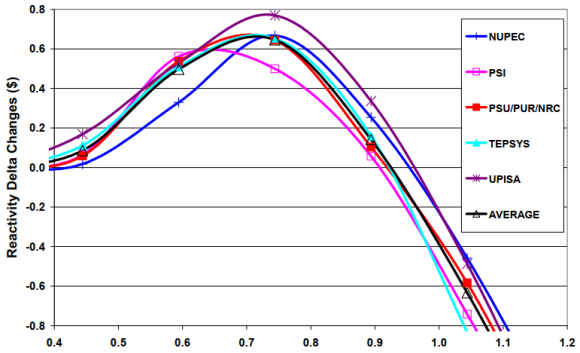

(b) Marginal change in the core reactivity in best estimate analysis

Figure 5.9: Comparison of core reactivity change against the benchmark data for best estimate analysis

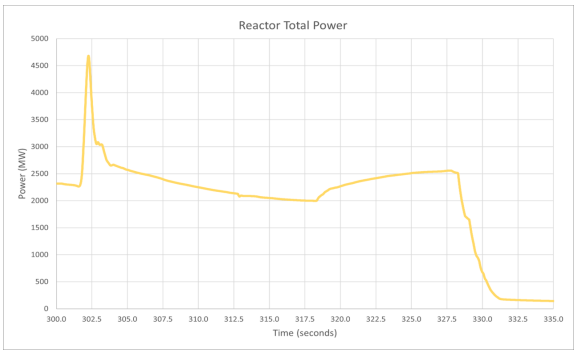

(a) Total core power response during turbine trip transient

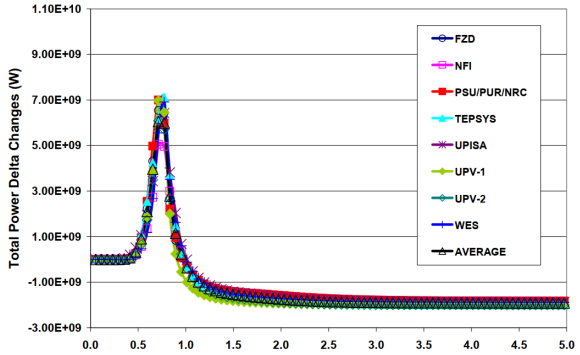

(b) Marginal change in total power in best estimate analysis

Figure 5.10: Comparison of core power history against the benchmark data for best estimate analysis

Owing to the inherent reactivity feedback mechanism, the core power demonstrates an excursion as shown in Figure 5.10a in response to the collapse of the void around the fuel elements. The core power level peaks at almost 4600 MW within milliseconds following the valve closure. The trend of the increase in total power

matches the trend in the benchmark result in Figure 5.10b. However, in comparison to the approximately 600 MW marginal increase in total power, the calculated value could be found underestimated.

The reactor SCRAM safety system is designed to be activated at predefined high power safety set-points. Although this level is usually adjusted based on the particular reactor design and the acceptance criteria of the regulatory bodies, the safety limits are scattered between 110% full power and 120% full power. Due to technical limitations during the programming phase we could not able to define this set point in the reference case. However, our calculations show that in the reference case the 110% full power level is achieved within 0.81 seconds after the TSV closure. Besides that the total core power reaches 120% full power level 0.87 seconds following the transient initiation. These examples clearly reveals the fast nature of the turbine trip transient. Therefore, the health and reliable action of the safety systems are vital during such transient events.

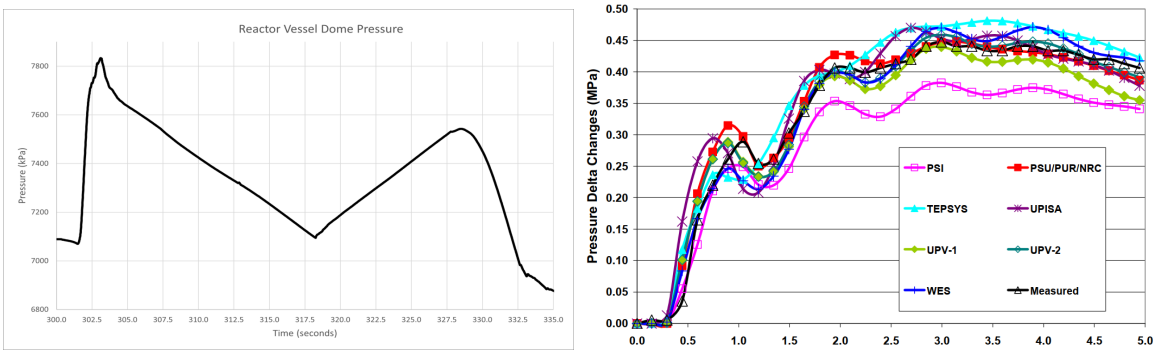

(a) Vessel dome pressure evolution during turbine trip transient

(b) Marginal change in vessel dome pressure in best estimate analysis

Figure 5.11: Comparison of dome pressure response against the benchmark data for best estimate analysis

Due to the introduction of the pressure waves into the reactor core, the turbine trip

with stop valve closure is often categorized as a pressurization event. Therefore the relation between the neutronic phenomena and system dynamics plays an important role in the plant response. The magnitude of the neutron flux transient is strongly affected by the initial rate of pressure rise. In Figure 5.11a it can be seen that the vessel dome pressure during the transient experiences a rise in excess of 700 kPa. We can argue that the code overestimated the dome pressure since Figure 5.11b shows a maximum 470 kPa increase during the transient.

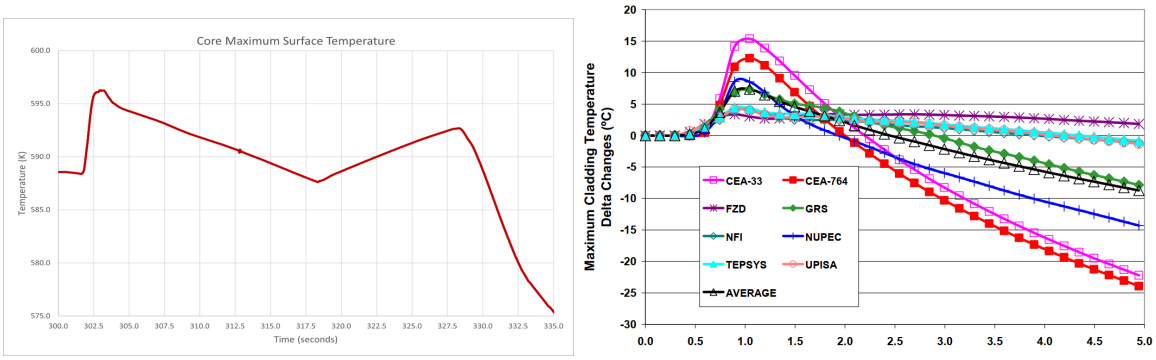

(a) Maximum cladding temperature during turbine trip transient

(b) Marginal change in maximum cladding temperature in best estimate analysis

Figure 5.12: Comparison of maximum cladding temperature against the benchmark data for best estimate analysis

Zircalloy fuel cladding material is designed to be able to withstand high temperatures. The maximum allowed limit for the cladding is limited to be less than 1480 K. Considering the low thermal conductivity of the UO2 fuel and the fast nature of the transient, the energy unleashed during the power spike becomes concentrated within the fuel pellet. Maximum surface temperature results, given in Figure 5.12a, remained below 600 K.

Considering the cladding temperature trend no temperature excursion occurred. This shows that the CHF limit is not exceeded in this case. Despite the discrepancies

that appeared in the prediction of pressure and power values, the maximum cladding temperature in Figure 5.12a and in Figure 5.12b are very close.

In this scenario, one of the most important aspects of the analysis is the prediction of the secondary power pulse occurring around 15 seconds after the first excursion. The reason for this behavior could be attributed to the excessive cooling of the reactor core after the first power transient. While the temperature is reducing under the effect of reduced reactivity in the core, evaporation around the hot fuel rods maintains a rising trend in the void fraction level.

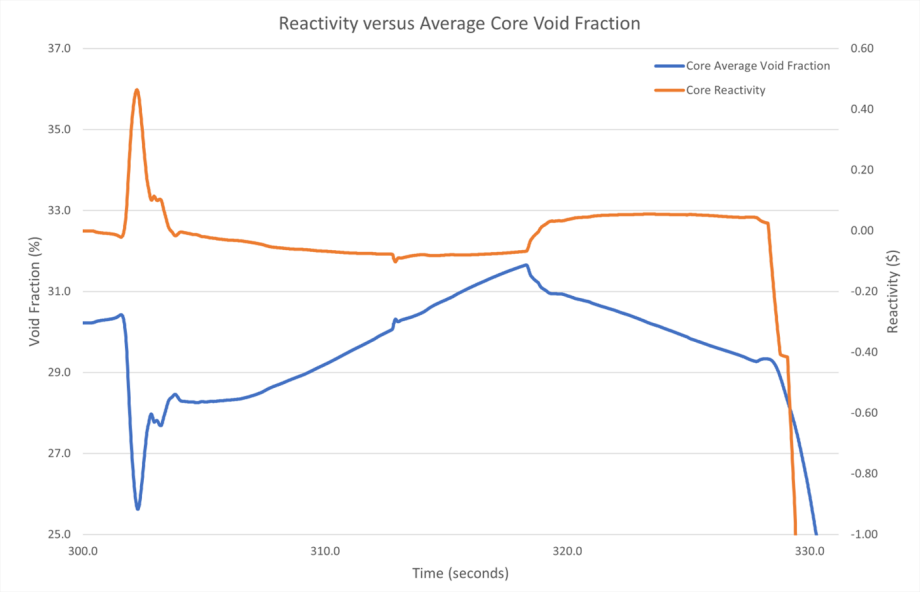

Figure 5.13: Relation between reactivity and average core void fraction during transient

Since control rods are not inserted at this stage the reactivity in the fuel pins is yet to be fully suppressed. Once the void fraction level is reached around 32% void reactivity feedback once again triggers the production of more reactivity and more power. However, as shown in Figure 5.13 since this transient occurs at a relatively lower power level and the rate of increase in the void fraction is relatively slow its

effect on power and pressure levels is not as significant. Also, the effect of the SCRAM mechanism should not be neglected.

The rising water level in the core caused the recirculation pumps to get tripped due to the high water level set-point. In conjunction with this tripping of the recirculation pumps reactor scram is activated (approximately 28 seconds after turbine trip initiation) which is suppressing entire reactivity in the core. The reactor scram then inserted additional negative reactivity and completed the power reduction and eventual core shutdown.

5.4 Postulated Turbine Trip Scenarios

Within the scope of this work, the following three hypothetical scenarios have been analyzed as variations of the best estimate turbine trip scenario calculation. Problem configurations and event sequences were adopted from the PBTT2 Benchmark [30].

- Hypothetical Scenario 1: Bypass valve opening failure
- Hypothetical Scenario 2: SCRAM actuation failure
- Hypothetical Scenario 3: Bypass valve opening failure combined with SCRAM failure.

Hypothetical Scenario 1:

The purpose of this test is to investigate the influence of the bypass valve movement on the reactor behavior. In this scenario, a turbine trip event is assumed to be accompanied by the failure of the bypass valve opening. Additionally, the SCRAM signal is manually activated 0.63 seconds after the initiation of the turbine trip signal.

The logic behind manually tripping the SCRAM mechanism is that in the reference input model configuration, the activation of the control rods is directly linked to the recirculation pump trip feedback. Once the recirculation pumps are tripped, the SCRAM signal is activated to limit the power excursion. However, in the benchmark, the SCRAM signal is activated upon violation of the overpower threshold. Due to the limitations, we are not able to assign an overpower limit. Yet as a remedy to this issue, we activate the SCRAM signal at the same activation time in the benchmark.

Figure 5.14a demonstrates the core power behavior in scenario 1. The result reveals that the insertion of the rods significantly limited the power surge. In comparison to the results from the reference case, the power peak value has been reduced by around 500 MW. With reference to Figure 5.14b the total power level in the hypothetical scenario 1 is significantly underestimated. The reason behind this difference could be the time when the control rod insertion is commenced.

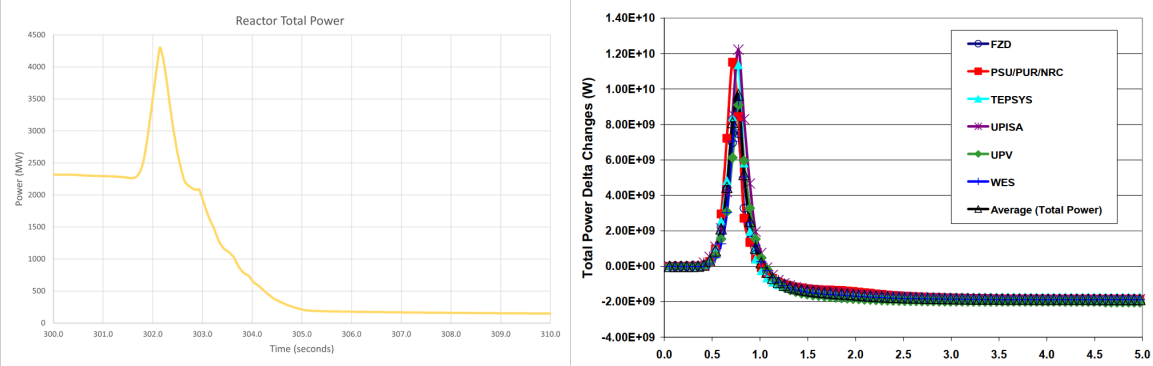

(a) Calculated total power

(b) Marginal change in total power in extreme scenario 1

Figure 5.14: Comparison of total power history against the benchmark data for extreme scenario 1

Figure 5.15a demonstrates that the vessel dome pressure change during the transient is affected by the control rods and the amplitude of the dome pressure is reduced

by roughly 100 kPa in comparison to the reference case. On the other hand, the benchmark values in Figure 5.15b predicts almost 1MPa increase in dome pressure.

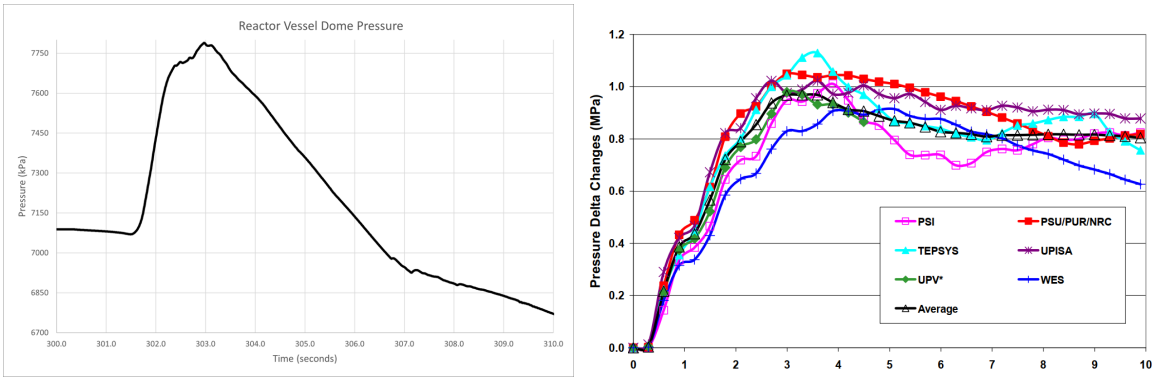

(a) Vessel dome pressure evolution

(b) Marginal change in dome pressure in extreme scenario 1

Figure 5.15: Comparison of dome pressure evolution against the benchmark data for extreme scenario 1

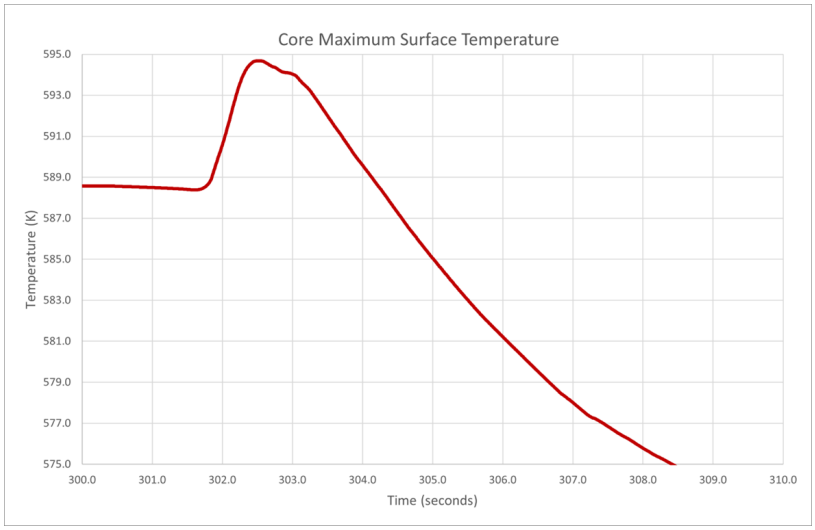

Figure 5.16: Core maximum surface temperature in hypothetical scenario 1

Similar behavior is observed in Figure 5.16 representing the evolution of the maximum cladding temperature. Even though a significant amount of power surge is lost

during this transient, the peak value of the maximum core surface temperature is nearly managed to reach the value in the reference case (595 K) before the scram went into action.

Hypothetical Scenario 2:

In this scenario, the turbine trip event is postulated with an error in the scram mechanism. To cancel the negative reactivity insertion as a result of the scram signal, we neutralized the amount of negative reactivity to be inserted into the system in case of shutdown. Figure 5.17a demonstrating the power surge, Figure 5.18a showing the vessel dome pressure response, and Figure 5.19 representing the maximum core surface temperature history charts will be evaluated to describe the overall plant behavior during this event.

Practically this scenario is equivalent to the reference case scenario presented in the previous sections. In the early seconds of the transient both cases do not have any SCRAM mechanism to limit the power excursion. Therefore, in terms of the most important period of the turbine trip analysis, hypothetical scenario 2 produces the same predictions as the reference case scenario.

The only difference between the two calculations could be found at the later stages of the transient where the scram signal is activated at the reference case. Since there is no insertion of the control rods in extreme case 2 the reduction in the change parameters occurs relatively slower than the change in the reference case results.

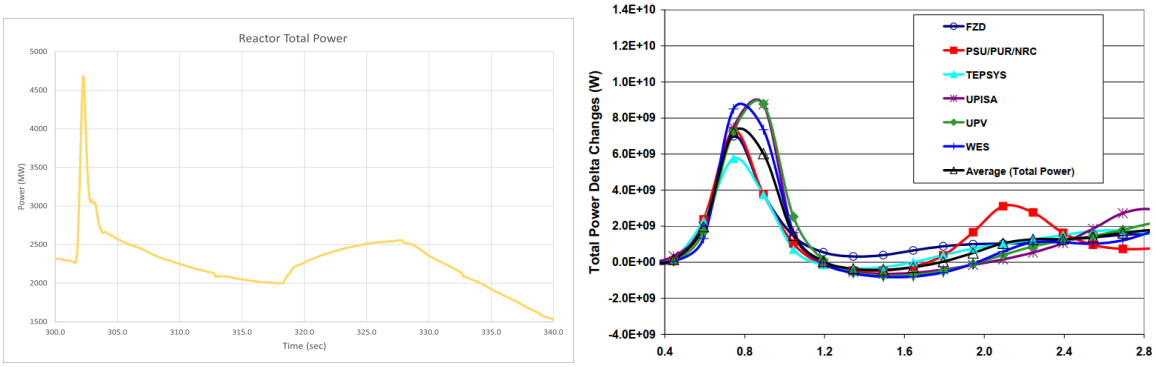

(a) Reactor total power response

(b) Marginal change in total core power in extreme scenario 2

Figure 5.17: Comparison of total core power against the benchmark data for extreme scenario 2

Figure 5.17a shows the rise in the core power in response to the turbine trip transient. Similar to the behavior at the reference case calculation the power history follows a steep trend up to almost 4700 MW until the natural limiting behavior of BWR results in a rapid decrease.

Comparison with the benchmark data in Figure 5.17b shows that code successfully achieved a similar trend. Differences with the benchmark are observed in the peak power value and the magnitude of the second power peak.

The pressure response shown in Figure 5.18a reaches the peak level of approximately 7800 kPa within nearly 1 second after the valve closure. This rate of rise in the dome pressure is slightly underestimated in comparison to the benchmark prediction shown in Figure5.18b.

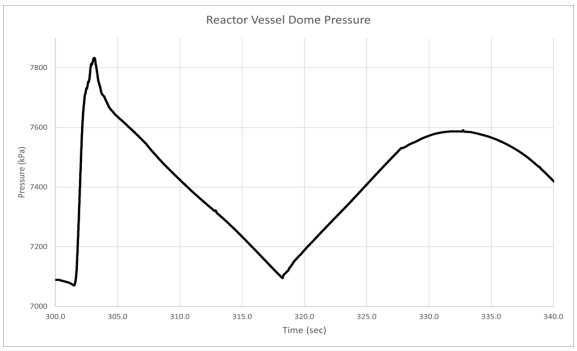

(a) Vessel dome pressure evolution

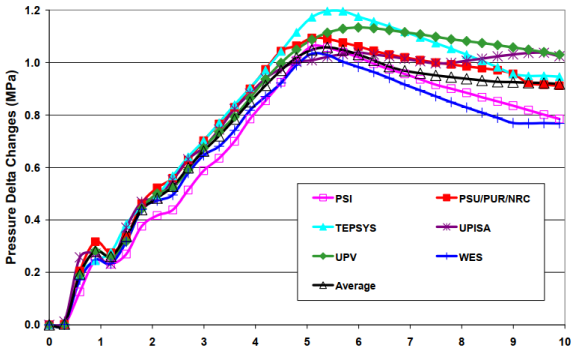

(b) Marginal change in vessel dome pressure in extreme scenario 2

Figure 5.18: Comparison of vessel dome pressure against the benchmark data for extreme scenario 2

In the early stages of the event, the course of the trend in Figure 5.19 also shows a strong resemblance to the results in the reference case. The maximum core surface temperature is calculated to be around 596 K.

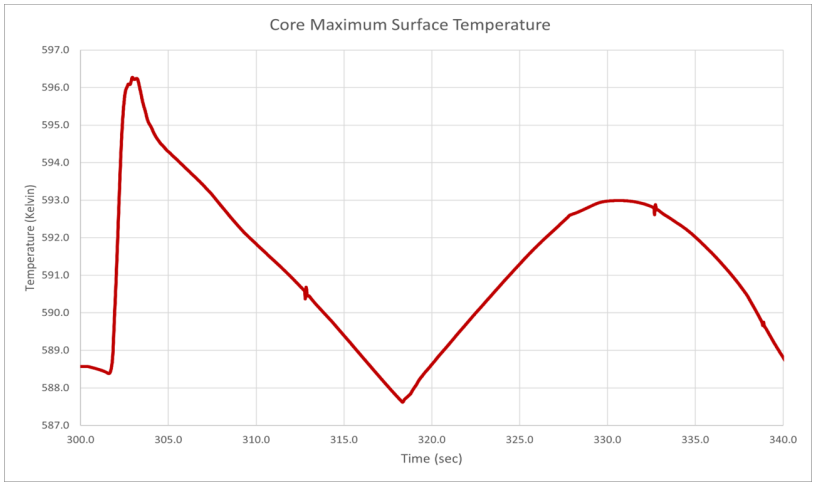

Figure 5.19: Core maximum surface temperature in hypothetical scenario 2

Hypothetical Scenario 3:

In this scenario turbine trip transient is postulated with the failure of the steam

bypass relief system and an error in the SCRAM mechanism. For this analysis, we blocked the bypass valve opening mechanism so that the valve remains closed throughout the simulation. To cancel the scram effect, we neutralized the amount of negative reactivity to be inserted into the system as a result of the scram initiation signal. Figure 5.20a demonstrates the vessel dome pressure response, Figure 5.21a showing the change in the core power, and Figure 5.22 representing the maximum fuel cladding temperature history charts will be introduced to describe the overall plant behavior during this scenario.

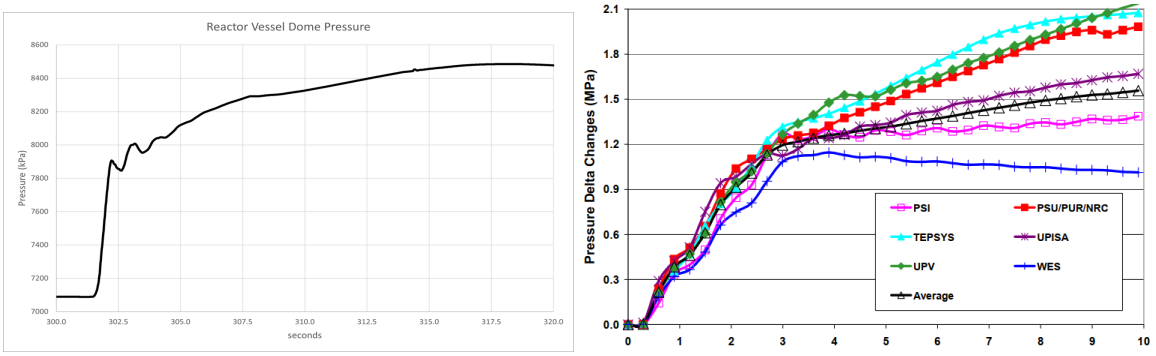

(a) Vessel dome pressure evolution

(b) Marginal change in vessel dome pressure in extreme scenario 3

Figure 5.20: Comparison of vessel dome pressure against the benchmark data for extreme scenario 3

According to the results shown in Figure 5.20a without opening the steam bypass valve, the first peak of the pressure wave is predicted to be greater by roughly 200 kPa than the pressure peak of the reference case. In the following seconds, the dome pressure level exceeded 8500 kPa. Comparison with the benchmark data in Figure 5.20b shows that the overall trend of the dome pressure evolution matches the benchmark data. When we compared the pressure levels 10 seconds after the starting point, we saw that our calculation predicted roughly a 1.3 MPa pressure increase

while the benchmark predicted 1.6 MPa.

The effect of higher pressure amplitude is shown its effect in Figure 5.21a. In comparison to the reference case power amplitude, a significantly higher (by nearly 50%) power excursion (nearly 6500 MW) is recorded during the hypothetical scenario 3 calculations.

The overall comparison of the results from a hypothetical scenario with the benchmark data given in Figure 5.21b shows that the code successfully generated a total power trend matching the benchmark result. However, the magnitudes of the first and second power peaks are significantly underestimated.

It is noteworthy that in this simulation the oscillatory behavior following the power surge is captured. Since the bypass valves are closed system is not able to discard the excess steam to the condenser. Therefore, the trapped steam caused power oscillations as a result of the reciprocal action of the void reactivity feedback.

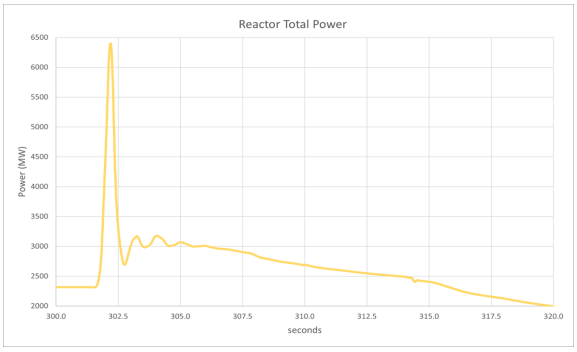

(a) Reactor total power response

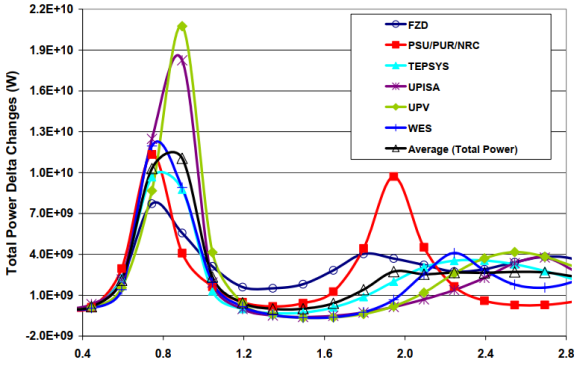

(b) Marginal change in total core power in extreme scenario 3

Figure 5.21: Comparison of total core power against the benchmark data for extreme scenario 3

On the other hand, the significant difference in this case appears immediately after the effects of the first excursion are suppressed by the negative void reactivity

feedback. Although the power level drops significantly within 1 second the pressure level records new highs since the release of pressurized steam from the safety relief valves is not sufficient.

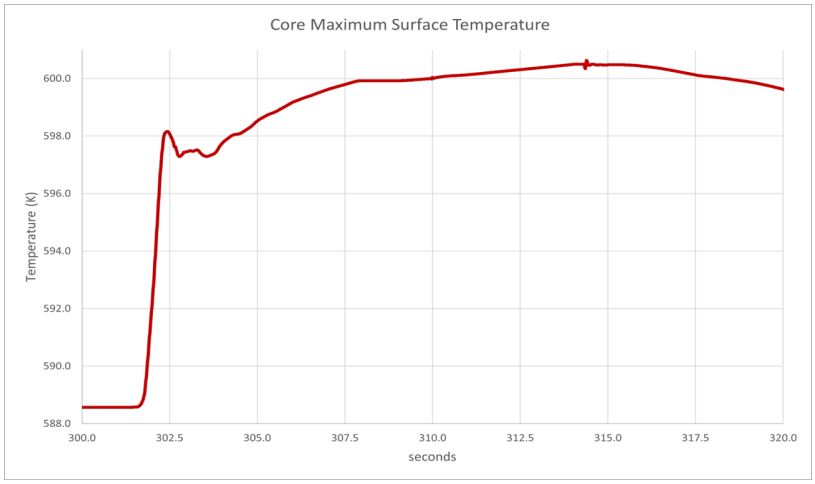

Figure 5.22: Core maximum surface temperature in hypothetical scenario 3

Figure 5.22 reveals that the increasing pressure level is accompanied by the increasing maximum core temperatures on the fuel cladding material. The figure shows that the first rise in the power and pressure levels resulted in exceeding 600K in the maximum cladding temperature. This experiences a slight decrease due to the change in the pressure level. In the following sequences of the simulation, higher values have been reached. Analyses in the literature [44] show that this simulation may result in the core meltdown in the later stages of the calculation. However, in our case, we observed that the thermal limits are not violated.

6

Sensitivity Analysis Results

In this chapter, we will provide the results of the sensitivity analyses that are conducted to find out how the calculation parameters and plant variables influence the important reactor responses. Since the first 5-10 seconds of the turbine trip cases include the important phenomena, we only plotted the charts for this time window.

6.1 Maximum Time Step

In this assessment, we evaluated the effect of the maximum time step on the vessel dome pressure response and reactor core power behavior. The time step in RELAP is an important input that influences the accuracy of the algebraic finite difference approximation of the time derivative. While smaller time steps are generally expected to improve accuracy, very small time steps can in fact reduce accuracy through increases in numerical truncation errors. For the best estimate turbine trip case linearly increasing maximum time steps has been explored. Vessel dome pressure in Figure 6.1 and total reactor power outputs in Figure 6.2 have been plotted against four different maximum time step values (0.1 ms, 1 ms, 10 ms, and 100 ms respectively). The data sampling frequency corresponding to each time step value is adjusted to

yield a record for every 0.1 seconds. This helps to maintain the consistency of the data gathered for each calculation.

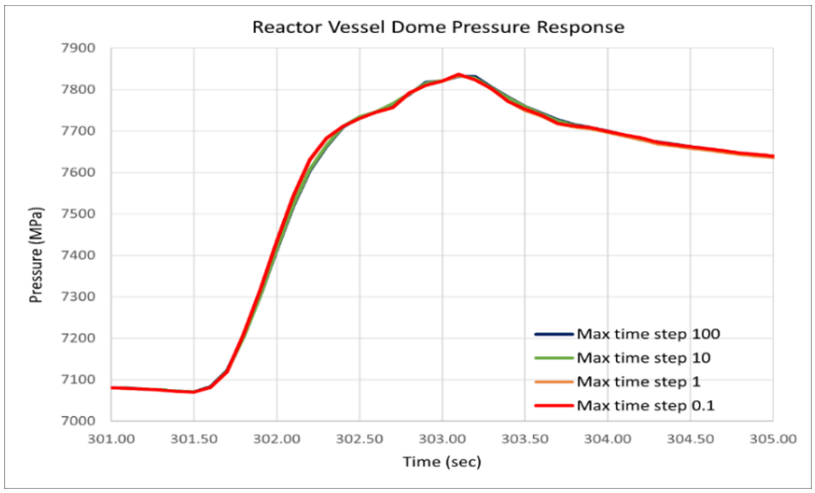

Figure 6.1: Vessel dome pressure response under different maximum time steps

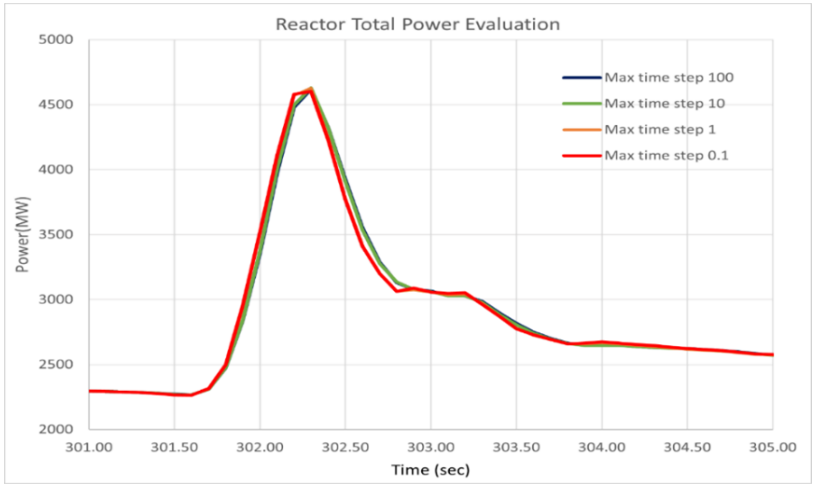

Figure 6.2: Reactor power response under different maximum time steps

Results in Figure 6.1 and Figure 6.2 revealed that the pressure and power response of the system during a turbine trip accident is not severely sensitive to the maximum time step value of the calculation. Yet, it is noteworthy that results for the

higher maximum time step values tend to diverge in a positive or negative direction depending on the direction of the trend.

Although the level of divergence is merely a small fraction of the value, the time step values between 1 ms and 10 ms would be safer to avoid the risk of overpredicting or underpredicting the pressure response of the reactor dome.

In terms of duration of calculation, computation takes around 550 seconds for the maximum time steps 100ms, 10ms, and 1ms, computation time increases up to 45 minutes if the maximum time step is chosen 0.1ms.

6.2 Direct Gamma Heating Coefficient

Gamma radiation is a high-energy electromagnetic radiation emitted in various nuclear processes, including neutron capture, nuclear fission, and radioactive decay. Gamma heating refers to the thermal energy produced as a result of the interaction of gamma radiation with a matter where the gammas largely are emitted by fission products in the fuel.

In this section, we present the analysis results about the effects of different gamma heating coefficients during turbine trip transient. Since the gamma heating coefficient can not be changed using restart problem input files, coefficients are defined at the beginning of each problem. In addition to the reference case calculation, two more calculations for different gamma heating coefficients (0.024 and 0.028 respectively) have been conducted. To demonstrate the effect of using different gamma heating coefficients, the reactor core power response in Figure 6.3 and maximum core surface temperature level in Figure 6.4 have been plotted.

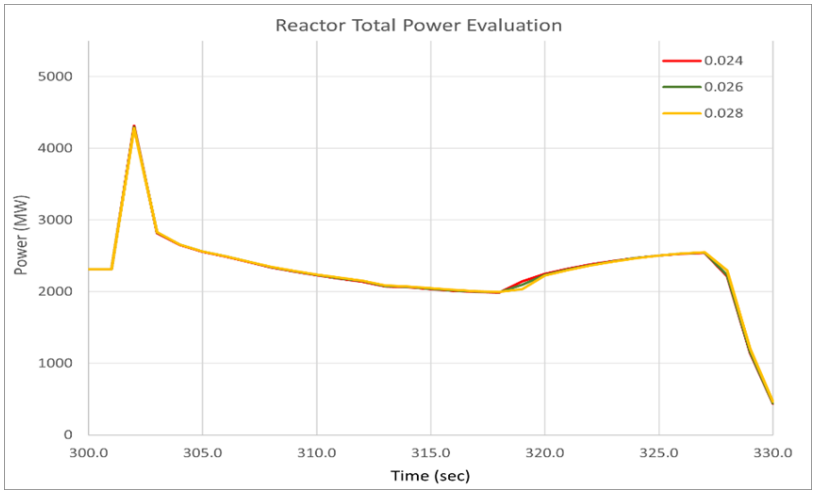

Figure 6.3: Reactor power behavior under different gamma heating coefficients

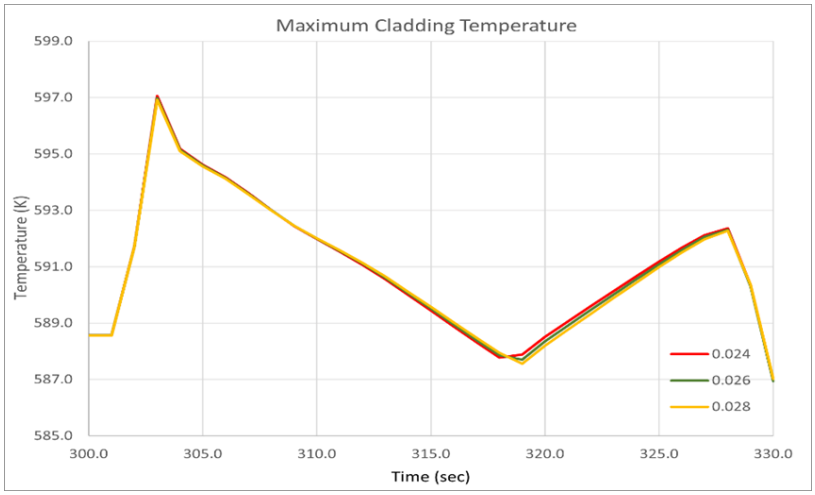

Figure 6.4: Cladding temperatures under different gamma heating coefficients

Results plotted in Figure 6.3 and Figure 6.4 are significantly overlapping. Despite the change in the direct gamma heating coefficient in the calculations, no considerable variation from the results of the base scenario calculations has been observed in the core power or maximum cladding temperature responses. This is consistent with expectations because the heating capacity of gamma interactions is significantly lower

than the heating capacity of thermal neutron interactions. That is the main reason why the nuclear power reactors mostly rely on the thermal neutrons.

6.3 Turbine Stop Valve Closing Speed

In this section, we present the results from sensitivity analyses conducted to investigate the influence of the TSV closing speed on the system parameters. For this purpose we plotted the vessel dome pressure response in Figure 6.6, the total reactor power history in Figure 6.5, and the change in the maximum cladding temperature in Figure 6.7 for reference case result as well as for a faster closing speed (0.1 sec) and a slower closing speed (1.0 sec) cases.

The results of the sensitivity analysis indicate that the TSV closure speed has a significant impact on the reactor parameters.TSV dynamics influence the pressure pulse in the core regions, and hence can significantly influence void collapse and hence the power pulse.

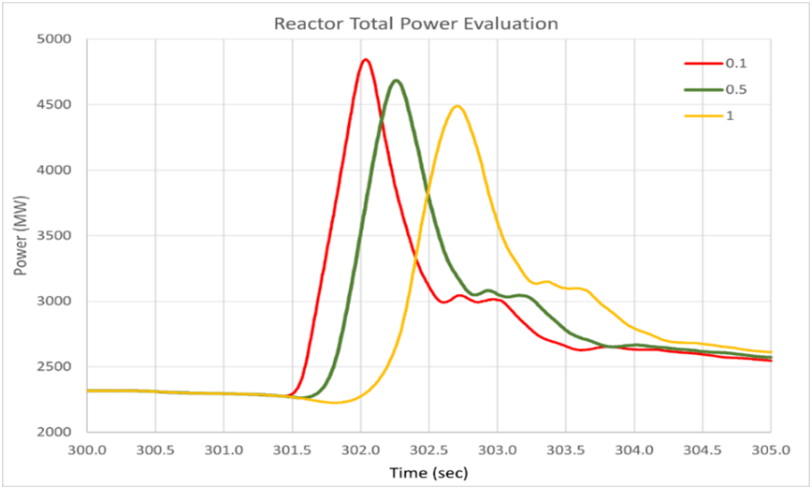

Figure 6.5: Effect of different TSV closing speeds on reactor power response

When the valve is closed suddenly, a power excursion is generated in the reactor. The characteristics of this power surge are heavily tied to the operational aspects of the valve, demonstrating its crucial role in the overall system dynamics. Figure 6.5 suggests that the changing TSV closing speed generates different power excursions. A faster TSV closure speed results in larger pressure waves, leading to higher power levels in the reactor.

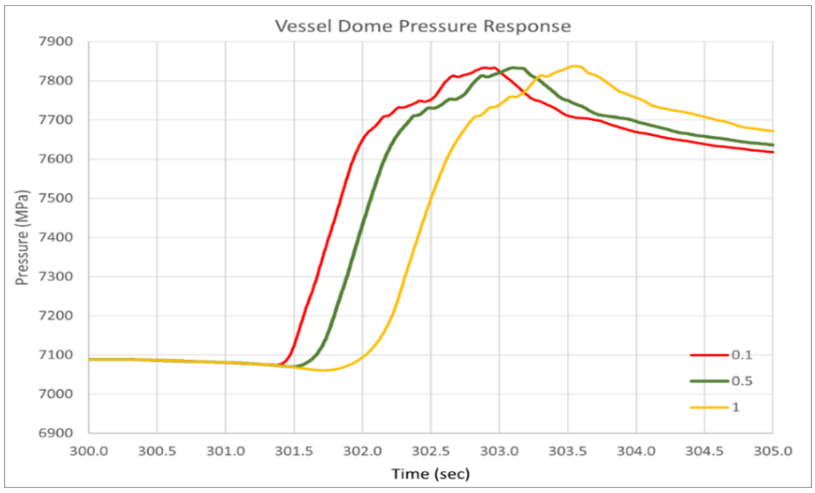

Figure 6.6: Effect of different TSV closing speeds on vessel dome pressure behavior

We expected to observe changing pressure wave amplitudes for the cases of slower and faster TSV closure speeds. Because the speed of TSV closure directly affects the amplitude of the pressure wave in the vessel dome. A slower TSV closure speed leads to a smaller amplitude of the pressure wave. This reduction in pressure wave amplitude may limit the power surge that occurs upon TSV closure, potentially providing a lower power excursion all other things being equal. However, Figure 6.6 predicts no change in the pressure amplitudes yet it just delays the time when the pressure is peaked. A similar response can be observed in Figure 6.7.

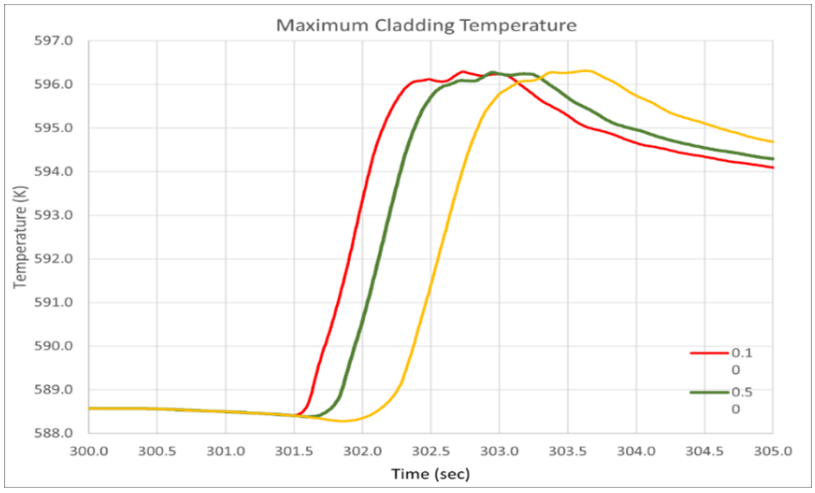

Figure 6.7: Effect of TSV closing speeds on maximum cladding temperature

It is known that the surge in power due to faster TSV closure could increase the risks associated with sudden shutdowns, including potentially higher maximum cladding temperatures. Higher cladding temperatures could increase the likelihood of fuel damage or more severe consequences, compromising the safety of the reactor.

These findings suggest that careful consideration and control of the TSV closure speed are vital to ensuring safe reactor operation and shutdown processes. Future investigations might focus on finding the optimal TSV closure speed that minimizes pressure wave amplitude and cladding temperatures while ensuring a controlled power reduction.

6.4 Bypass Valve Opening Speed

Given that the system's pressure response is significantly affected by the characteristics of the BPV valves, influences of a range of BPV opening speeds on the system

dynamics need to be investigated. In addition to the reference case (0.3 to 1.2) results one slower opening (0.3 to 1.4) and one faster opening (0.3 to 1.0) have been evaluated. In this section, we plotted the vessel dome pressure response in Figure 6.8, the total reactor power history in Figure 6.9, and the change in the maximum cladding temperature in Figure 6.10.

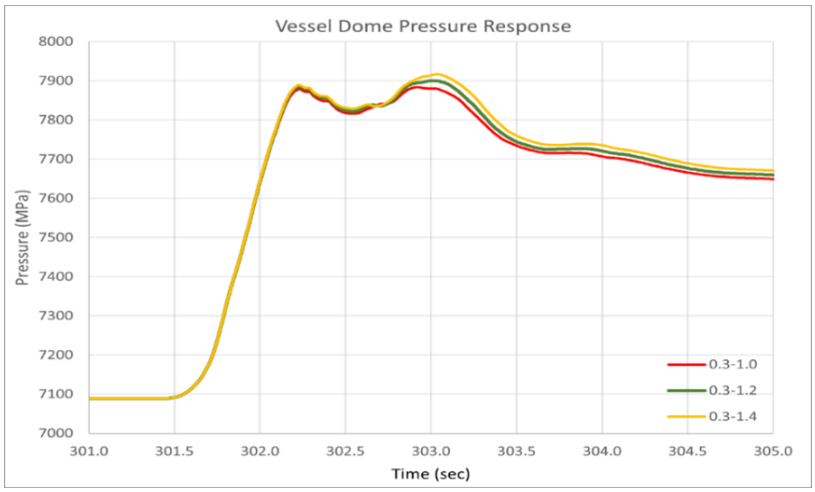

Figure 6.8: Effect of different BPV opening speeds on vessel dome pressure response

Results plotted in Figure 6.8 demonstrated a reduction in the BPV opening speed resulting in an increasing pressure wave amplitude in the steam dome.

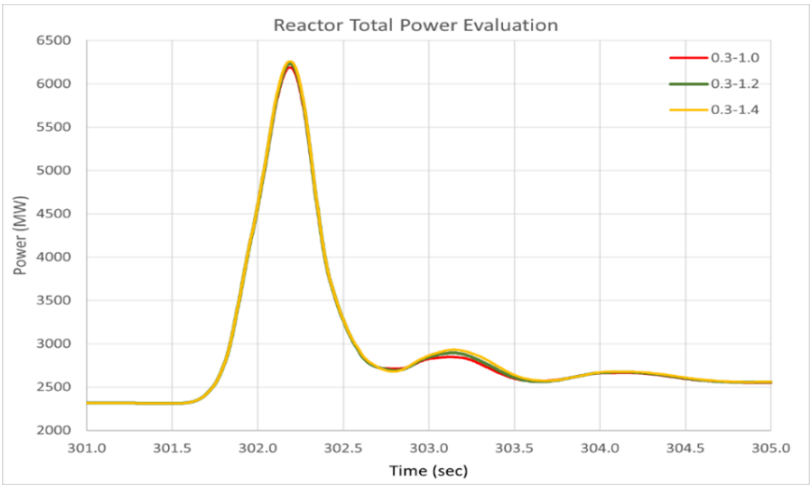

Figure 6.9: Effect of different BPV opening speeds on reactor power response

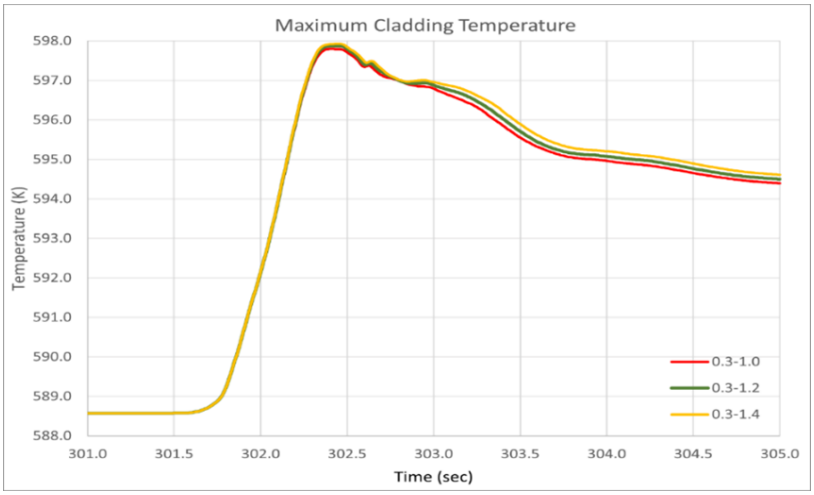

Figure 6.10: Effect of different BPV opening speeds on cladding temperature

From Figure 6.9 the peak point in the core power history is shifting below with the increasing BPV opening speeds. Similarly, the peak level of the maximum core surface temperature value experiences an upward shift if a slower BPV opening speed is employed.

Based on the results from this sensitivity analysis, it's clear that the characteristics

of the power excursion following the closure of the TSV are closely related to the operational and functional aspects of the BPV. However, it is noteworthy that despite the change in the parameter the trends in the figures did not shift too much. This means that even though the faster-acting bypass valves could be helpful in reducing power spikes, due to the fast nature of the turbine trip transient it may not be able to prevent accidents alone.

6.5 Bypass Valve Initial Actuation Time

Knowing that the pressure evolution within the vessel dome is significantly influenced by the behavior of the bypass valve, a range of valve initial actuation times have been investigated. In addition to the reference case (0.3 to 1.2) results one earlier action (0.1 to 1.0) and one delayed action (0.5 to 1.4) have been evaluated. In this section the vessel dome pressure response in Figure 6.8, the total reactor power history in Figure 6.9, and the change in the maximum cladding temperature in Figure 6.10 will be introduced.

From Figure 6.11 it is clear that the early actuation of the bypass valve has successfully reduced the amplitude of the pressure wave in the vessel dome.

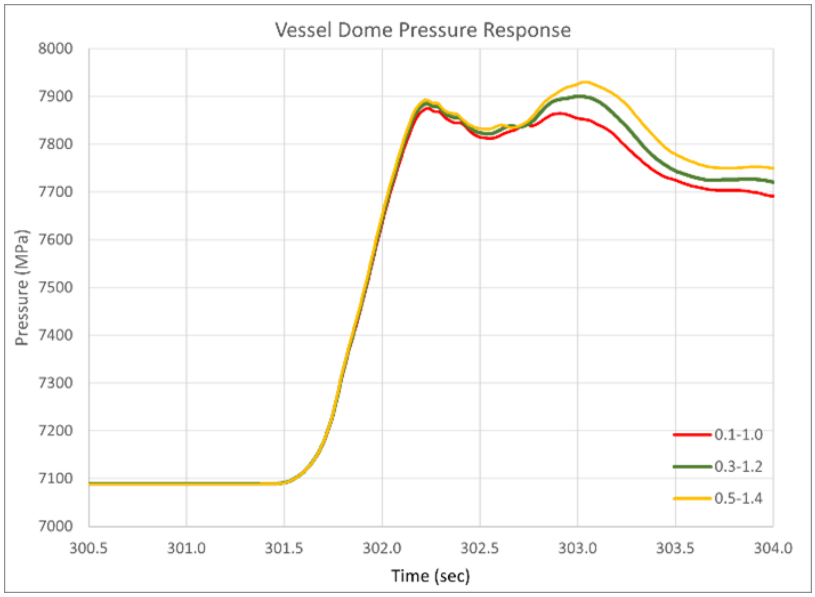

Figure 6.11: Vessel dome pressure response to different BPV actuation times

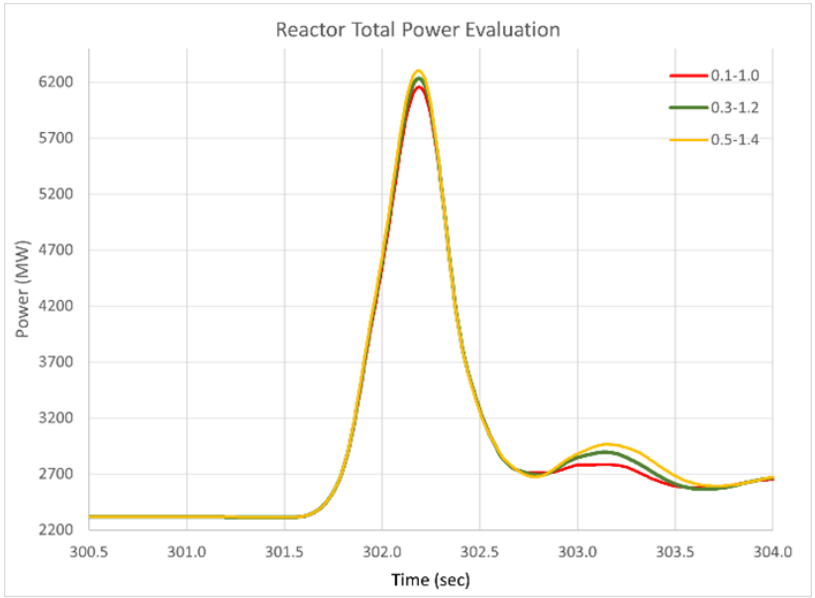

Figure 6.12: Reactor total power production with different BPV actuation times

Figure 6.12 shows that the suppression of the pressure rise in the vessel by early

BPV action also resulted in a lower level of power pulse which means that the characteristics of the power excursion following the closure of the TSV are significantly related to the initial actuation time of the steam bypass valve.

Consequently, the reduction in pressure and power pulses is also followed by the reduction in the maximum cladding temperatures in Figure 6.13.

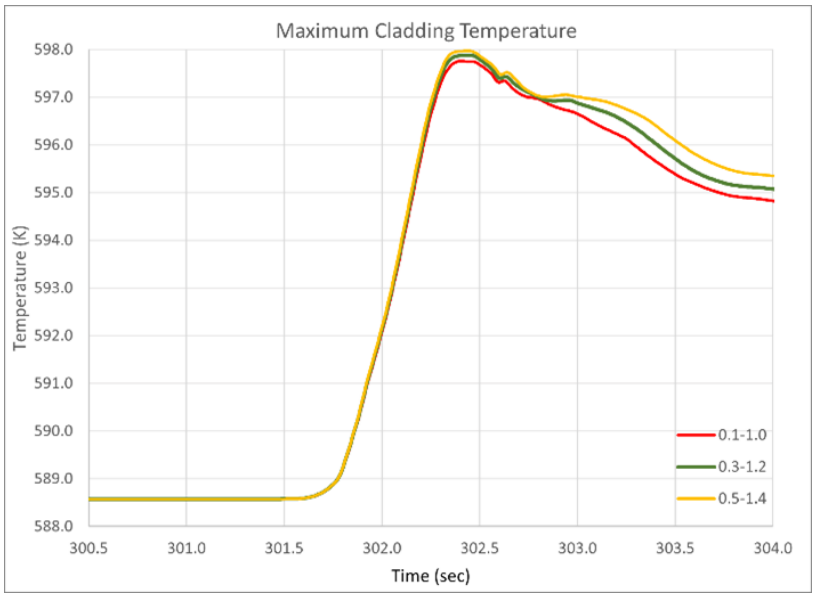

Figure 6.13: Maximum cladding temperatures with different BPV actuation time

Altogether, it is clear that the nature and progression of the transient are strongly dependent on the valve characteristics, thereby highlighting the valve's critical role in governing the system response to the turbine trip transient.

6.6 SCRAM Activation Time

In this sensitivity analysis, we evaluated the effect of the time when the control rods are inserted into the reactor core on the reactor responses. It should be noted that the

control rod insertion speed given in the Boundary condition section is preserved in this analysis. In addition to the base case (SCRAM activated at 0.63 sec) simulation, four sensitive cases(0.3 sec earlier action, 0.2 sec earlier action, 0.2 sec later action, and 0.3 sec later action) have been investigated. Findings from this analysis are presented in the vessel dome pressure response in Figure 6.15, the total reactor power history in Figure 6.14, and the change in the core maximum surface temperature in Figure 6.16 will be introduced.

Results plotted in Figure 6.14 revealed that rapid activation of the control rods is helpful for reducing the power response to the turbine trip transient. In comparison to the base case, 0.30 seconds earlier response time helped reduce the power peak by roughly 35%. In terms of late response times, it appears that there is an upper limit because of the inherent negative feedback system. For the response times of 0.93 seconds and above 0.93 the power amplitude is automatically suppressed. However, it is clear that in case of a 0.20-second delay in the SCRAM activation power peak increases significantly by approximately 10%.

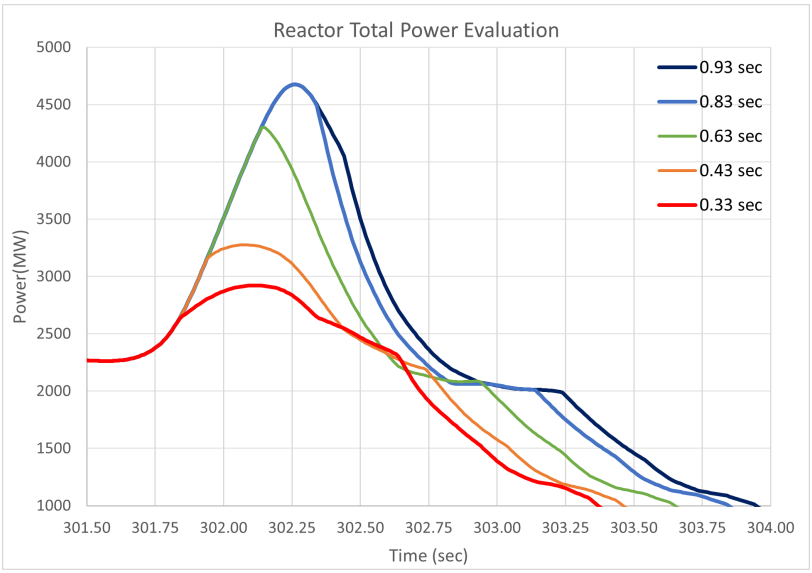

Figure 6.14: Reactor total power production with different SCRAM activation times

Although the pressure responses in Figure 6.15 acted in a similar way to the power history, the rate of change in the dome pressure response is not as drastic. However, even the slightest difference in dome pressure shows a noticeable difference in the maximum cladding temperature chart in Figure 6.16.

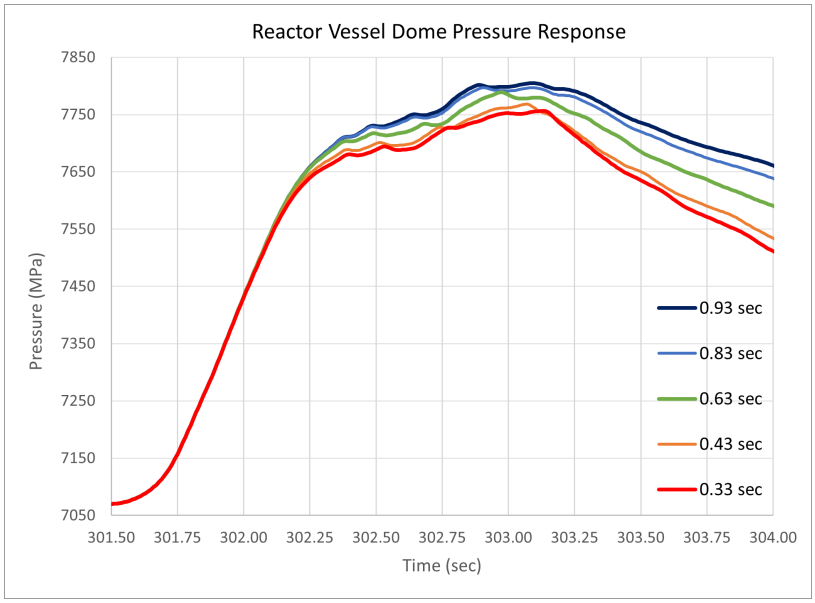

Figure 6.15: Vessel dome pressure response with different SCRAM activation times

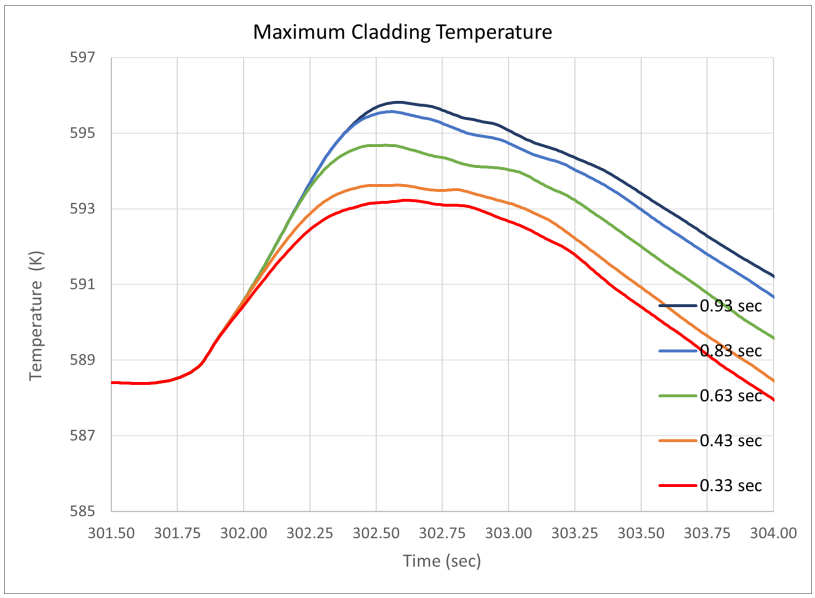

Figure 6.16: Maximum cladding temperatures under different SCRAM times

7

Conclusion and Future Work

7.1 Conclusions

The primary objective of this study is to investigate the behavior of a Boiling Water Reactor during a turbine trip scenario triggered by the sudden closure of the turbine stop valve. A best-estimate case is formulated to investigate if the increase in power can pose a risk to the cladding temperature through the occurrence of CHF on the fuel sheath. The RELAP5/Mod3.4 thermal-hydraulic analysis code is employed for this analysis. Calculations are run on the plant input model of the Laguna Verde Nuclear Power Plant provided by ISS. To determine the event sequence and initial boundary condition of the plant components we adopted the guideline published in the Boiling Water Reactor Turbine Trip 2 Benchmark created by NEA. Steady-state simulations demonstrated the model's capability to achieve design parameters and establish a stable trend. Similarly, the code testing routine indicated the code's capability to handle dynamic transient events.

Reference case analyses showed that closing the TSV resulted in the collapse of the in-core void fraction in the core. Although core power nearly doubled, the

inherent negative feedback feature of BWR effectively countered the power increase. Importantly, the maximum cladding temperature remained comfortably below the Critical Heat Flux (CHF) level. This is attributed to both the fuel's low thermal conductivity and the rapid nature of the transient event.

Within the framework of this thesis, three hypothetical scenarios were developed to push the boundaries of the computer model for the plant. The third scenario combines elements from the first two, resulting in elevated parameters (6500MW core power, 598K cladding temperature, and 7900kPa dome pressure), as anticipated. In the absence of control rod insertion, pressure, and temperature exhibited a rising trend. However, the negative feedback mechanism led to a decrease in power. A comparison with existing literature suggests that the plant could face a core dry out and even core meltdown risk in the later stages of this calculation. Remarkably, in our case, the CHF limit remains uncompromised.

A series of sensitivity assessments are conducted to determine how the plant parameters are responsive to the changes in the plant and computation variables. Results indicate that the changes in the gamma heating coefficient or the maximum time step of the calculation do not notably affect the responses of core power or maximum cladding temperature. Conversely, parameters were discovered to be most responsive to the initial actuation of control rod insertion. The outcomes revealed that a quicker rod response time significantly reduced the power peak by approximately 35%.

Analyses investigating the influences of different BPV opening speeds showed that peak power, dome pressure, and core maximum surface temperature levels are decreasing as the BPV opens faster, the opposite also holds true. When the effect of the initial actuation time of BPV is investigated, findings showed that early action

of the BPV could be helpful for suppressing the pressure wave thereby allowing the controller to reduce the power peak and maximum cladding temperatures. However, the amount of changes caused by the changing valve characteristics is not very significant. When the impact of TSV closing speed on system parameters is investigated the power trend indicates the significance of carefully controlling TSV closure speed for safe reactor operation and shutdown. Yet, pressure and temperature parameters created questionable results. Therefore, we believe that future research could focus on determining the optimal TSV closure speed to minimize pressure wave amplitude and cladding temperatures while ensuring controlled power reduction.

7.2 Recommendations for Future Work

Within the scope of this work, we investigated a nuclear plant operation from a safety point of view. However, due to the limitations in time, skill, tools, and publicly available data, some of the results may not satisfy the reference data or expert opinion. In this section, we highlight the points in this thesis open for improvement.

As we stated in the previous section, a future study could be conducted to determine the optimal TSV closure speed minimizing the pressure wave amplitude and fuel sheath temperature while allowing controlled power reduction. Similarly, the progression of the pressure wave in the main steam line plays and important role in the turbine trip event. A steam-water hammer analysis on the main steam line could contribute to understanding the scale and dynamics of the pressure wave entering the core. This analysis may also be helpful for assessing the dynamic loads affecting the pipes and other components in the main steam line.

Since the turbine trip event is a fast transient it is highly affected by the spatial

distribution neutron flux. A future work using a thermal-hydraulic and neutronic coupled analysis method could achieve a better representation of in-core neutronic behavior and hence better temperature and void distribution. We also believe that future work applying the high power set-point for the control rod insertion signal could achieve more realistic results as this is the method suggested in the benchmark.

A

Appendix

In thermal-hydraulic analysis, hands on experience in analytical tools and understanding of physical phenomena is crucial. A strong foundation of knowledge and expertıse is necessary for an effective analysis. Within the scope of this thesis a progressive learning approach was adopted for skill acquisition and confidence building. Some RELAP input nodalization diagrams and corresponding calculation results are presented. By conducting these relatively simpler analysis we aimed to gain insights into the performance of analytical tools and their applications.

Model 1: Single Pipe with a Heating Element:

This model is intended to be a simplified representation of a horizontal fluid flow test circuit located between two control volumes. Main idea behind this model is to simulate a frictional pressure drop along the horizontal pipe. The heat transfer from a constant power supply to the moving fluid is also investigated in this model.

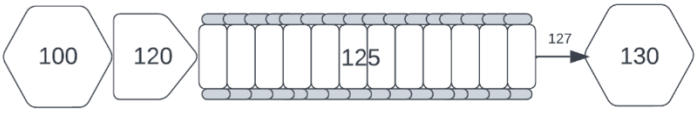

Figure A.1: Nodalisation diagram of a single pipe with heat element model

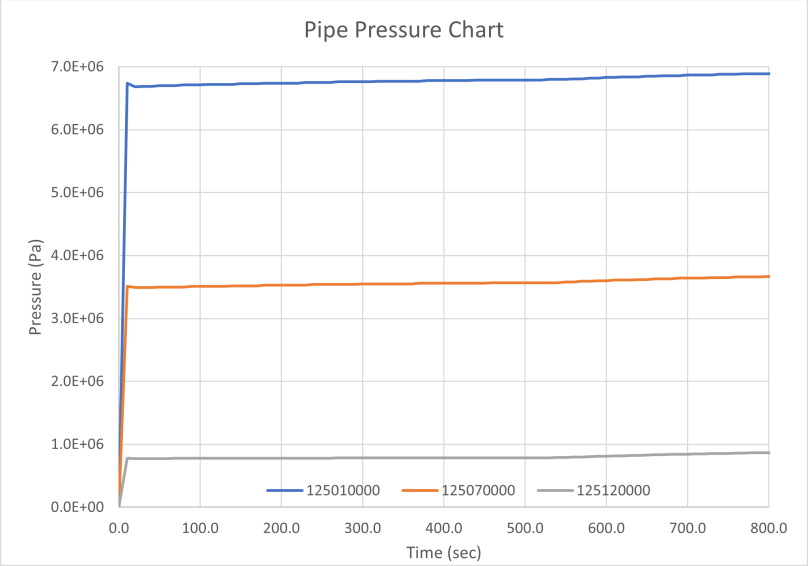

Figure A.2: Pressure drop behavior in a single pipe model

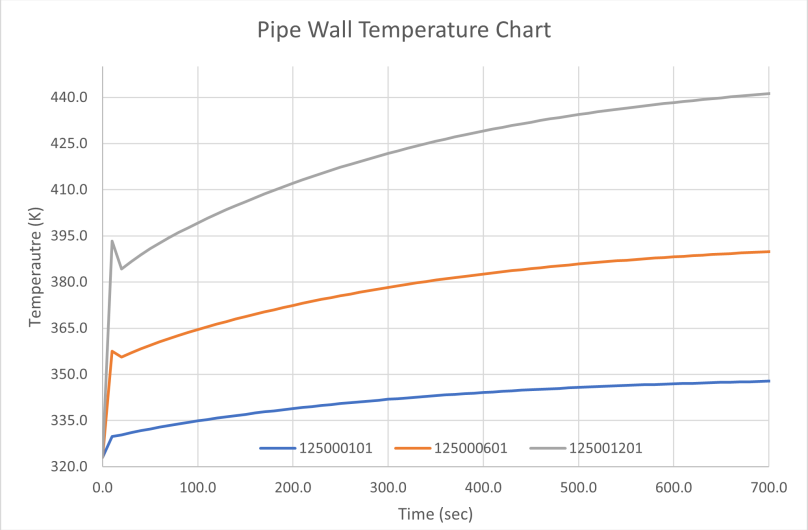

Figure A.3: Change in the pipe wall temperature in single pipe model

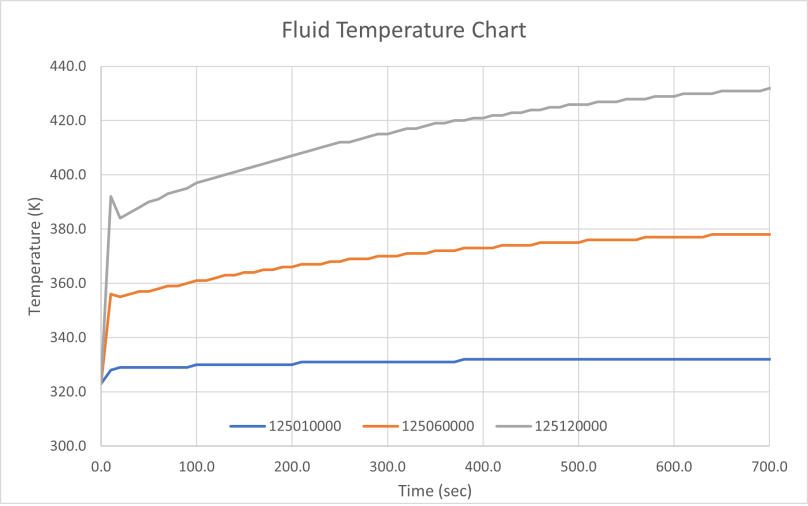

Figure A.4: Change in the fluid temperature in single pipe model

Model 2: Simplified Thermal-Hydraulic Loop Model:

This model is intended to be a simplified representation of a thermal-hydraulic loop system. Various system configurations are assessed by applying different combinations of trip adjustments.

Some of the scenarios are:

- Boiling Crisis in a Simplified Loop
- Effect of Accumulator in the Event of Boiling Crisis in a Simplified Loop
- Small Inlet Break Scenario in a Simplified Loop

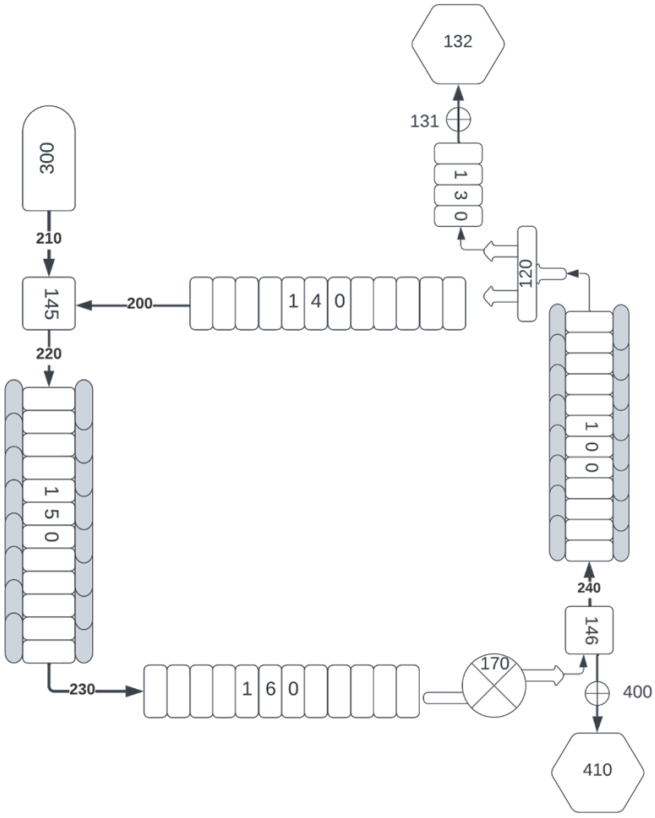

Figure A.5: Nodalisation diagram of a simplified thermal-hydraulic loop model

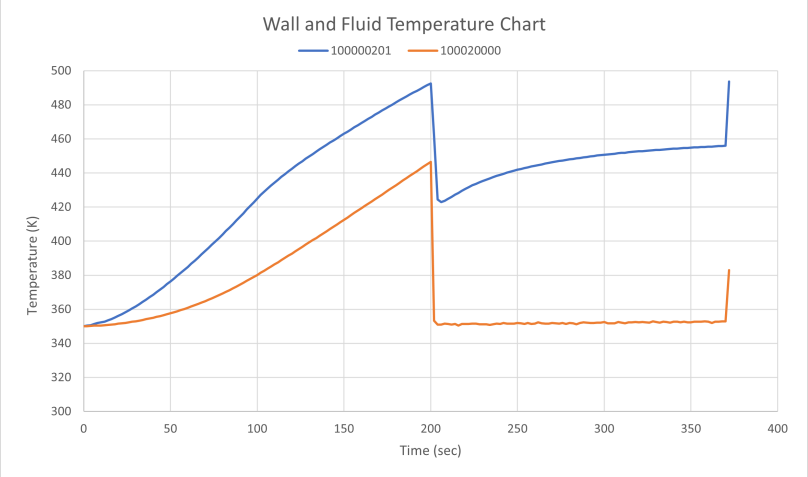

Figure A.6: The effect of accumulator action on fluid and pipe wall temperatures in a loop model

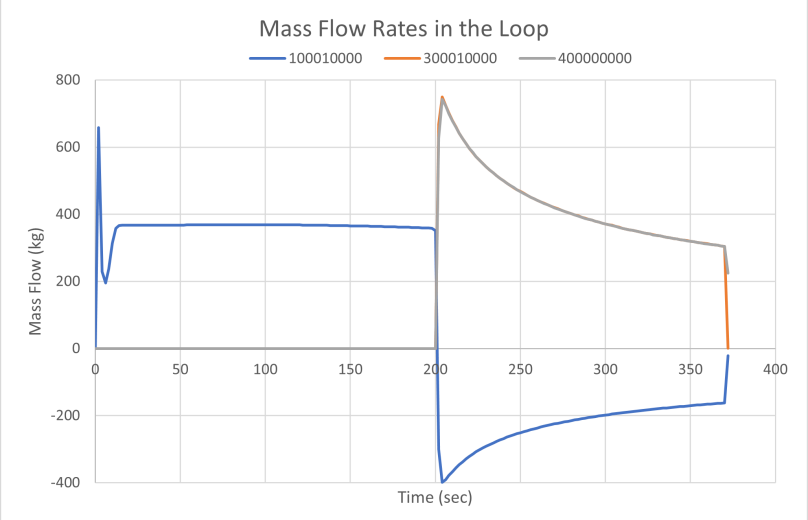

Figure A.7: The effect of accumulator action on mass flow rates within the pipes in a loop model

Model 3: Natural Circulation Experiment in Simplified Thermal-Hydraulic Loop:

This model is created with an intention to understand the dynamics of natural circulation in a simplified representation of a thermal-hydraulic loop. In order to physically allow the natural flow existing simplified thermal-hydraulic loop model is

customed and pump trip command is introduced. The natural circulation of fluid in a heated and cooled loop is assessed as different rate of heating and cooling applied to the system. Without achieving the balance in applied thermal energies system would not sustain a fluid flow without pressure difference provided by the pump.

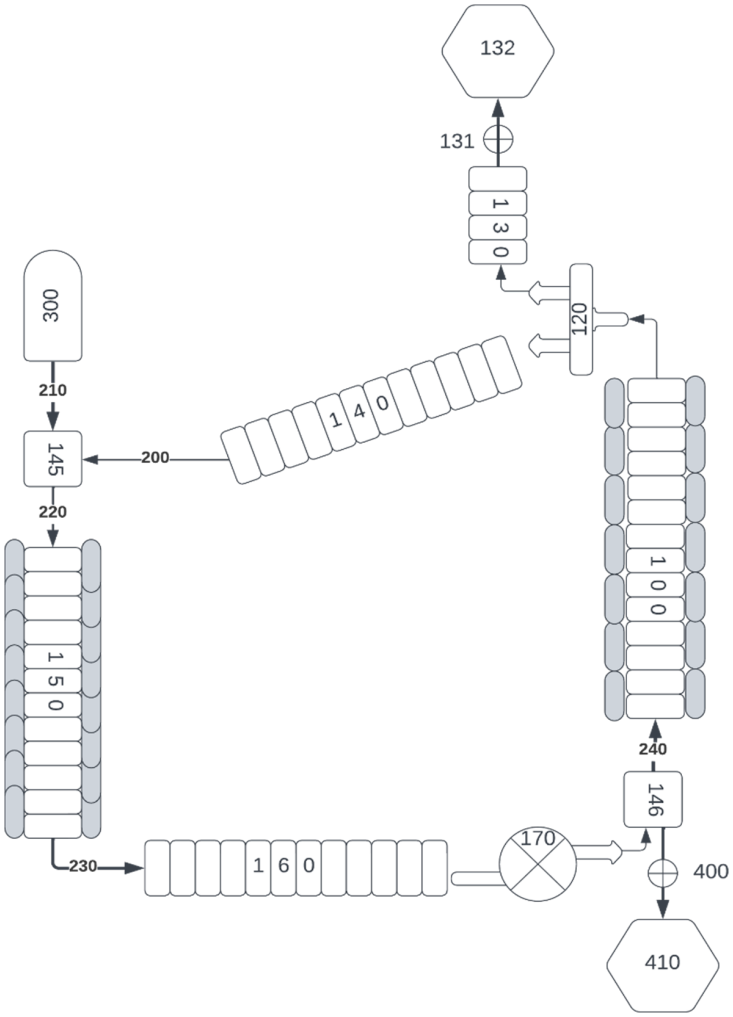

Figure A.8: Nodalisation diagram of a simplified natural flow loop model

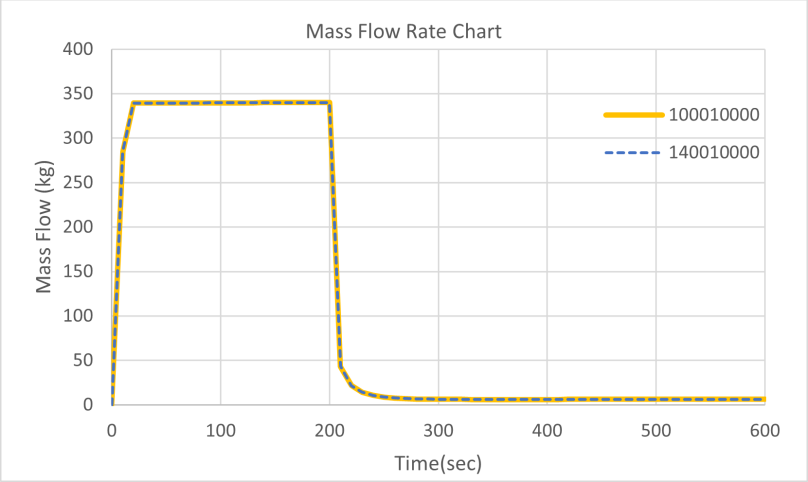

Figure A.9: Mass flow rates maintaining the natural flow in a loop model

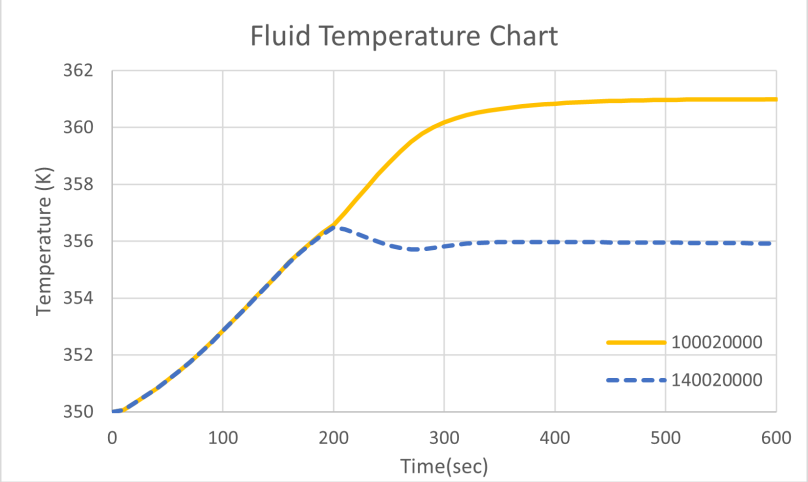

Figure A.10: Temperature difference in different pipes creating the natural flow in a loop model

Bibliography

[1] US Nuclear Regulatory Commission NRC General Electric Boiling Water Reactor BWR4 Technology Manuals. URL https://www.nrc.gov/docs/ML1125/ML11258A231.html.

[2] *Paris Agreement 2015*. United Nations Environment Programme. URL https://wedocs.unep.org/20.500.11822/20830.

[3] *Safety of Nuclear Power Plants: Design*. Specific Safety Requirements SSR-2/1 (Rev. 1). International Atomic Energy Agency (IAEA), 2016. URL https://www.iaea.org/publications/10885/safety-of-nuclear-power-plants-design.

[4] *Safety Assessment for Facilities and Activities*. General Safety Requirements GSR Part 4 (Rev. 1). International Atomic Energy Agency (IAEA), 2016. URL https://www.iaea.org/publications/10884/safety-assessment-for-facilities-and-activities.

[5] *Deterministic Safety Analysis for Nuclear Power Plants*. Specific Safety Guides SSG-2 (Rev.1). International Atomic Energy Agency (IAEA), 2019. URL https://www.iaea.org/publications/12335/deterministic-safety-analysis-for-nuclear-power-plants.

[6] *Computer Codes*. US Nuclear Regulatory Commission (NRC) Website, 2021. URL https://www.nrc.gov/about-nrc/regulatory/research/safetycodes.html.

[7] *Nuclear Power Reactors in the World*. Reference Data Series No.2. International Atomic Energy Agency (IAEA), Vienna, 2022. URL https://www.iaea.org/publications/15211/nuclear-power-reactors-in-the-world.

[8] B. Akdeniz, N. K. Ivanov, and M. A. Olson. *Boiling Water Reactor Turbine Trip (TT) Benchmark - Volume II*. Nuclear Energy Agency (NEA), Organisation for Economic Cooperation and Development(OECD), 2005.

[9] C. M. Allison, J. K. Hohorst, B. S. Allison, D. Konjarek, T. Bajs, R. Pericas, F. Reventos, and R. Lopez. Preliminary Assessment of the Possible BWR Core/Vessel Damage States for Fukushima Daiichi Station Blackout Scenarios Using RELAP/SCDAPSIM. *Science and Technology of Nuclear Installations*, 2012.

[10] J. R. Baratta, Anthony John; Lamarsh. *Introduction to Nuclear Engineering*. Pearson, 3rd edition, 2014.

[11] S. E. Bays, A. Abou Jaoude, and G. Borlodan. Reactor Fundamentals Handbook. 4 2019. doi: 10.2172/1615634. URL https://www.osti.gov/biblio/1615634.

[12] A. Bousbia-Salah and F. D'Auria. Analysis of the Peach Bottom 2 BWR Turbine Trip Experiment by RELAP5/3.2 Code. *Nuclear Technology and Radiation Protection*, 2002.

[13] A. Bousbia-Salah, F. D'Auria, and M. Bambara. Sensitivity Analysis of the Peach Bottom Turbine Trip 2 Experiment. 2004.

[14] A. Bousbia-Salah, J. Vedovi, F. D'Auria, K. Ivanov, and G. Galassi. Analysis of the Peach Bottom Turbine Trip 2 Experiment by Coupled RELAP5-PARCS Three-Dimensional Codes. *Nuclear Science and Engineering*, 2004.

[15] A. Bousbia-Salah, G. M. Galassi, F. D'Auria, and B. Končar. Assessment Study of the Coupled Code RELAP5/PARCS Against the Peach Bottom BWR Turbine Trip Test. *Nuclear Engineering and Design*, 2005.

[16] S. Bozzola. Fundamentals of Boiling Water Reactor (BWR). Technical report, International Atomic Energy Agency (IAEA), 1982. URL `http://inis.iaea.org/search/search.aspx?orig_q=RN:15025513`.

[17] G. O. Brown. The History of the Darcy-Weisbach Equation for Pipe Flow Resistance. 2004.

[18] Y. A. Cengel and A. J. Ghajar. *Heat and Mass Transfer Fundamentals and Applications*. Mcgraw-Hill Education, 6th edition, 2020.

[19] Comision Federal de Electricidad. *Laguna Verde Nuclear Power Plant Specifications*. Gerencia de Centrales Nuceluoeletricas, 1976. URL `https://www.nrc.gov/docs/ML0125/ML012500140.pdf`.

[20] G. Espinosa-Paredes, R. Camargo-Camargo, and A. Nuñez-Carrera. Severe Accident Simulation of the Laguna Verde Nuclear Power Plant. *Science and Technology of Nuclear Installations*, 2012.

[21] L. Fennern. *Design Evolution of BWRs: Dresden to Generation III+*. Elsevier Ltd, 2018.

[22] T. Filburn and S. Bullard. *Three Mile Island, Chernobyl and Fukushima: Curse of the Nuclear Genie*. Springer International Publishing, 2016.

[23] P. Gerland, S. Hertog, M. Wheldon, V. Kantorova, D. Gu, G. Gonnella, I. Williams, L. Zeifman, G. Bay, H. Castanheira, Y. Kamiya, L. Bassarsky, V. Gaigbe-Togbe, and T. Spoorenberg. World Population Prospects 2022: Summary of Results. 2022.

[24] J. Hohorst. *RELAP/SCDAPSIM Input Deck Manual Mod3.4/3.5/4.0*. Innovative Systems Software, 2012.

[25] International Atomic Energy Agency (IAEA). Safety Standards Series: Fundamental Safety Principles. *Fundamental Safety Principles No. SF-1*, 2006.

[26] International Atomic Energy Agency (IAEA). Best estimate safety analysis for nuclear power plants: Uncertainty evaluation. *Safety Reports Series No.52*, 2008.

[27] International Energy Agency (IEA). *Nuclear Power and Secure Energy Transitions*. 2022. URL `https://www.iea.org/reports/nuclear-power-and-secure-energy-transitions`.

[28] K. Ivanov, A. Olson, and E. Sartori. OECD/NRC BWR Turbine Trip Transient Benchmark as a Basis for Comprehensive Qualification and Studying Best-Estimate Coupled Codes. *Nuclear Science and Engineering*, pages 195–207, 2004.

[29] N. K. Ivanov, B. Akdeniz, and M. A. Olson. *Boiling Water Reactor Turbine Trip*

(TT) Benchmark - Volume III. Nuclear Energy Agency (NEA), Organisation for Economic Cooperation and Development(OECD), 2006.

[30] N. K. Ivanov, B. Akdeniz, and M. A. Olson. *Boiling Water Reactor Turbine Trip (TT) Benchmark - Volume IV*. Nuclear Energy Agency (NEA), Organisation for Economic Cooperation and Development(OECD), 2010.

[31] R. T. Lahey and F. J. Moody. *The Thermal-Hydraulics of a Boiling Water Nuclear Reactor*. American Nuclear Society, 2nd edition, 1993.

[32] G. Laura. Meet Oklo, the Earth's Two-Billion-Year-Old Only Known Natural Nuclear Reactor. 2018. URL `https://www.iaea.org/newscenter/news/meet-oklo-the-earths-two-billion-year-old-only-known-natural-nuclear-reactor`.

[33] S. Marguet. *The Physics of Nuclear Reactors*. Springer International Publishing, 2018.

[34] L. Marquez. Laguna Verde Nuclear Power Plant: An Experience To Consider In Advanced BWR Design. 2001. URL `https://inis.iaea.org/collection/NCLCollectionStore/_Public/32/048/32048869.pdf`.

[35] Nuclear Energy Agency (NEA). *BEMUSE Phase II Report: Re-Analysis of the ISP-13 Exercise, Post Test Analysis of the LOFT L2-5 Test Calculation*. Paris, 2006.

[36] Nuclear Energy Agency (NEA). *BEMUSE Phase IV Report: Simulation of a LB-LOCA in Zion Nuclear Power Plant – Appendices A to D*. Paris, 2008.

[37] A. Núñez-Carrera, R. Camargo-Camargo, G. Espinosa-Paredes, and A. López-García. Simulation of the lower head boiling water reactor vessel in a severe accident. *Science and Technology of Nuclear Installations*, 2012.

[38] R. L. Panton. *Incompressible Flow*. John Wiley Sons, Inc., 4th edition, 2013.

[39] R. Pericas, C. M. Allison, and J. K. Hohorst. RELAP/SCDAPSIM Fukushima Related Activities. *17th International Topical Meeting on Nuclear Reactor Thermal Hydraulics, NURETH 2017*, 2017.

[40] G. Petrangeli. *Nuclear Safety*. Butterworth-Heinemann, 2nd edition, 2020.

[41] J. Solis, N. K. Ivanov, and B. Sarikaya. *Boiling Water Reactor Turbine Trip (TT) Benchmark - Volume I*. Nuclear Energy Agency (NEA), Organisation for Economic Cooperation and Development(OECD), 2001.

[42] K. Theriault. *Nuclear Engineering Handbook Chapter 5 Boiling Water Reactors*. CRC Press, 2016.

[43] E. Togashi, J. Nakagawa, and H. Muramatsu. Effects of Ancient Egypt Hypostyle Halls on the Thermal Environment. *Japan Architectural Review*, 5, 2022.

[44] A. Trivedi. Application of RELAP/SCDAPSIM for Severe Accident and Safety Analysis of Nuclear Reactor Systems. 2017. doi: 10.13140/RG.2.2.29857.20328.

[45] A. Trivedi, P. Munshi, and C. M. Allison. Fukushima Type Severe Accident Analysis of Laguna Verde Nuclear Power Plant Using RELAP5/SCDAPSIM. 2012.

[46] A. Trivedi, C. Allison, A. Khanna, and P. Munshi. *RELAP5/SCDAPSIM/MOD3.4 Analysis of the Influence of Water Addition on the Behavior of a BWR During a Fukushima-like Severe Accident*. 2013.

[47] UNENE. *A Textbook on the CANDU Nuclear Power Plant Technology THE ESSENTIAL CANDU*. 2014. URL `www.unene.ca/education/candu-textbook`.

[48] USNRC. SCDAP/RELAP/MOD3.2 Code Manuals. NUREG/CR-6150, INEL-96/0422, US Nuclear Regulatory Commission, 1998.

[49] L. Zeghadnia, J. L. Robert, and B. Achour. Explicit Solutions for Turbulent Flow Friction Factor: A Review, Assessment and Approaches Classification. *Ain Shams Engineering Journal*, 2019.

[50] B. Zohuri. *Thermal-Hydraulic Analysis of Nuclear Reactors*. Springer International Publishing, 2017.